Mineralia Slovaca, 48 (2016), 1 – 60
Web ISSN 1338-3523, ISSN 0369-2086

Geothermometry techniques in reservoir temperature estimation and conceptual site models construction: Principles, methods and application for the Bešeňová elevation hydrogeothermal structure, Slovakia

BRANISLAV FRIČOVSKÝ[1], LADISLAV TOMETZ[2] and MARIÁN FENDEK[3]

[1]Department of Hydrogeology and Geothermal Energy, State Geological Institute of Dionýz Štúr, Mlynská dolina 1, SK-817 04 Bratislava, branislav.fricovsky@geology.sk
[2]Institute of Geosciences, Faculty of Mining, Ecology, Process Control and Geotechnologies, Technical University of Košice, Park Komenského 15, SK-042 00 Košice, ladislav.tometz@tuke.sk
[3]Department of Hydrogeology, Faculty of Natural Sciences, Commenius University in Bratislava, Mlynská dolina, SK-842 15 Bratislava; fendek@fns.uniba.sk

(Received 15. 2. 2016, accepted for publishing 19. 4. 2016)

Abstract The Bešeňová elevation hydrogeothermal structure has been analysed applying the ion-solute (silica, cation) and multicomponent equilibrium geothermometry techniques. Instead of a simple model of infiltration, transition and discharge, the multiple mixing stages have been proven, whether referring to the infiltration zone, transition – accumulation area, or discharge zone, where most of a focus has been oriented to the Vyšné Sliače area. Only multicomponent equilibrium and silica geothermometry based on chalcedony conductive cooling models appears adequate in the reservoir temperature estimation. Application of the cation geothermometers suffers of the deep reservoir thermal waters immaturity, driven by the separate convection cells due to unconform aquifer base overheating. In the Vyšné Sliače area, warm springs are related to both reservoir zones by lateral leaking (driven by density, hydraulic and pressure gradient), later diluted at a contact with the shallow and cold groundwater. Qualitative use of geothermometers proves its adequacy in construction of conceptual site models for low enthalpy geothermal systems. Quantitative application, however, remains limited in essence.

Key words: Bešeňová elevation, conceptual site models, muticomponent equilibrium geothermometry, solute geothermometry, thermodynamics

Graphical abstract

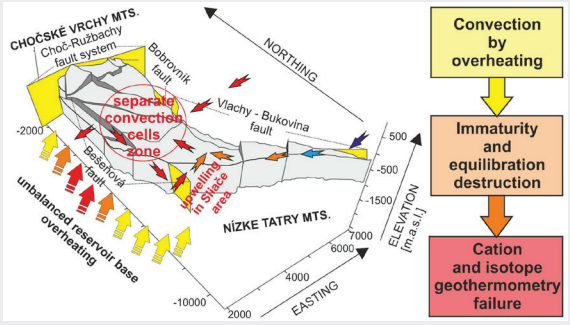

Highlights

- Complex geothermometry applied for a first in conditions of the W. Carpathians in CSM construction
- Separate convection cells form within the deep reservoir
- Immaturity of thermal waters due to convection and carbonate environment
- Minor (SW) discharge zone in the Sliače area
- Dry CO_2 fluxes in the Sliače area due degassing during upwelling

FOREWORD

In the past decades, geothermometry gained conclusive credits worldwide since first of them have been developed (e.g. Fournier and Truesdell, 1971), whether for reservoir temperature assessment, reservoir dynamics identification (mixing, boiling, dilution, leakage, etc.), field development perspectives, geothermal history matching and reservoir production response monitoring, or conceptual site models (CSM) construction. Both aspects of geothermometry application, quantitative temperature estimation or qualitative analysis, require comprehensive understanding of theory beyond, local thermodynamics and basic site concepts.

Essentially, geothermometers either formulate a degree of deep particular constituents concentration conservation over a reservoir fluid history, or determine a magnitude of equilibration of fluids to the dissolved mineral assemblage or wallrock.

A skepticism towards geothermometry in conditions of the Western Carpathian stems from misunderstood convention of its use for temperature estimation only, subsequently considering it undue, as being derived from high

enthalpy fields. The same disbelief, however, contravenes the principal philosophy of geothermometry application.

In contrast, this contribution explains principles and application conditions of geothermometry at tough background, with consequent demonstration of its qualitative and quantitative analysis in CSM construction for the Bešeňová elevation hydrogeothermal structure. We also provide an extended review on most important and well established publications, explaining this topic in details and in extension that our contribution could not cover.

THE BEŠEŇOVÁ ELEVATION STRUCTURE

The Bešeňová structure represents pre-Paleogene basement elevation (Maďar, 1997), trending N-S within the western part of the Liptov Basin (Fig. 1a), limited tectonically to its surroundings. Limitation to neighboring structures of the Liptovská Mara depression (E) and the Ivachnová depression (W) is formed by the N–S trending Vlachy – Lubeľa – Vrch Hája and Bešeňová fault respectively. Fault swarms of NW–SE to NE–SW trend terminate the structure at the Nízke Tatry Mts. on the south. To the north, the Choč fault provides a tectonic contact of the Bešeňová elevation structure with the Chočské vrchy Mts. (Remšík et al., 1998).

Pioneering research on local mineral waters assumed the springs nearby the town of Bešeňová as being associated with the deep and thermal water reservoirs due to the travertine domes formation, and connection of the groundwater basin (the Liptov Basin) with the massif of Nízke Tatry Mts. (Franko et al., 1974), later extending the conception to delineate both areas as the discharge and recharge zones (Franko, 1984). Meanwhile, temperature and density measurements of dry CO_2 fluxes in the Vyšné Sliače area assigned them a petrogene origin (Zbořil et al., 1972). The analysis of springs and artesian wells at the southern margin of the basin has provided an argument to assume several infiltration channels at different depths towards the basin. Soon Zembjak et al. (1986) concluded that the infiltration and recharge propagation differentiation realizes at open fault systems at southern periphery of the basin, whilst local springs are not just of barrier, but the tectonic origin as well.

Geothermal prospection on thermal waters began in the late 1970s, installing a 450 m deep BEH-1 well. Thermal waters, found in the Choč Nappe (CHN) Mid Triassic carbonates and a secondary permeable top of the Krížna Nappe (KNA) Jurassic–Mid Cretaceous variegated pelite limestones, have recorded the transient Ca-Mg-HCO_3-SO_4 type of waters at $T_{btm} \approx 35$ °C, unconform to the host rock environment, arising an impression of their origination in deeper, Krížna Nappe (KNA) Mid Triassic carbonate complexes (Franko et al., 1979). Completion of the ZGL-1 Bešeňová in 1987 documented deep reservoir thermal waters with $T_{wh} \approx 61.5$ °C, compared to the formation temperature of $T_{btm} \approx 68 – 71$ °C. Sampling revealed three geochemical facies at different positions: carbonatogene (Ca-Mg-HCO_3) to transient (Ca-Mg-SO_4-HCO_3) and sulphatogene (Ca-SO_4) geochemical types (Fendek et al., 1988). Later, the FBe-1 well (400 m) replacing the BEH-1 well after its failure, has produced the shallow reservoir waters of Ca-Mg-HCO_3 to Ca-Mg-HCO_3-SO_4 type waters at $T_{wh} \approx 25$ °C (Vandrová et al., 2009). Problems with ZGL-1 well called for a completion of the FGTB-1 Bešeňová well (1833 m) in 2011 that proved sulphatogene Ca-SO_4 to transient Ca-Mg-SO_4-HCO_3 character of deep reservoir waters at $T_{btm} = 69$ °C and $T_{wh} = 66$ °C (Vandrová et al., 2011). Hydraulic connection between both reservoirs and shallow reservoir extension to the Borové Formation (IWCP) has been concluded continuously (Remšík et al., 1998; Vandrová et al., 2009).

Since the beginning, thermal waters have been found as oversaturated with respect to calcite (e.g. Fendek et al., 1988). Geothermometry application resulted in marginal constatations on immaturity to the Na/K system (Remšík et al., 1993), silica geothermometry inadequacy and uncertain validity of temperature – aqueous SO_4 concentration relation (Bodiš and Borosová, 1996). Only $\delta O_{SO_4} – \delta O_{H_2O}$ oxygen isotope geothermometry application (Remšík et al., 1998) yielded some success in temperature estimation ($T_{est} = 40 – 52$ °C).

Geology and tectonics

The Liptov Basin is a typical Tertiary intramountain depression of the Western Carpathians. Its recent arrangement into N–S elevated or depressed blocks has originated by the combination of (1) the pre-Paleogene relief segmentation and onset of the first karstification period (Mesozoic mass reduction; Činčura and Köhler, 1995); (2) Late Eocene–Oligocene synsedimentary tectonic activity regionally limiting deposition rate of the IWCP (Inner Western Carpathian Paleogene) sediments (Gross et al., 1979); (3) Neogene basin dissection and IWCP mass reduction along N–S, NW–SE and SW–NE faults (Němec and Bartková, 1987); and (4) Late Neogene–Early Quaternary rejuvenation of W–E faults inverting a relief to balance uplift tendencies of surrounding massifs (Jurewycz, 2005).

Review on geology

Vertical arrangement of the structure corresponds to its geotectonic evolution and recent tectonic position. *Devonian–Mid Carboniferous* magmatites and metamorphites form Tatricum Crystalline (TCR) bedrock beneath the *Early Triassic–Mid Cretaceous* para-autochthonous Tatricum Envelope Unit (TEU) and allochtonous Krížna Nappe (KNA) system or *Mid Triassic* Choč Nappe (CHN) tectonic slag respectively; all carbonates domina-

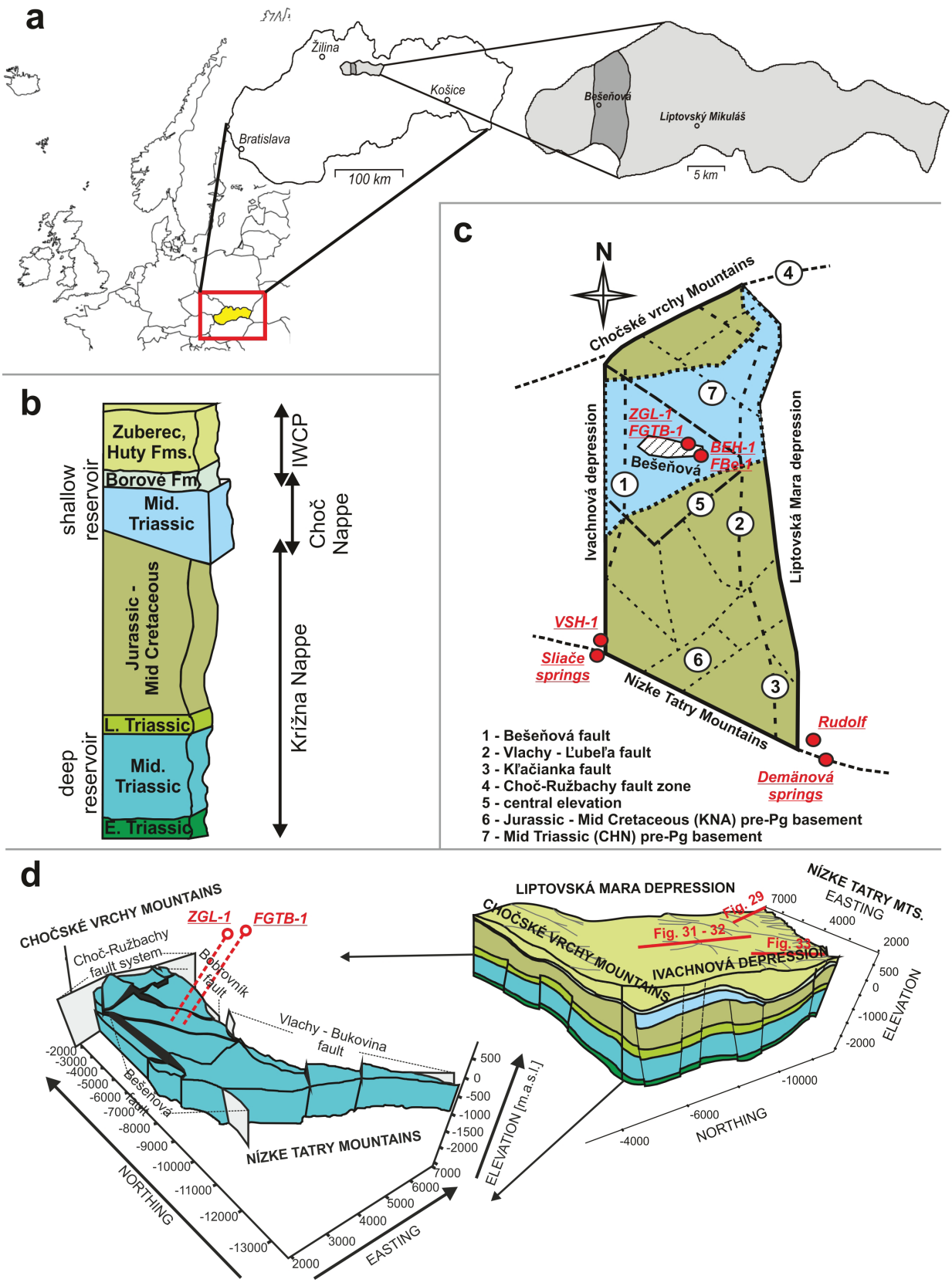

Fig. 1. The Bešeňová elevation definition: Geographic position (a), simplified vertical profile (b), major faults delineation (c) and 3D tectonic scheme with deep reservoir body (Krížna Nappe Mid Triassic carbonates) detail (d).

ted. Above, a *Mid Eocene–Latest Oligocene* succession of the Inner Western Carpathian Paleogene (IWCP) forms a siliciclastics dominated envelope (Gross et al., 1980), reduced in thickness centrewards the system (Gross et al., 1980). Atop, continental *Quaternary* sedimentary cover forms some meters thick cover (Remšík et al., 1998).

The geothermal system encompasses two reservoirs (Remšík et al., 2005). The *deep reservoir* associates with KNA Mid Triassic carbonates (limestones, dolomites, transient varieties), forming a solid body through an entire system, being segmented into several blocks in depths between 660–3 200 m and sealed by the Early Triassic (base) and Late Triassic (top) rich-in-evaporites siliciclastics (quartzites, pelite shales) dominated aquicludes. The *shallow reservoir* is recognized in the CHN Mid Triassic dolomites, hydraulically connected to conglomerates, breccia and detritic carbonates of the Borové Formation (IWCP). Atop, typical claystones-dominated (Huty Formation) and flysch-dominated (Zuberec Formation) horizons, both of IWCP group, form regional top insulator, while Jurassic–Mid Cretaceous KNA duplexed pelitic and organogene carbonates (Fig. 1b–d) represent a central aquitard (Fendek et al., 1988). Even the occurrence of thermal waters associated with the Mid Triassic TEU carbonates can not be excluded, though it has neither been proven yet.

Role of tectonics

Intersection of W–E and SW–NE faults at SE periphery allows the groundwater to enter the deep circulation regimes from the massif (Franko et al., 1979). Obviously, NW–SE and NE–SW faults towards the central part allow either further submerging of thermal waters already in the circulation, or hydraulic communication between CHN and KNA reservoirs (Fendek et al., 1988; Fričovský et al., 2015). The Choč–Ružbachy fault of trending W–E and located on the north, however, hydraulically separates thermal waters of the basin to waters documented in the Lúčky area (Fendek et al., 2013). To the south, contact of W–E, N–S and NW–SE faults respectively triggers upwelling of springs from moderate to deep circulation from the Nízke Tatry Mts. (e.g. Franko, 2002a; Remšík et al., 2005), or provide upwelling conditions for thermal waters from the basin (Fričovský and Tometz, 2013). It is fair then to assume those faults are open down to the KNA profile. If we accept some possibility on closed, TEU carbonates hosted structure, faults must be healed at a horizon of KNA Early Triassic, as any of mixing models gave a valuable indices on invasion of TEU thermal waters into the KNA carbonates (Fričovský and Tometz, 2013). Unlike, the Choč–Ružbachy fault zone is healed secondary, providing a lithological trap for hydraulic communication between structures of Bešeňová and Lúčky (Fendek et al., 2013; Franko, 2002b).

Review on geochemistry

The system has been concluded as open hydrogeological structure. Lateral inflow realizes along N–S faults from the Liptovská Mara depression, whilst runoff tendency is rather of intraformation character to the Ivachnová depression (Remšík et al., 1998). The infiltration zone is located towards the Nízke Tatry Mts. (Fendek et al., 1988) – Kľačianka valley area (Fričovský et al., 2015). Even there is a general agreement on discharge zone in the central part of the structure nearby Bešeňová, this paper discusses existence of second, minor, southwest located discharge zone of the Sliače area.

The BEH-1 and FBe-1 wells represent the shallow reservoir, along with ZGL-1 and FGTB-1 screening the deep aquifer. Both encompass the accumulation – transition zone. In the Vyšné Sliače area, waters are analysed by the Sliače springs and the VŠH-1 well. The recharge zone chemistry is approximated for shallow circulation by the Demänová springs and deep circulation by the wells in the Demänová valley area. Analyses are listed in Appendix C.

Review on facies analysis

Groundwaters are atmospheric in origin and petrogenic in chemistry. The shallow reservoir (SRTW) contains transient Ca-(Mg)-HCO_3-SO_4 to Ca-SO_4-HCO_3 and carbonatogene Ca-Mg-HCO_3 waters (Franko et al., 1979; Vandrová et al., 2009). Carbonatogene character is conformal to wallrock, defining this facies primary. Origin of sulphates is, however, expected for the KNA Early or Late Triassic formations (e.g. Fendek et al., 1988). These must then be secondary, resultant to deep reservoir waters evasion and mixing. Deep reservoir (DRTE) water samples at a bottom record sulphatogene (Ca-SO_4) and transient (Ca-SO_4-HCO_3) character, whilst at a top, carbonatogene Ca-Mg-HCO_3 to transient Ca-Mg-HCO_3-SO_4 facies were documented (e.g. Remšík et al., 1998). Variation in SO_4 content is due to vertical reservoir dynamics (Fričovský and Tometz, 2013). In central discharge zone, springs record mixed Ca-Na-HCO_3-SO_4 type, owing to Quaternary hosted groundwaters with the SRTW evasions. Waters of VSH-1 are of transient character. Mixed to hydrosilicatogene chemistry of springs (Franko et al., 1979) is, probably, due to the mixing of VSH-1 facies with the groundwater hosted in the Quaternary or Paleogene at shallow altitudes (Fričovský et al., 2015). Infiltrated waters from the N-slopes of the Nízke Tatry Mts. attain both, carbonatogene type for the shallow and transient type for deep transition.

Review on mixing models application

After Tshc diagram (Giggenbach, 1988), waters of accumulation zone are classified as immature and acid

to soda-springs (Fig. 2a), whilst both, discharge and recharge zone samples plot within the peripheral fluids only (Fričovský and Tometz, 2013). At Schoeller's plot (e.g. Marini, 2004), the thermal waters of deep reservoir are relatively stable in cation abundance, varying SO_4/HCO_3 ratio because of dissimilar contact with the sulphate source (Fričovský, 2014). There are no indices of adiabatic boiling (Fig. 2b) as curves do not change a shape signiffi-cantly. Some vertical dispersion is rather an implication of instable reservoir accommodation and, possibly, separate convection cells formation. Use of Gibb's plots (Gibbs, 1970) reveals a general lack in Na^+ for all facies. All waters may be classified as of continuous recharge insensitive to precipitation intensity (Fričovský and Tometz, 2013), but subjected to polystageous mixing because of facies similarities in between (Fig. 2c).

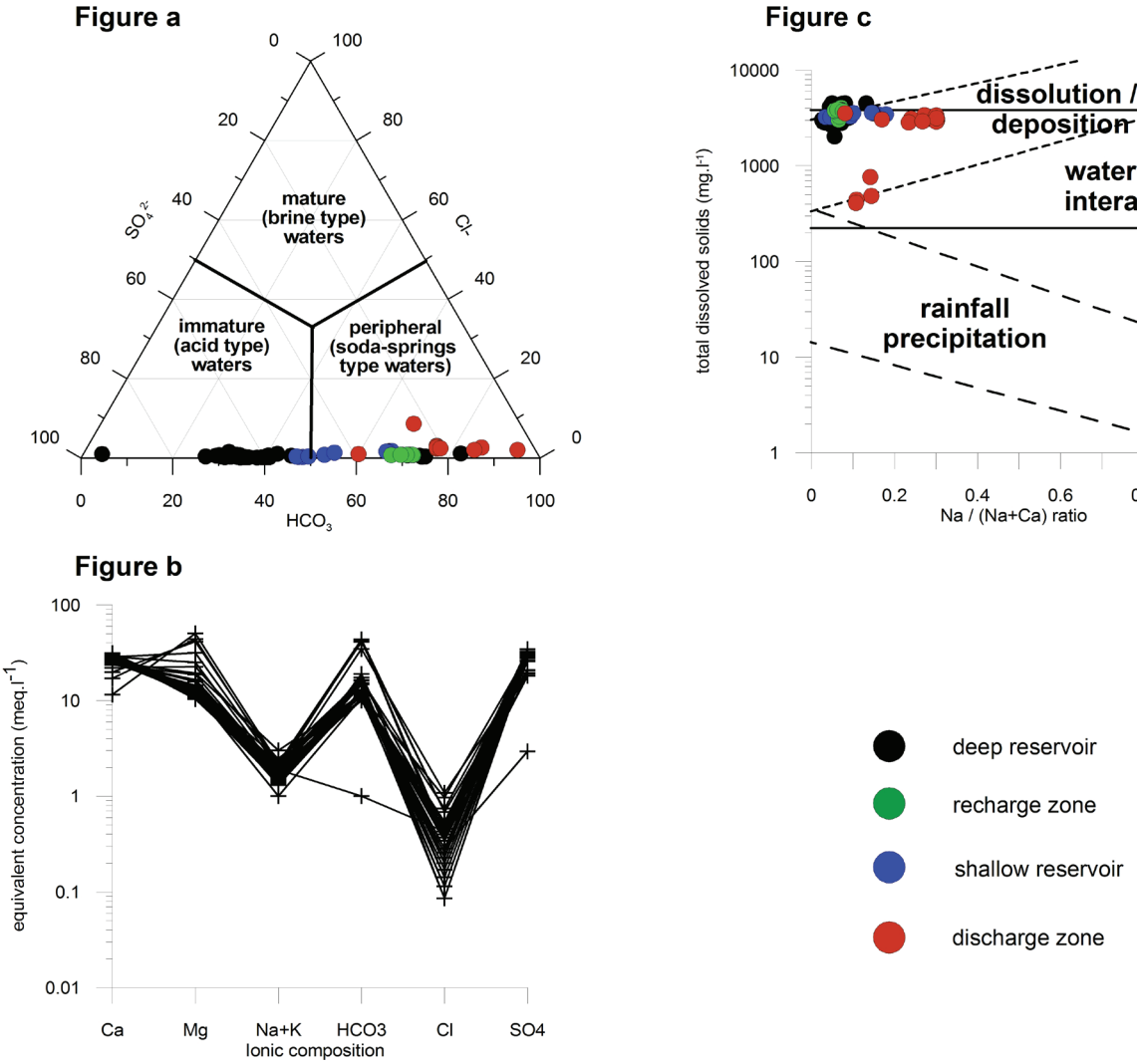

Fig. 2. Review on classification and mixing diagrams: The maturity Tshc plot (a), the Schoeller's plot for deep reservoir samples (b), and the Gibb's plot (c).

BACKGROUND

Understanding the nature and characteristics of the targeted system is key for its successful exploration, development and (sustainable) utilization. This is best achieved by conceptual model development (Axelsson, 2009), visualizing or interpreting relation between its particular components of physical and chemical provenience (Cummings, 2009). In other words, the conceptual model displays in-situ situation and relations generally.

Interpretation and validation of results, obtained by geothermometry application, necessitates as much knowledge on the processes the sample could underwent as possible. There is, thus, a need to understand its conceptual history, under which we understand every chemical, physical, dynamic and thermodynamic process, the fluid

or sample experienced since it entered a hydrogeothermal structure until it has been discharged or sampled. Improving the knowledge on conceptual model helps understanding the conceptual history and vice versa. The conceptual history must then be accepted as an inherent integrant of the CSM. Both must be considered and known, to some extension, before geothermometry application.

Geothermometers – classification and limitations

Geochemical composition of fluids projects saturation states for mineral assemblage(s) in solution (Browne, 1978), derived from a host rock environment and a conceptual history of a fluid. A chemical or isotope geothermometer is a model, based on temperature-dependent chemical reactions or isotope equilibrium fractionation of which reservoir equilibrium temperatures can be derived (Pang, 2001). These reactions are variably slow in re-equilibration at cooler temperatures and after effective phase separation, thus the equilibration temperature is believed as "printed" in a form of concentrations or ionic ratios (Karingithi, 2009).

Geothermometers consider individual constituents or their combination, of which three groups are distinguished conventionally (D'Amore and Arnórsson, 2000):

- solute geothermometers (silica and cation geothermometers)
- gas geothermometers (master gasses, noble gasses); and
- isotope geothermometers

Recent interest aims at thermodynamic equilibrium analysis, considering a fluid as a complex of solutes at various saturation states, introducing a multicomponent geothermometry (e.g. Spycher et al., 2011).

Yet the critical consideration in reservoir temperature estimation is a conservation of deep fluid chemical composition at a sampling point, assuming (Fournier et al., 1974):

- chemical reactions in a reservoir are temperature-dependent
- chemical and isotopic reactions do not change reservoir fluid chemistry significantly
- solids for equilibration reactions are sufficiently abundant in a host formation
- water–rock equilibration takes place at reservoir temperature
- the geofluid suffers little or no re-equilibration, mixing or dilution in upflow

Fluids meet all the criteria unlikely as they always loose heat by conductive cooling or boiling. Conductive cooling does not necessarily change a composition, but may change the saturation states of solutes, modifying the composition by precipitation or dissolution optionally. Adiabatic boiling (flashing) changes chemical composition immediately, subsequent to CO_2 evasion, variation in residual concentrations or pH (Marini, 2004). Isotopic composition of flashed water depends upon whether the steam fraction remained with the boiling water until it separated in once, or there had been a continuous steam removal from a fluid, relying upon a number of flashing stages (Truesdell et al., 1977).

Amount of a heat lost during conductive cooling is proportional to vertical distance traveled and inversely proportional to the flow rate or discharge. To some extension, duration of conductive cooling results in some pH variation, which, in a consequence, buffers dissolution–precipitation processes (Arnórsson, 2000a). The heat lost by adiabatic boiling is proportional to boiling rate and propagation. Chemical composition of a vapor in its wet-steam or dry-steam form always experiences modification by condensation or air attainment (Marini, 2004).

The actual reservoir fluid composition is then representative at no-boiling, no-mixing conditions prior sampling, otherwise parental composition must be reconstructed. Regardless of conformity in results, geothermometry bears substantial information for CSM construction.

SILICA GEOTHERMOMETRY

The silica geothermometry reflects solubilities of its polymorphs (quartz, chalcedony, amorphous silica, LT/HT opal), being not too sensitive to hydrostatic pressure changes and salt additions below 300 °C (Fournier and Potter, 1982). Temperature is then the factor to control silica thermodynamics in fluids, forth the use of temperature – aqueous silica concentration correlations becomes valuable for the most of geothermal systems worldwide.

Silica solubility and aqueous SiO_2 control

Silica solubility

First studies on silica solubility (Fig. 4) were carried out by Morey et al. (1962), defining an essential reaction to control the process (Eq. 1):

$$SiO_{2(s)} + 2H_2O = H_4SiO_4 \quad \text{(Eq. 1)}$$

for which the equilibrium constant (Eq. 2) is given (Fournier and Rowe, 1966):

$$K_{eq} = \frac{[H_4SiO_4]}{[SiO_{2(s)}]\,[H_2O]^2} \quad \text{(Eq.2)}$$

which reduces to (Eq. 3) as activity of pure phases equals 1

$$K_{eq} = [H_4SiO_4] \quad \text{(Eq. 3)}$$

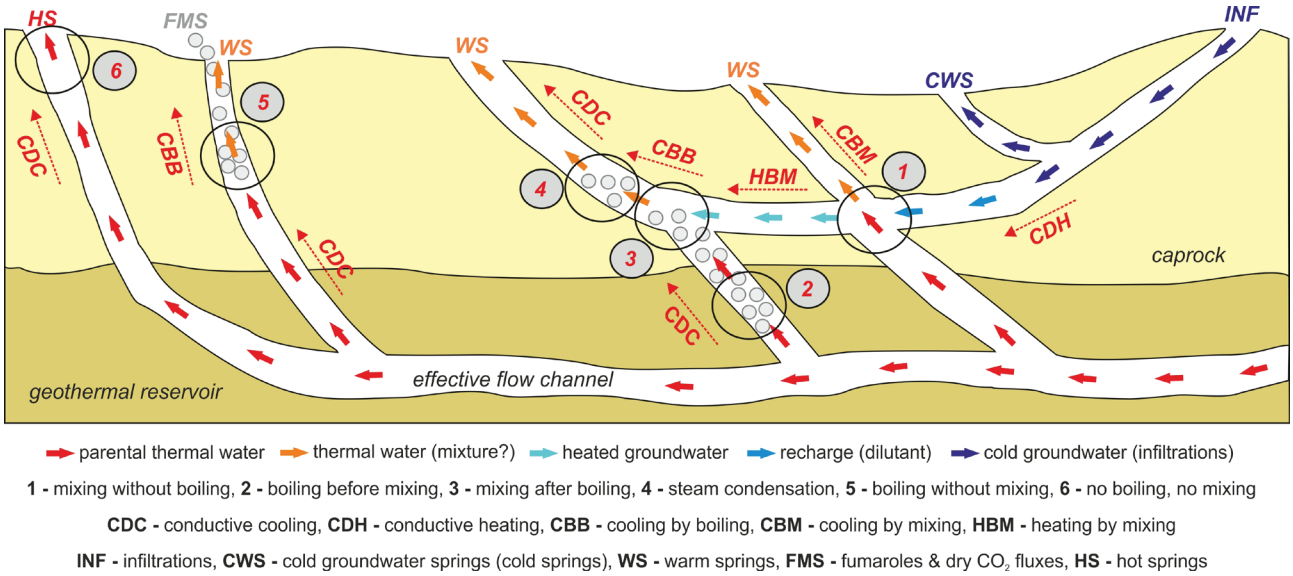

Fig. 3. Basic conceptual histories of geofluids.

The silica solubility decreases dramatically with adiabatic or conductive cooling (Fig. 4). Silica may, however, precipitate before reaching surface or the wellhead, forth sampling concentrations can not be assumed representative in some occasions.

The quartz is the most stable silica polymorph at T = 180–330 °C (Walther and Helgeson, 1977; Fournier and Potter, 1982), controlling aqueous SiO_2 concentration in high enthalpy fields. At T = 120–180 °C (low enthalpy or cooled/boiled high enthalpy fluids), the chalcedony becomes metastable and dissolved SiO_2 depends on conceptual history of the water. Below T = 120 °C (most low enthalpy or dramatically boiled thermal waters) it is likely the solubility of chalcedony is in control (Fournier, 1989). Activity of other polymorphs is rather rare in geothermal systems, even they may express higher solubility (Fournier, 1977).

Silica regime

If the fluid boils before sampling, the SiO_{2aq} concentration increases in the residual liquid proportionally to the amount of evaded steam, overestimating calculations (Fournier, 1989). This is the reason the chalcedony (Arnórsson et al., 1983) and quartz (Fournier, 1973) geothermometers were modified to correct for aqueous silica increase (see app. A).

Onset of silica precipitation is observed in conjunction to boiling, causing SiO_{2aq} concentrations at sampling points lower than those in parental reservoir that counteracts effect of relative silica concentration increase. Analogously, geothermometers, which do or do not involve boiling correction, may yield good results (D'Amore and Arnórsson, 2000). According to that, both should be used simultaneously and considered as probably providing a fairly reasonable range of temperature estimates.

An effect of silica solubility increase with pH is pronounced at above pH = 7.5 and T > 175 °C. Correction upon silica enrichment is necessary if a solution became alkaline prior dissolving additional silica in a response to increase in pH (Fournier, 1981) as a consequence of boiling. Then, the aqueous SiO_2 is possible to originate from hydrolytic dissociation of alkali silicates, instead of hydrolysis of wallrock silica polymorphs (Fournier, 1977).

High enthalpy fluids record most likely pH < 7.5, being resultant to buffering the hydrogen ions by hydrolytic reactions involving silicates (Fournier, 1977). At lower temperatures (T_{res} < 100 °C), thermal waters may have high CO_2 content and low pH because of, for example, dissolution of calcite.

Dilution decreases the silica content consequent to the onset of silica precipitation due to cooling. Because of fast response to reservoir dynamics, most of the equilibrium re-attainment with the silica causes the estimate to give a temperature of re-equilibration, otherwise parental temperatures tend to be underestimated (Fournier, 1980a).

Quartz geothermometers work best for T_{res} > 150 °C. For plutonic systems the usual validity range for chalcedony geothermometry is T_{res} = 120–180 °C, whilst the lower limit drops in carbonate, basaltic and sedimentary reservoirs to T_{res} = 60–180 °C. Amorphous silica and cristobalite geothermometry is trendless, depending on their control only.

The majority of silica geothermometers (see Appendix A) applies to solely cooling springs at sub-boiling temperatures or

borehole samples (Arnórsson et al., 1983; Fournier, 1973, 1977, 1991; Truesdell and Fournier, 1975), assuming reservoir equilibration conservation, thus vertical velocity of upwelling fluids is higher than silica re-equilibration and any dilution. These are labeled as "conductive cooling". Silica geothermometers with correction for boiling "adiabatic boiling geothermometers" (Fournier, 1973; Arnórsson et al., 1983) compensate the steam loss and residual SiO_2. Modifications obtain precious results for boiling springs of high discharge (> 2 kg·s^{-1}) or samples that undergo reservoir boiling prior sampling (Fournier, 1977).

Application: silica solubility analysis

One of accented arguments against silica geothermometry applicability in carbonate reservoirs is a "sufficient source" objection. Indeed, the silica is definitely not excessive in pure carbonates. Referring to local conditions, some minor silica sources must be accounted:

- siliciclastic IWCP formations in early downflow/late upflow stages
- pelitic Jurassic–Mid Cretaceous carbonates in early downflow/late upflow stages
- siliciclastics and impure detritic carbonates in late downflow/early upflow stages
- siliciclastic intercalations and silica impurities in reservoir carbonates
- siliciclastic and detritic carbonates hosted shallow reservoir

Analytical approach in controlling silica polymorph analysis is an alternative, if the primary or alteration mineralogy data are missing. This is grounded by sit-and-cluster principle along solubility functions (Fig. 4), correlated to temperature and reservoir homogeneity criteria.

With a great confidence, the chalcedony is a controlling polymorph on aqueous SiO_2 in local conditions. At relatively low wellhead (T_{wh} = 51–62 °C) and deep borehole (T_{res} = 61–69 °C) temperature differences, the SiO_2 oscillates considerably ($cSiO_2$ = 35–80 mg·l^{-1}) in deep reservoir, lacking any trend with the temperature. Under expected reservoir homogeneity where carbonates dominate over siliciclastic intercalations and thin sandstone beds, the variation records unstable dissociation of silicates (Fig. 4). Because it is not possible for quartz to take over a control in the shallow reservoir, clustering along a chalcedony and quartz metastability line at higher temperature is rather a record of two different facies. The metastability is rather attributed to silica shortage in the deeper parts of the system (BEH-1; $cSiO_2$ = 10–17 mg·l^{-1}, T_{wh} = 32–34 °C) due to its deposition after evasion from DRTE. The upper parts of the reservoir (FBe-1; $cSiO_2$ = 27–30 mg·l^{-1}, T_{wh} = 25–27 °C) do not suffer a lack in source as connected to the IWCP formations. By a contrast, samples of the discharge zone plot well onto chalcedony solubility line, definitely answering a controlling silica polymorph question.

Application: silica saturation analysis (deep reservoir)

The deep reservoir is found a key uncertainty in understanding the complex silica stability at a site. We inspected opal (low temperature), chalcedony (moderate temperature) and quartz (high temperature) to review SiO_2 thermodynamics within. Plotting saturation indices against extended temperature range (Fig. 5) eliminated opal of any influence on SiO_{2aq} concentration in thermal fluids as it remains undersaturated within the entire interval.

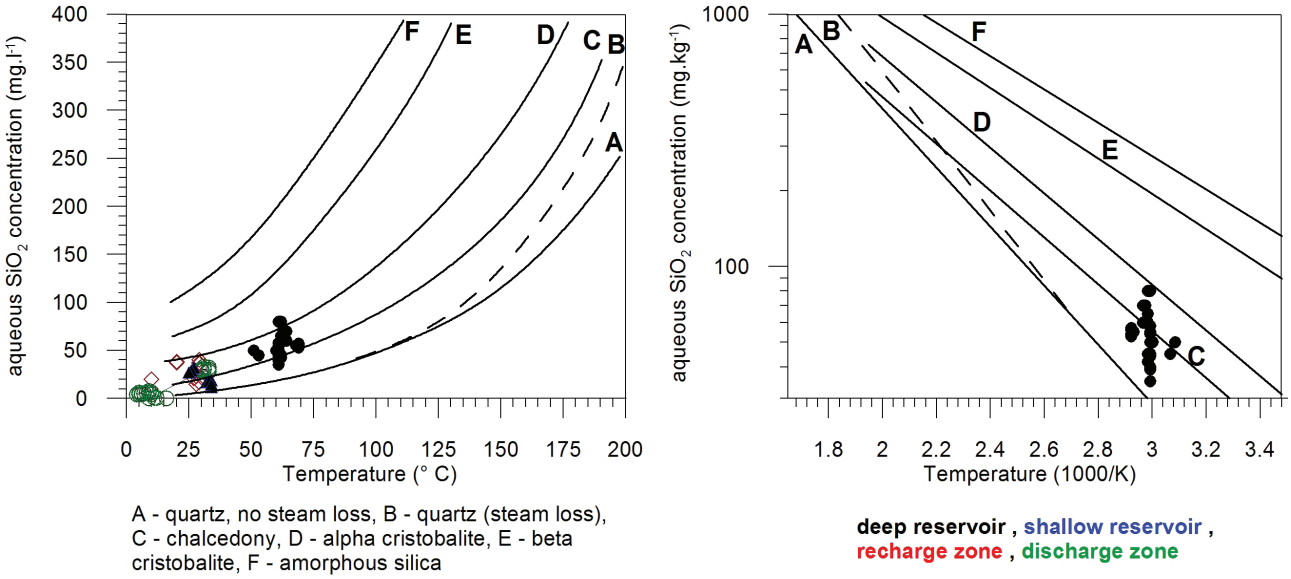

Fig. 4. Silica solubility analysis with (a) and against (b) the inverse of temperature. Modified after Morey et al. (1962).

The chalcedony equilibrates at T = 56–94 ˚C (Fig. 5) completely, with only two samples not attaining saturation below T = 90 °C. Most of samples intercepts SI = 0 at T = 65–70 ˚C. Irregularity in equilibration dispersion is either a consequence of the deficiency in silica source or unstable contact with the silica source (and hydrolysis reactions) within a deep reservoir. Thus this may be considered an indirect evidence on vertical reservoir filtration.

On a face of saturation curves distribution, the quartz may be of influence onto silica concentration in the water. This is because 14 out of 20 samples record equilibration at T = 80–100 ˚C. In fact, reservoir temperature of over 90 ˚C is an optimistic assumption, reducing SI = 0 interception to 4 samples only.

A clear trend of the increase in SiO_2 with p-T, depth, residential time and distance from an infiltration zone is missing (Fig. 4). The lack accounts to (1) the reservoir (intraformation) dynamics (mixing, vertical filtration); (2) insufficient source of silica for hydrolysis; and (3) silica origin by the water-rock cation exchange reactions. The controlling polymorph in the shallow filtration regime within the recharge zone may be opal, proceeding towards chalcedony metastability with the increase in p-T conditions during submersion. Both, SiO_2 concentration and saturation variation is resultant either to vertical mass flux in reservoir and insufficient available silica. Reservoir chalcedony saturation (Fig. 5) turns it available for cation exchange reactions with the wallrock, with minor deposition only (if any). Thus the deep SRTW facies are deficient in silica, explaining their affinity to plot onto quartz solubility line. By a contrast, the VSH-1 well records no lack in silica, even it should be implicit under given geological, p-T and initial DRTE conditions, evidencing other silica source to balance its loss. The compensation must then be due to mixing with SiO_2 rich source (SRTW evasions, groundwater hosted in IWCP or Jr/Cr-2 succession), or proportional to decrease in filtration velocity of DRTE facies towards discharge zone.

Reservoir dynamics and processes

Silica – enthalpy mixing model (XSih)

The silica – enthalpy mixing/geoindicator model (Fournier and Truesdell, 1974) is developed to determine reservoir temperatures regardless of dilution and steam loss. Use of enthalpy instead of temperature takes an advantage in the heat (energy) conservation in a reactive system. Involved silica solubility function must correspond to the polymorph controlling SiO_{2aq} concentration.

For geothermal waters at T_{res} = 50–340 °C (Fournier and Potter, 1982) proposed polynomial functions to determine the enthalpy H_L for liquid (Eq. 4) or vapor (Eq. 5) component, including liquid enthalpy for low temperature systems (Eq. 6) of T_{res} < 50 °C. Unknown dissolved silica (cSi) may be derived with (Eq. 7) below fluid enthalpy of H < 1 670 J·kg^{-1}. Besides (Eq. 4 to Eq. 6) enthalpies can be read from steam tables or calculated (e.g. using REFPROP). Silica concentrations may be taken from analyses.

$$H_L = 418.84 + 10.286T - 0.05092T^2 + 2.6309\cdot10^{-4}T^3 - 6.9303\cdot10^{-7}T^4 + 7.4566\cdot10^{-10}T^5 - 1209.8T^{-1} + 11.99T^{-2} - 353.76\log T \quad \text{(Eq. 4)}$$

$$H_L = 2\ 035 - 5.0499T + 0.057399T^2 - 3.0426\cdot10^{-4}T^3 + 7.909510\cdot10^{-7}T^4 - 8.6968\cdot10^{-10}T^5 + 1\ 342.4T^{-1} - 13.298T^{-2} + 396.29\log T \quad \text{(Eq. 5)}$$

$$H_L = 4.1868\cdot T \quad \text{(Eq. 6)}$$

$$cSi = -3.5532 + 0.146H_L - 4.927\cdot10^{-4}H_L^2 + 1.2305\cdot10^{-6}H_L^3 - 4.9421\cdot10^{-10}H_L^4 \quad \text{(Eq. 7)}$$

Procedure for non-boiling CSMs is relatively straight-forwarded. The point (A) represents a non-thermal, cold groundwater at its silica concentration and enthalpy, the fluid is expected to mix with. The point (B) is stated for the sampled thermal spring depart of (sub) boiling conditions. Straight line (A–B) drawn intercepts the silica (quartz or chalcedony) solubility curve at point (C). Vertical line onto X-axis gives the enthalpy of resultant member, forth read from steam tables at pure water vapor pressure. The same model gives an opportunity to check for possible reservoir boiling. Usual assumption expects the fluid to boil under atmospheric pressure that equals the enthalpy of H = 419 kJ·kg^{-1}. From that, vertical line along Y-axis intercepts the mixing (A–C) line at point (D). Contouring the horizontal line towards maximum steam loss curve gives the initial (intraformation) enthalpy of hot-water component (E), projected onto X-axis.

Reasonable result represents a reservoir temperature of parental thermal water before it has been mixed, so the horizontal line onto Y-axis gives initial reservoir silica concentration (Fournier, 1980a). For either case (no-boiling and boiling model), overestimation of derived initial reservoir temperatures is a hint on boiling prior mixing or silica addition after mixing. If lines do not intercept, it may be a consequence of cooling without silica deposition. Derived initial temperatures below the expected range give a vital sign on silica deposition prior isenthalpic mixing or steam loss (Truesdell and Fournier, 1977).

Application: shallow reservoir and discharge zone silica-enthalpy analysis

In this model, we accepted archive data (Appendix C) for DRTE because of no evidence on boiling/mixing correction necessity. Meanwhile, (Eq. 6) and (Eq. 7) were used to determine thermodynamic silica concentrations and temperatures in other zones, assuming isenthalpic mixing without boiling.

For DRTE, we calculated the reservoir enthalpy by REFPROP for pure water phase at atmospheric pressure, obtaining H_{res} = 336–355 kJ·kg^{-1}. For the SRTW, we pre-

ferred silica concentrations computed (Eq. 7) of $cSiO_2$ = 11–14 mg·l^{-1} under a mean enthalpy of H_{res} = 105–142 kJ·kg^{-1} to minimize effect of silica hydrolysis or deposition. Mixing line (Fig. 6) between both facies is given by their median enthalpy and concentration values. This yields the enthalpy of H_{res} = 580 kJ·kg^{-1}, equal to overestimated T = 138 °C. For the shallow reservoir (cold-water component), the temperature excision implies silica deposition in deeper parts of the horizon. Cooler subfacies against DRTE individually give the final temperature of T = 116 °C, thus the rate of silica inbalance decreases proportionally, as they compensate loss in SiO_2 by its hydrolysis from IWCP formations.

Similar principles were adapted to carry an analysis at the discharge zone facies. Samples of cold Sliače springs represent cold water component at sampled concentrations. VSH-1 represent a thermal water mixture, with concentrations ($cSiO_2$ = 12–13 mg·l^{-1}) and enthalpy (H_{res} = 163–176 kJ·kg^{-1}) substituted according to (Eq. 6) and (Eq. 7). After solubility line extrapolation, springs samples sit onto. Drawing a mixing line between springs and VSH-1 (Fig. 6) overestimates temperature (T = 70 °C) and enthalpy (H = 295 kJ·kg^{-1}). VSH-1 waters must be enriched with SiO_2 prior mixing with S-CGW. If mixing line is plotted between deep reservoir representative sample and VSH-1, the overestimate counts H = 555 kJ·kg^{-1} (or T = 133 °C). The yield is excessive because VSH-1 samples evidently loose some silica compared to deep reservoir they are expected to be relative with (Fig. 6).

Silica – carbonate mixing model (XSiCo)

Geofluids worldwide recorded strong correlation between total carbonate ($\sum CO_3$) and temperature, with most

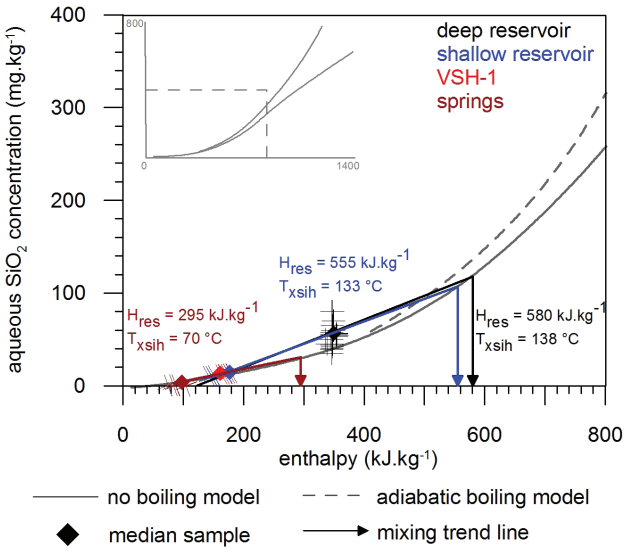

Fig. 6. Silica – enthalpy mixing model. Modified after Fournier and Truesdell (1974).

of it partitioned into CO_2 (Arnórsson et al., 1983). Amount of aqueous silica in a sample relates to solubility of its polymorphs at fixed temperatures (Fournier et al., 1974). Most of silica speciates into H_4SiO_4. The relation between CO_2 as total carbon, Ct, and SiO_2 in aqueous solution is, however, not linear. A model curve is obtained by plotting relative CO_2 (Eq. 8) and SiO_2 (Eq. 9) concentration at fixed T in Kelvin (Arnórsson, 1985).

$$SiO_2 = -15.433 - \frac{151\,.\,6}{T} - (2.977\,.\,10^{-6}T^2) + 5.464(\log T) \quad \text{(Eq. 8)}$$

$$CO_2 = -1.09 - \frac{3894.55}{T} + 2.532(\log T) \quad \text{(Eq. 9)}$$

Resultant concentrations are in logs of molality. Silica concentration may be optionally modified by the chalcedony geothermometers. Boiled waters plot above the line or tend to cross the curve. Non-boiling samples are usually positioned below the line. Unmixed fluids plot onto the curve or cluster close around. If fluid boils before sampling, the aqueous CO_2 level is depleted proportionally to produced vapor, whilst aqueous SiO_2 increases in residual fluid. Therefore, the CO_2/SiO_2 ratio drops. Dilution of the fluid without boiling retains CO_2 in a liquid phase causing CO_2/SiO_2 ratios high relative to parental conditions (Arnórsson, 1985). Overestimated temperatures are resultant to silica removal (deposition) after mixing due to a conductive cooling. Temperatures below reasonable range for parental (reservoir) fluid may be a sign of partial degassing after earlier dilution or mixing respectively (Nicholson, 2012).

Relation between CO_2 and SiO_2 aids solute geothermometry application. Besides interpretation of positions, the model is used as geoindicator, extending a trend line from provenienced populations to intercept the curve at point A. Drawing a line onto X-axis gives CO_2 content in a parental fluid. The initial silica concentration is obtained by projecting A onto Y-axis. This is correct only for a case where the supportive hints on mixing or boiling are present, as well as for a case where quartz controls the aqueous silica in the water. Temperature is given by substitution of yielded parental SiO_2 concentration into quartz geothermometer (Eq. 10) by Fournier and Potter (1982). In other cases, this procedure should not be used to estimate reservoir temperature, or the plot must be modified for the chalcedony geothermometers. Inserted concentrations (c) are in mg·kg^{-1}.

$$T(K) = -53.5 + 0.11236c - 0.5559.10^{-4}c^2 + 0.1772.10^{-7}c^3 + 88.39 \log c \quad \text{(Eq. 10)}$$

Application: discharge zone silica – total carbonate analysis

We used (Eq. 8–9) to draw the cross equilibrium function. The conversion of initial (mg·l^{-1}) into mass (ppm)

concentrations was carried in WATCH v.2.4 package that accounts for H_2CO_3 dissociation under given pH and temperature. The Sliače springs (S-CGW) are identified as cold water component ($cSiO_2$ = 56–128 ppm; cCO_2 = 79–1 830 ppm). Thermal waters of VSH-1 well represent a mixture ($cSiO_2$ = 44–53 ppm; cCO_2 = 230–867 ppm). Samples of ZGL and FGTB-1 wells stand for thermal end-member ($cSiO_2$ = 56–128 ppm; cCO_2 = 79–1 830 ppm). All facies were upscaled to representative values by median concentrations.

Facies plot in the non-boiling region, disproving any boiling in the structure. Deep reservoir samples organize along a logarithmic trend line (Fig. 7), similar to the equilibrium function by Arnórsson (1985), secluded deep within the non-boiling region because of the general lack in silica typical for carbonates. This evidences DRTE stability to dilution. Samples of VSH-1 must be distinguished into D-LTC (discharge zone – low total carbonate) and D-HTC (discharge zone – high total carbonate), as they plot discontinuously.

A mixing line is drawn between S-CGW and D-LTC, fairly striking DRTE median, implying some influential facial relation (Fig. 7). Extended mixing line intercepts the equilibrium curve at 521 ppm of SiO_2. Later, we substituted the inferred concentration into chalcedony conductive geothermometers (see App. A), obtaining a temperature of T = 190–205 °C, which is definitely an overestimate. Apparently, D-LTC loses CO_2 and SiO_2, compared to parental conditions by silica consumption into hydrolysis reactions and minor precipitation.

To explain the D-HTC population, we introduce a shallow reservoir (SRTW) facies ($cSiO_2$ = 16–48 ppm; cCO_2 = 110–1 090 ppm), that is, however, not a geothermal end-member. A line connecting the S-CGW and D-HTC facies intercepts a region of median shallow reservoir, but does never cut the XSiCo model (Fig. 7). Then, if there is some facies relation between the shallow reservoir and thermal waters, the D-HTC may originate by mixing with DRTE (increase in CO_2 and SiO_2), prior dilution by S-CGW (D-HTC → D-LTC), which would drop CO_2 instantaneously because of cooling.

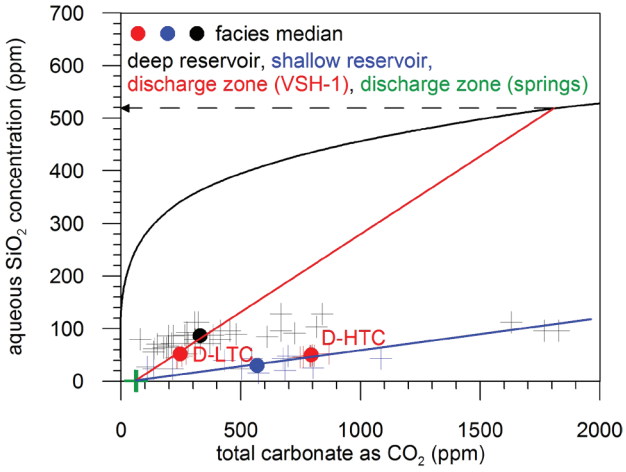

Fig. 7. Silica – total carbonate model. Equilibrium curve after Arnórsson et al. (1983).

Silica – enthalpy (no boiling) fraction model

Sampling and analysing geothermal springs is, by far, one of the easiest and cost-effective approaches in the early stages of geothermal field exploration. Warm springs or two-phase springs represent solid indices on underground geothermal reservoir and possible water evasion suffering some mixing with the shallow groundwater (early case) or degassing (latter case). Samples experiencing either of these, however, yield erroneous results (not only) for silica geothermometers application, except of those designed to correct estimates for boiling.

The fraction model based on enthalpy (Eq. 11) and mass balance (Eq. 12), developed by Fournier et al. (1974), is capable to infer the endmember temperature and a rate of parental chemistry modification by a dilution rate:

$$H_{gw} \cdot X + H_{tw} \cdot (1-X) = H_{spg} \qquad \text{(Eq. 11)}$$

and

$$CS_{gw} \cdot X + CS_{tw} \cdot (1-X) = CS_{spg} \qquad \text{(Eq. 12),}$$

where H is the enthalpy of components ($kJ \cdot kg^{-1}$), X is the cold water fraction in the spring, and CS stands for aqueous silica concentration ($mg \cdot l^{-1}$), with following subscripts: "gw" for (cold) groundwater, "tw" for modeled thermal water component and "spg" for springs.

The enthalpy remains conserved in the system, as the thermal spring heats the groundwater. Some silica deposition due to parental water cooling is, in some extension, balanced with the aqueous SiO_2 added by the groundwater. The model assumes a spring with parental thermal water component originated in homogeneous reservoir below or at sub-boiling conditions (Sheridan et al., 1980). The parental fluid wells up towards surface and is diluted by encountering shallow and cold groundwater, which fixes a steam phase in the liquid to form the warm or hot spring (Fournier et al., 1974).

Due to enthalpy conservation, the weighting factor for cold water component "X_H" is given by transcription of "X" in (Eq. 11) towards (Eq. 13), whilst silica weighting component "X_{CS}" (Eq. 14) is derived from "X" in (Eq. 12):

$$X_H = \frac{(H_{tw} - T_{spg})}{(H_{tw} - T_{gw})} \qquad \text{(Eq. 13)}$$

and

$$X_{cs} = \frac{(CS_{tw} - CS_{spg})}{(CS_{tw} - CS_{gw})} \quad \text{(Eq. 14)}$$

where enthalpy is in cal·g^{-1}, T is the temperature in °C and CS is in mg·l^{-1}.

A procedure is simple and straightforward. In a first, one must assume a reasonable temperature range for parental thermal water in natural, deep reservoir (origin) conditions. The X_H is calculated substituting variables into (Eq. 13) for every temperature, and plotted onto cross-diagram against temperature. Next step involves calculation of possible silica content (Sheridan et al., 1980) in unmixed and unboiled parental fluid per each designed temperature, here for a case a chalcedony controls the silica solubility in water (Eq. 15):

$$CS_{tw} = \frac{10^{\left[\frac{-1032}{t+273,15}\right]} - 0,09}{1665.10^{-5}} \quad \text{(Eq. 15)}$$

In following, the X_{CS} (Eq. 14) is determined for each silica content of parental fluid at each of fixed temperatures designed above, where the CS_{tw} is the only variable and CS_{spg} and CS_{gw} are constants. Next, the X_{CS} is plotted into the same graph as the X_H was in previous. Because of sensitivity to input data, a great certainty in representativity of a spring for thermal water is mandatory, requiring cross-correlation with other facial geochemical techniques.

Intersection projects a cold water fraction on the X and parental water temperature on the Y axis. Overestimate is then a hint on additional silica dissolution owing to a water-rock contact with glassy rocks or amorphous silica layers. If curves do not intercept, it is possible that the parental fluid lost steam before dilution (Fournier et al., 1974).

Application: deep reservoir fraction model analysis

Enthalpy of DRTE has been taken from REFPROP calculations, modified by a conversion factor of 0.239 to get a scale in cal·g^{-1}. While the mixture (VSH-1) was identified at T = 40 °C and $cSiO_2$ = 30 mg·l^{-1}, the cold water component attributes at T = 9 °C and $cSiO_2$ = 0.4 mg·l^{-1}. The chalcedony model (Eq. 15) represents the DRTE component in the mass balance. The model was scaled for T = 50–300 °C (Fig. 8).

Fraction functions (X_H, X_{CS}) intercept at T = 130 °C and X = 0.79. The temperature is supposed to correspond to that of deep reservoir, geothermal end-member composition, however, there is a distinct overestimation. Under given undisturbed parental (DRTE) conditions, the high temperature is a result of SiO_2 addings after mixing. Another explanation is cooling of VSH-1 waters with S-CGW. Both explanations are, in fact, reasonable under local conditions. This is, however, in confidence to XSih and XSiCo plots. Moreover, temperature overrate makes the coldwater fraction estimate (X = 79 %) excessive.

Cross-check for post-mixing silica addition by use of amorphous silica solubility (Eq. 16) is recommended if resultant temperatures are overestimated. In this case, the (Eq. 16) replaces (Eq. 15) for DRTE silica upscaling at external variables and enthalpy balance constant.

$$\log CS = -\frac{731}{t + 273.15} + 4.52 \quad \text{(Eq. 16)}$$

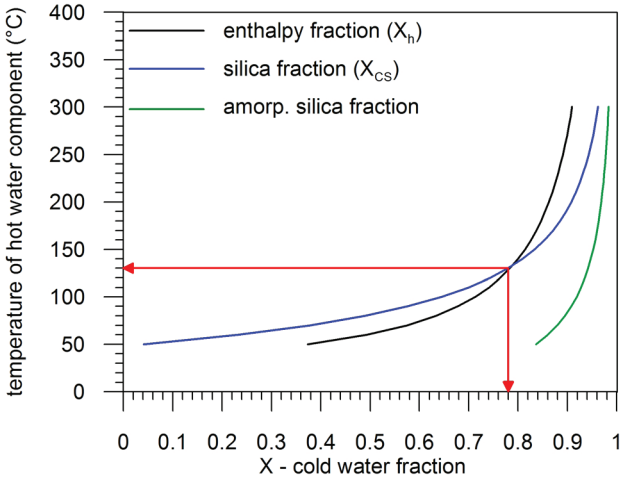

Fig. 8. Fraction model analysis.

At local conditions, the amorphous silica curve does not intercept the enthalpy function (Eq. 16). Therefore, silica addition is less probable after final mixing stage (see XSiCo model), and the temperature overestimate is rather resultant to cooling of VSH-1 wells subsequent to mixing with S-CGW and upflow.

Quantitative SiO_2 geothermometry application

Under known conception, the DRTE is expected to yield most precise results because of missing factors to modify reservoir geochemistry, although skewing by vertical reservoir filtration must be taken accounted. Chalcedony geothermometers (GSC1 – GSC4A) match best the expected deep reservoir temperature range (Fig. 9), varying the calculated temperature of T_{chalc} = 51–98 °C. This includes the chalcedony adiabatic boiling (Arnórsson et al., 1983) geothermometer too (GSC4A), which gives T_{chalc} = 62–97 °C. Yet this is a solid evidence of chalcedony control on aqueous SiO_2 concentrations in thermal waters.

The median of chalcedony conductive cooling equilibration $T_{chalc\text{-}m}$ = 74.8 °C increases to $T_{chalc\text{-}m}$ = 76.7 °C if adiabatic boiling model is included. Because of no boiling, this can be further neglected. Most of temperature estimates fall within the T_{chalc} = 75–85 °C interval. In general, temperatures given by chalcedony geothermometers are

greater than those by solubility analysis (Fig. 5), with median T_{chalc} = 67 °C. In essence, the difference is because of variable sensitivity of geothermometry functions to local SiO_2 content, which is generally less than that at moderate to high volcanic fields, which they were derived from.

Variation in temperature estimates is, however, not only a function of relative sensitivity of geothermometry functions to aqueous silica level. We rather adjust the variation in estimate and absolute concentrations to unstable contact of thermal waters with a silica source, regardless it is because of its various incorporation in hydrolysis reactions or due to vertical intraformation filtration induced by unbalanced reservoir base overheating. Either way, results oppose a statement by Bodiš and Borosová (1996) on chalcedony geothermometry inadequacy. Instead of comparing results to the wellhead temperature, temperatures must be referenced to deep bottomhole (reservoir) conditions, as this is the environment where the equilibration is, due to principles of geothermometry, supposed to take place.

Both, the shallow reservoir and the discharge zone represent not an end-member but a mixture. In shallow reservoir, any silica geothermometry must simply account on two subfacies, different in the depth and silica content. The deeper subfacies (BEH-1) lacks silica, because of its deposition or consumption, after the parental, DRTE waters evade vertically the reservoir. The subfacies in shallower positions (FBe-1) are comparatively enriched with silica by its low grade (low temperature) dissociation from the IWCP and recharge. Because of numerical confidence (see Appendix D), there may be some re-equilibration with chalcedony within the formation.

For the discharge zone, inferred temperatures are lower than those expected at shallow parts of deep reservoir, where we set a parental fluid origination prior lateral leaking. Temperature estimates (Appendix D) may then point to temperature of chalcedony last equilibration during propagation towards discharge zone, or are simply skewed by multiple mixing episodes prior sampling. Because of mixture character, we would rather prefer the second scenario, and do not recommend to use quantitative silica geothermometry to either of these.

CATION GEOTHERMOMETRY

Cation geothermometers refer to numerous ion-exchange reactions, mostly partitioning of alkalis, of various temperature dependent equilibrium constants (Fournier, 1989). This is because e.g. sulphates and carbonates adjust to changes in physical or chemical environment much faster, and so they equilibrate with the system rapidly, whilst Na^+, K^+ or Li^{2+} silicates (i.e. tectosilicates, feldspars or micas) do so slowly even at high temperatures (Giggenbach, 1981). In other words, equilibrium preservation is more likely a case of alkali system rather than those of carbonates. Obtaining about the same results applying various cation geothermometers for a same sample at the same time is, thus, fairly rare (Fournier, 1989).

Complex mineral assemblages attain fluid–rock equilibrium rarely, as complete isochemical recrystallization of a primary rock matrix to a thermodynamically stable alteration assemblage is likely to take part in stagnant systems of an infinite age (Giggenbach, 1968; Ellis, 1970) only.

Obligatory "sufficient source" condition, especially for alkalis, fits for magmatic systems. Quantifying application of alkali geothermometers to carbonate systems often suffers from a lack of a source within reservoir and unstable water–source contact. If not for a temperature estimation, the Na-K-Mg and K-Mg-Ca thermodynamic subsystems are, at least, effective in analysis of reservoir maturity and reservoir dynamics at a site (Giggenbach, 1981).

Alteration and equilibration

A knowledge on controlling alteration assemblage is one of mandatories necessary to get a gain prior applying cation geothermometry. Most of alteration systems relate to Na-K and K-Mg alteration (thermodynamic) pairs at a base of alteration and partitioning of silicates.

Na/K geothermometry

The recalled Na/K geothermometers (Appendix B) are based on partitioning of Na^+ and K^+ between alumno-

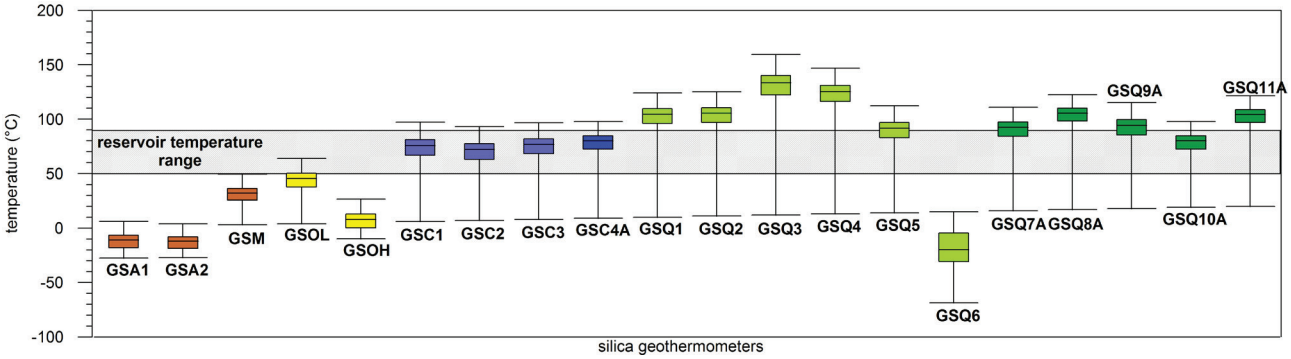

Fig. 9. Silica geothermometry results distribution: deep reservoir. See Appendix A for symbols and references.

silicates (feldspars) and water (Eq. 17), with temperature dependent equilibrium constant (Eq. 18) in control of the process (Fournier, 1979):

$$Albite + K = Adularia + Na \rightarrow NaAlSi_3O_8 + K^+ = KAlSi_3O_8 + Na^+ \quad \text{(Eq. 17)}$$

$$K_{eq} = \frac{[KAlSi_3O_8]\,[Na^+]}{[NaAlSi_3O_8]\,[K^+]} \quad \text{(Eq. 18)}$$

The equilibrium constant (Eq. 18) assumes unity in reaction activities, that means reactants are pure end-members, thus activities of dissolved species are about equal to their molar concentrations (Truesdell, 1976). Then, for dilute solutions, the (Eq. 18) transforms to (Eq. 19), where Na^+ and K^+ are in desired units.

$$K_{eq} = \frac{Na}{K} \quad \text{(Eq. 19)}$$

Also, for many geothermal systems, not only feldspars participate in cation exchange equilibrium reactions involving Na^+ and K^+, but e.g. montmorillonites may do so (Eq. 20–21). Equilibrium constant for the reaction equals the Na/K ratio (Eq. 19), however, the aqueous Na/K ratio resultant to a cation exchange reaction at a given temperature controlled just by montmorillonites fairly differs to that controlled by alkali feldspars (Fournier, 1989).

$$Na^+ - montmorillonite + K^+ = K^+ - montmorillonite + Na^+ \quad \text{(Eq. 20)}$$

$$Na_{0.33}Al_2(Al_{0.33}Si_{3.67}O_{10})(OH_2) + 0.33K^+ = K_{0.33}Al_2(Al_{0.33}Si_{3.67}O_{10})(OH_2) + 0.33Na^+ \quad \text{(Eq. 21)}$$

After Fournier (1989b) albite may not be present at low enthalpies, and the Na/K exchange reaction is controlled by adularia – sodic clay – silica and hydrogen system (Eq. 22), equilibrated at (Eq. 23)

$$3Na - montmorillonite + 7K^+ + 10SiO_2 = 7K - feldspar + Na^+ + 6H^+ \quad \text{(Eq. 22)}$$

$$K_{eq} = \frac{[Na^+]\,[H^+]^6}{[K^+]^7} \rightarrow \log K_{eq} = \log[Na/K] - 6\log[K/H] \quad \text{(Eq. 23)}$$

Numerous other reactions contribute in geothermal systems at various temperatures, either involving water and equilibrium reactions with hydrogen or not. The variation in Na/K and suites controlling the Na/K ratios reasoned a range of empirically derived Na/K geothermometers (i.e. Truesdell, 1976; Tonani, 1980; Arnórsson et al., 1983; Fournier, 1979; Nieva and Nieva, 1987; Giggenbach, 1986; Giggenbach, 1988; Verma and Santoyo, 1997; Simmons, 2013), thereupon precision of temperature estimation applying these depends on involved mineral assemblage and structural states of solids in local conditions (Fournier, 1980). Possibly, the Na/K equilibration may not be reached at T < 100 °C, as well as micas and zeolites may control the Na/K exchange, or the Na^+ and K^+ participation is rather a consequence of preferential cation leaching than exchange reactions (Fournier, 1979).

There is no universal Na/K geothermometer as one may give a correct estimation in one place and an erroneous temperature in another (Fournier, 1989), thus the use of Na/K geothermometry should be grounded by cautious mineral assemblage analysis.

The Na/K geothermometer re-equilibrates slowly in comparison to others at T < 350 °C, thereby it is less sensitive to dilution (dilutant is expected to have lower Na^+ and K^+ concentrations than the parental fluid) providing an ability to evaluate deeper parts of the high enthalpy systems (Fournier, 1980) by conservation of absolute concentrations at thermodynamic conditions the other models would fail in (Davraz, 2014). Thus it yields highest temperature estimates. Unfortunately, the highest temperature is not necessarily the correct temperature of equilibration, nor a reservoir temperature. Indeed, thermal waters may invade shallow reservoir zones prior upwelling and targeted aquifer may then be of lower temperature that the Na/K geothermometer may not recognize.

Cation geothermometers work best for reservoir fluids of T_{res} > 150 °C (Nicholson, 2012). The necessary cation exchange equilibrium state is scarcely reached at T_{res} < 100 °C, and Na^+ and K^+ are rather resultant to Na^+ and K^+ leaching instead. Yet caution must be paid for carbonate reservoirs (rich in CO_2^- which transforms Na-silicates), and waters originated in organic sediments rich in NH_4^- (Fournier, 1980b).

Graphical tests for Na/K geothermometry application and interpretation are carried by conclusious cross charts (Fournier, 1980b; Marini, 2004) plotting a relative Na/K ratio over a reciprocal of absolute temperature, either to correlate the aqueous Na^+ and K^+ concentrations with a particular mineral assemblage and/or inspection of chemistry formation processes; or to correlate the ratios to particular equilibrations. Reservoir chemistry and dynamics are accessible for evaluation regarding position and spatial organization of samples within one or more systems (i.e. stratified reservoirs with mixing, conceptual fluid flow etc.).

Application: Na/K alteration system analysis

All facies suffer a lack of alkalis (Fig. 10), decreasing the Na/K ratio with temperature. Position of facies is far of any equilibration, whether for low (LT albite – microcline) or high (albite – adularia) enthalpy assemblage. Equilibrium pairs (Eq. 17–23) are not valid in local conditions. The inequilibration results then in temperature overestimates (see Appendix D).

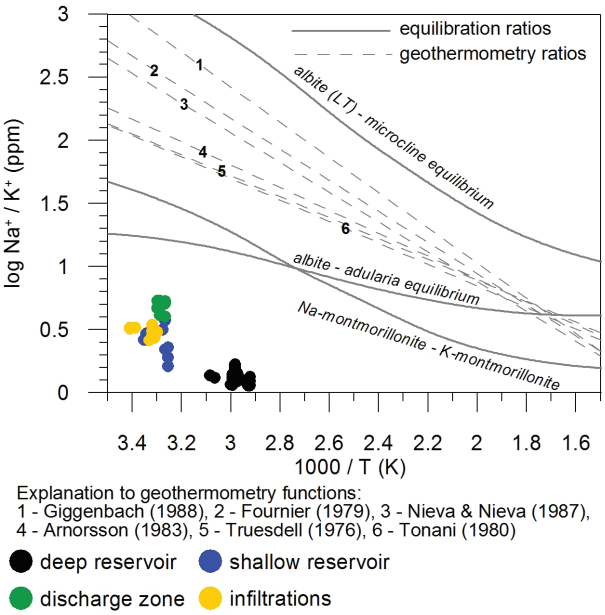

Fig. 10. Equilibrium ratios with Na-K system.

Inequilibration in deep reservoir is due to rock dissolution in control of Na/K ratio, suffering to insufficient source in carbonates and excess CO_2 which switches activities of Na-silicates to K-micas (Fig. 11). While rock dissolution controls alkali chemistry for DRTE originated subfacies in the shallow reservoir (slightly increasing Na/K due to drop in CO_2 by deposition of carbonates), subfacies recognized as recharged record preferential Na^+ and K^+ leaching from IWCP in a downflow regime. This is well correlated with records from many recharge waters (e.g. Marini). Preferential leaching inferred for VSH-1 samples is rather due to enrichment of DRTE evasions with SRTW rich in Na^+, later enriched with Na^+ added by dilution of a mixture with cold groundwater (S-CGW) or from a wallrock acquire.

K/Mg geothermometry

Dynamic systems rarely attain overall equilibrium because of much faster reaction velocity for a thermodynamic system involving Mg^{2+} than that for Na^+ and/or K^+ (Giggenbach, 1984). The velocity is buffered by conductive cooling of ascending thermal waters retaining high CO_2 and low pH. Drop in CO_2 and increase in pH under steam loss restricts reactivity of thermal waters in a consequence (D'Amore and Arnórsson, 2000). Except of carbonatogene facies, geothermal waters are usually low in Mg^{2+} thus even its little addition alters the concentration and changes equilibration immediately.

Empirical basis (Giggenbach et al., 1983) assumes equilibration of the fluid with the K-feldspar (adularia), K-mica (illite and muscovite), Mg-bearing silicate (chlorite, clinochlore) and chalcedony assemblage (Eq. 24–25) described at equilibrium activity (Eq. 26–27):

$$0.8muscovite + 0.2clinochlore + 5.4SiO_2 + 2Na^+ \leftrightarrow 2albite + 0.8K-feldspar + 1.6H_2O + Mg^{2+} \quad \text{(Eq. 24)}$$

respectively:

$$0.8muscovite + 0.2clinochlore + 5.4SiO_2 + 2K^+ \leftrightarrow 2.8K-feldspar + 1.6H_2O + Mg^{2+} \quad \text{Eq. 25)}$$

with equilibrium constant for Eq. 24 is:

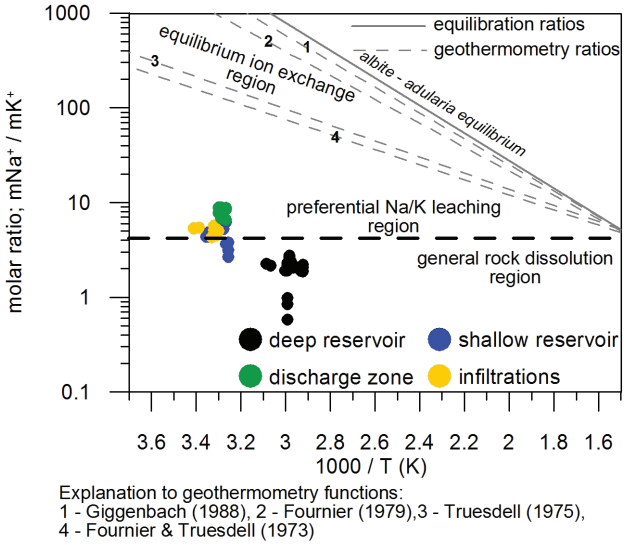

Fig. 11. Na-K system analysis: equilibration processes.

$$K_{eq} = \left[\frac{[Mg^{2+}]}{[Na^+]^2}\right]\left[\frac{[albite]^2[K-feldspar]^{0,8}}{[mus\ \mathrm{cov}\ ite]^{0,8}[clinochlore]^{0,2}}\right] \quad \text{(Eq. 26)}$$

meanwhile the latter equilibration reaction follows:

$$K_{eq} = \left[\frac{[Mg^{2+}]}{[K^+]^2}\right]\left[\frac{[K-feldspar]^{2,5}}{[mus\ \mathrm{cov}\ ite]^{0,5}.\ [clinochlore]^{0,2}}\right] \quad \text{(Eq. 27)}$$

These reactions are typical for magmatic environment or can stand sufficiently impure carbonates. Progressive water-rock interaction towards equilibrium to the Na/K system increases K/Mg ratio rapidly as the Mg^{2+} incorporates into magnesium alkalis, such as chlorite (Nicholson, 2012). Alkali alterations (Eq. 24–27) are questionable in low enthalpy sedimentary aquifers, including evaporates, siliciclastics or carbonates, as source of K^+ and Mg^{2+} is rather in dolomite or seawater brine leaching instead (Sonney and Vuataz, 2010).

Likely alteration for impure carbonate environment (Eq. 28) accounts for plagioclase/clay–calcite alteration assemblage (Giggenbach, 1981):

$$X{\cdot}microcline + 2{\cdot}epidote_{(LT)} + Y{\cdot}calcite + (4+Y){\cdot}CO_2 + 2{\cdot}H_2O \leftrightarrow X{\cdot}muscovite + (4+Y){\cdot}calcite + 6{\cdot}SiO_2 \quad \text{(Eq. 28)}$$

Graphical tests for Mg/Na and Mg/K equilibration are applied to inspect for overall equilibration to both thermodynamic subsystems (discussed below) and overall equilibration or chemistry formation.

Development of K-Mg geothermometer allowed its comparison to the silica thermodynamic system as both are relatively sensitive to fluid dynamics. Their comparable adaptation to new thermodynamic conditions (dilution, mixing, boiling) helps identifying causes of deviation in equilibrium for particular samples or populations. The chart plots equilibrium silica concentration (Eq. 29; Giggenbach et al., 1994) to the K-Mg equilibrium function (Eq. 30), that is, practically, the K-Mg geothermometer by (Giggenbach, 1988).

$$\log(cSiO_2) = 4.55 - \frac{1\,000}{T + 273.15} \qquad \text{(Eq. 29)}$$

where silica concentration is in mg·kg^{-1} and temperature is in °C; and

$$T_{KMg}\,(°C) = \frac{4\,410}{14 - \log\left(\frac{K2}{Mg}\right)} - 273.15 \qquad \text{(Eq. 30)}$$

where K^+ and Mg^{2+} concentrations are in mg·kg^{-1} and temperature is in °C.

Possible inspection on increase in aqueous concentrations in fluids due to partial or maximum steam loss is grounded by enthalpy and mass balance (Giggenbach et al., 1994), which gives correction functions for silica (Eq. 31) and K-Mg geothermometer (Eq. 32):

$$\log(cSiO_2)_b = 5.12 - \frac{1\,215}{T + 273.15} \qquad \text{(Eq. 31)}$$

and

$$\log(cK^2 / cMg)_b = 14.6 - \frac{4\,630}{T + 273.15} \qquad \text{(Eq. 32)}$$

where all concentrations are in mg·kg^{-1} and temperature is in °C.

The K-Mg geothermometer (Appendix B) is the fastest to adapt for Mg^{2+} dynamics quickly responding to re-equilibration. Because of that, the K-Mg geothermometer gives lowest temperature estimates (Giggenbach, 1988), most probably that of last equilibration. For barely real no mixing conditions, the K-Mg geothermometer yields temperature at shallowest reservoir zones. Consistency between K-Mg and silica geothermometers but overestimates for other cation geothermometers is most probably due to short residency and partial equilibration of water-rock system with most reactive phases only (Fournier, 1989).

Application: K-Mg alteration system analysis

Position of facies scatters between the rock dissolution and preferential leaching region (Fig. 12). Facies of DRTE are high in Mg/K ratio, because of poor K^+ but Mg^{2+} rich reservoir environment. Excess Mg^{2+} decreases estimated temperature ($T_{Mg/K} \approx 42–55$ °C) below T_{samp}, disqualifying equilibrium reactions in the microcline – muscovite system (Eq. 24–25).

The residential subfacies of the shallow reservoir dissolve K^+ during downflow off the IWCP horizon, implied by comparison to recharge samples and a region they plot within. Thermal waters derived of DRTE in deeper positions are still affine to parental conditions. Given ionic ratio infers $T_{Mg/K} \approx 38–42$ °C, which may be a temperature of last equilibration to silica (chalcedony) and dolomite system along with talc activation along an upflow ($T_{Mg/K} > T_{samp}$). Yet the temperature must be underestimated because SRTW facies intakes Mg^{2+} lost by Mc-calcite precipitation and talc activity. Samples of the VSH-1 plot well along a muscovite stability line, equilibrated at $T_{Mg/K} \approx 59–63$ °C. The temperature corresponds to upper (evasion) zones of the deep reservoir. Yet the stability accounts rather activation of talk and consumption of Mg^{2+}. The increased K^+ is preferentially a sign of its leaching controlled by IWCP hosted S-CGW and preservation, compared to SRTW (Fig. 12).

In fact, thermal waters attain equilibrium to illite and talc rather, varying dolomite and calcite saturation of during upflow/upwell regime. Then, equilibrium reactions given by K/Mg geothermometry (Eq. 24–28) are not valid at local conditions.

Application: Mg-SiO_2 alteration system analysis

We used the chalcedony (Arnórsson et al., 1983), conductive quartz (Eq. 29) and adiabatic quartz (Giggenbach et al., 1994; Eq. 31) models plotted against conductive cooling (Eq. 30) K-Mg geothermometer.

Because of high Mg/K ratio and variable SiO_2 absolute concentrations, DRTE facies tend to organize towards amorphous silica corner at $T_{SiO_2} \approx 50–90$ °C and $T_{Mg/K} \approx 30–70$ °C. At relatively stable (low) K^+ concentration, the scattering in temperature estimate reflects various Mg^{2+} level, because of change in saturation states of dissolved dolomite and, most probably, because of different dolomite dissolution intensity with vertical filtration. A trend towards amorphous silica is a sign of short reservoir residency. Somewhat reliable temperature estimations give a sign of equilibration with chalcedony, thus Mg^{2+} can either be consumed to activate a talc formation variably.

The SRTW population does not equilibrate to Mg-SiO_2 pair as any component yields reliable results. Inconsistency in a plot is (Fig. 13) evidence of mixed origin. Both

subfacies are undersaturated to chalcedony, which either precipitates or is consumed in dissociation of alkalis or talc activation. The same may be concluded for K/Mg variation, as K^+ enrichment is of low scale only. Discharge facies record more reliable conditions to quartz ($T_{SiO_2} \approx$ 55 °C) rather than chalcedony ($T_{SiO_2} \approx 30$ °C), yet overestimating the K/Mg temperature ($T_{Mg/K} \approx 60$ °C). The first is explained by only partial SiO_2 replacement by mixing. Again, high Mg^{2+} content gives more evidence on enrichment by dilution of a mixture with S-CGW, realizing in greater intensity than some K^+ leaching from IWCP or Jr/Cr2 horizon before sampling.

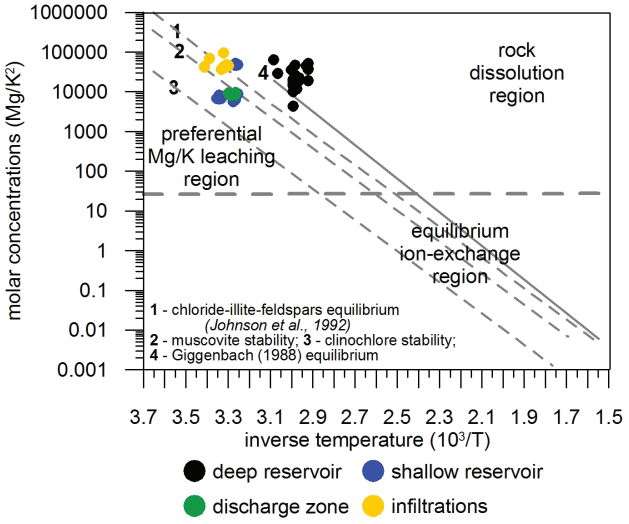

Fig. 12. K-Mg system chemistry forming processes.

Associated thermal waters, regardless of a facies position, are definitely not equilibrated with the Mg-SiO_2 system, forth they can not be considered equilibrated to Na^-, K^-, and Mg-alkalis. Besides calcite, the inequilibration is controlled by saturation of dolomite at deep reservoir conditions and variation in free Mg^{2+} and CO_2 controlling talc activity and Na-silicates modification to K-silicates.

Na-K-Ca geothermometer

The Na/K geothermometer gives poor precision for low temperature ($T_{res} < 150$ °C) geothermal waters rich in Ca^{2+} and aggressive CO_2. The amount of dissolved carbon dioxide in a geofluid is controlled by dissolution of calcite bearing carbonates or silicates, pH, T and CO_2 fugacity.

In these, the amount of Na^+ and K^+ is not controlled by alkalis saturation. Linearity in ionic ratios (Ca/Na, Ca/K, Na/K) over inverse of temperature at HT fields contrast to its scattering, observed in LT systems, has been referred as to Ca^{2+} entering silicate reactions (Eq. 33), thus influencing aqueous Na^+ and K^+, if equilibrated (Eq. 34) under the same assumptions as above (Fournier and Truesdell, 1973). As the absolute K^+ concentration in water is much less than that of Na^+, the change in K^+ is more evident than for the Na^+ in response to change in Ca^+ (Fournier, 1989), so the aqueous K^+ changes as so as the Ca/Na ratio satisfies (Eq. 34)

$$K^+ + Na_xCa_x - plagioclase + 4ySiO_2 = K - feldspar + xNa^+ + yCa^{2+} \quad \text{(Eq. 33)}$$

$$K_{eq} = \frac{Na^{(1-2y)} \cdot Ca^x}{K} \quad \text{(Eq. 34)}$$

where coefficients "y" and "x" represent a stoichiometry of particular reactions.

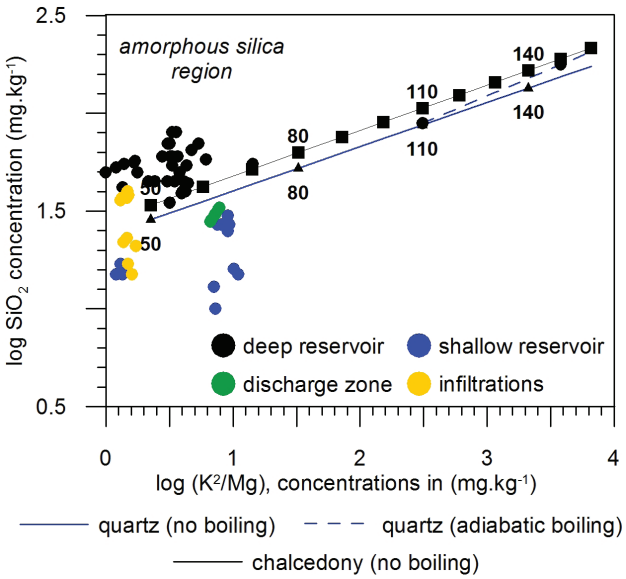

Fig. 13. K-Mg system chemistry forming processes.

Three Na-K-Ca system reaction configurations (Eq. 35–37) are usually observed, with unifying equilibration constant (Eq. 38)

$$(x + 2y)K^+ + solid = xNa^+ + yCa^{2+} + solid \quad \text{(Eq. 35)}$$

$$(2y - x)K^+ + xNa^+ + solid = yCa^{2+} + solid \quad \text{(Eq. 36)}$$

$$(x - 2y)K^+ + yCa^{2+} + solid = xNa^+ + solid \quad \text{(Eq. 37)}$$

$$\log K_{eq} = \log \frac{Na}{K} + \beta \log \frac{\sqrt{Ca}}{Na} \quad \text{(Eq. 38)}$$

where "solid" denotes the silica or alumosilicate respectively and "beta – β" depends on stoichiometry of particular reactions (Fournier and Truesdell, 1973).

To satisfy (Eq. 38), not only the excess silica must be present. Aluminum conservation in solids is rather accepted as

neglecting Al^{3+} contents in geothermal waters compared to other constituents, causing equality in deposition and dissociation of hydroxyle minerals so they cancel out of the equation (Fournier and Truesdell, 1973).

For the low temperature (T_{res} < 100 °C) systems, the β = 4/3 for the net reaction (Eq. 39), whilst for the high temperature waters the net reaction of base exchange transforms to (Eq. 40) and the stoichiometry derived parameter turns β = 1/3 (Fournier, 1989), except for waters of T_{res} < 100 °C where log √Ca/Na < 0 for which β = 1/3 (Fournier and Truesdell, 1973).

$$K^+ + \left(\frac{1}{3}\right) Na^+ + Ca_{\frac{2}{3}} - solid = \frac{2}{3} Ca^{2+} + K_{\frac{1}{1}} Na_{\frac{1}{3}} - solid \quad \text{(Eq. 39)}$$

$$K^+ + Na_{\frac{2}{3}} Ca_{\frac{1}{6}} - solid = \left(\frac{1}{6}\right) Ca^{2+} + \left(\frac{2}{3}\right) Na^+ + K - solid \quad \text{(Eq. 40)}$$

Both models account micas, silicates or clays to fix the aqueous Na-K-Ca system (Shikanozo, 1976). The Na-K-Ca geothermometer (see Appendix B) fits well for thermal waters of various temperatures rich in Ca^{2+}, fixing disregarding activities of Ca-silicates (Fournier and Truesdell, 1973).

Carbonate reservoirs usually lack any relation between actual temperature and cation chemistry of associated waters (Giordano and Swanberg, 1978). Most accurate temperature estimations are obtained for T_{res} > 200 °C. Erratic results are frequent for low temperature waters of T_{res} < 75 °C and fluids with partial pressure of $CO_2 > 10^{-4}$ atm (Pačes, 1975).

Cooler environments (evidenced by petrifying springs) are high in pCO_2 so the pH is controlled by carbonate equilibria rather than by exchange reactions of silicates (Fournier, 1989), thereupon the Na-K-Ca geothermometer scores only if calcite was not deposited after reservoir evasion. In fact, most of thermal waters in carbonate reservoirs are oversaturated to calcium carbonates, influencing their precipitation tendency. Thus the Na-K-Ca geothermometer overestimates reservoir temperatures (Fournier and Truesdell, 1973).

Either dilute (Na)-HCO_3 dominated waters rich in CO_2 are sensitive to Na-K-Ca equilibration (Eq. 39–40). In these, plagioclase likely converts to clay (kaolinite), modifying aqueous pH. Such a process involves interactions with additional Mg^{2+} or Al^{3+}. Typical underestimates are gained so for waters low in Ca^{2+} content and slow evasion velocities, within which a fluid–mineral system is able to react with a wallrock and re-equilibrate. The CO_2 rich springs, if boiled or cooled continuously, yield erratically high estimates owing to intense $CaCO_3$ deposition and slow Na/K reactions. Mixing has a little effect upon Na/K ratios and precision onto Na-K-Ca geothermometer if the difference in Ca^{2+} concentration is small. If the calcium rich water is diluted, the contact changes the final calcium content for fair (Fournier and Truesdell, 1973). Still, effect onto Na-K-Ca temperature prediction is negligible unless the parental thermal water component is reduced to less than 30 % (Fournier and Truesdell, 1974).

Mg-correction for Na-K-Ca geothermometer

The Na-K-Ca geothermometer routinely fails in temperature estimation for waters rich in Mg^{2+}. Elevated aqueous Mg^{2+} is expected to originate by dilution, easy uptake of Mg^{2+} out of the wallrock (e.g. chlorite, montmorillonite, dolomite, Mg-calcite) and, for coastal systems, by invasion of a seawater into reservoir (Fournier and Potter, 1978).

In fact, the more the sample deviates from the Na-K-Ca equilibration and purity conditions, the less precise is the $T_{Na\text{-}K\text{-}Ca}$ estimate, and the more is the water excess in Mg^{2+}. The magnesium proportion in equivalents is defined by (Eq. 41):

$$R = \frac{100\, Mg}{(Mg + Ca + K)} \quad \text{(Eq. 41)}$$

The empirical correction assumes thermal waters of R > 50 equilibrated at formation temperatures regardless of $T_{Na\text{-}K\text{-}Ca}$ estimate, or assumes their complex unequilibration (Fournier and Potter, 1978). Variation in Mg^{2+} and deviation in functional continuity pronounced mathematical corrections for samples at 5 < R < 50 (Eq. 42) and R < 5 (Eq. 43) to determine the temperature of magnesium correction Δt_{Mg} (Fournier and Potter, 1979).

$$\Delta t_{Mg}(°C) = 10.66 - 4.7415\log(R) + 325.87[\log(R)]^2 - 1.032\,\frac{10^5[\log(R)]^2}{T} \quad \text{(Eq. 42)}$$

$$\Delta t_{Mg}(°C) = 1.03 + 59.97[\log(R)] + 145.05[\log(R)]^2 - 36711\frac{[\log(R)]^2}{T} - 1.67\,\frac{10^7[\log(R)]}{T^2} \quad \text{(Eq. 43)}$$

where T is the $T_{Na\text{-}K\text{-}Ca}$ in Kelvins (Fournier and Potter, 1979).

The graphical technique (Fig. 14) is presentation of (Eq. 42–43). The X axis represents the $T_{Na\text{-}K\text{-}Ca}$ calculated temperature in degrees of Celsius, whilst the Y axis plots desired Δt_{Mg}. Solid curvatures represent the calculated proportion (R) of Mg^{2+} in the sample (Eq. 41). The correction temperature is obtained drawing a vertical line from the X axis at calculated $T_{Na\text{-}K\text{-}Ca}$ temperature to intercept the appropriate R function, with later projection of horizontal line onto the Y axis. Each correction must, however, match (Eq. 44):

$$T_{Na\text{-}K\text{-}Ca(C)} = T_{Na\text{-}K\text{-}Ca} - \Delta t_{Mg} \quad \text{(Eq. 44)}$$

where temperatures are in °C (Fournier, 1980b).

The empirical correction does not account on structural characteristics of reactants and complexing of dissolved solids,

thus it is not based on particular activity coefficients or reaction stoichiometry (Fournier and Potter, 1979). Overestimation preservation after correction is a solid hint on secondary enrichment in Mg^{2+} (usually by dilution).

Lithium geothermometry review

Lithium geothermometers, i.e. Na/Li and Mg/Li (see Appendix B) are the least used in analyses. This is because: (a) there is no immediate geochemical reaction that grounds the relationship between Na^+/Li^+ or Mg^{2+}/Li^+; (b) any explicit equilibrium alteration between Na^+ and Li^+ has been proven; (c) both geothermometers appear sensitive to host rock, thus application may be fairly limited by initial lithium concentrations. Best results for both are obtained in sedimentary reservoirs rich in magmatic clasts (Nicholson, 2012). The general relation of Li^{2+} involvement (Eq. 45) rewritten to (Eq. 46) obviously realizes in deeper parts of geothermal systems (Marini, 2004), still, there is a question of contribution of lithium pure end-member silicates (Sanjuan et al., 2003).

$$Li - clay + H^+ \leftrightarrow H - clay + Li^+ \qquad \text{(Eq. 45)}$$

$$albite + K - feldspar + 2kaolinite + Li^+ \leftrightarrow muscovite + Li - mica + 4SiO_2 + 2H_2O + Na^+ \qquad \text{(Eq. 46)}$$

Li^{2+} is less reactive compared to Mg^{2+}, Ca^{2+}, Na^+ or K^+, thus comparison of Na/Li and Mg/Li ratios between springs and borehole samples may give a solid note on upflow velocity (D'Amore and Arnórsson, 2000).

Application: Summary on alkali alteration

The recharges originate by infiltration at various altitudes in the Kľačianka valley area. Because of primary dissolution of carbonates, CO_2 concentration increases with sink and temperature. At this conditions, LT albite dissolved in a downflow off the IWCP and the Tr3–Cr2 formation transforms to K-micas, i.e. muscovite, even hypothetical, activates just before recharges enter deep reservoir. The oscillation in Ca/Mg, Mg/Na and Mg/SiO_2 recorded for DRTE supports assumption on vertical reservoir filtration within deep reservoir, varying CO_2 level by saturation regime of carbonates and, possibly, LT talc. Upflow regime consumes CO_2 and increases pH stabilizing Na-silicates partially by reduction of activities (not necessarily oversaturating) of illite and muscovite (Figs. 15 and 24), whilst onset of talc activity. Yet chalcedony turns oversaturated (Fig. 5), thus available for LT initial and weak metamorphosis of impure reservoir dolomites (at least at a scale of thermodynamic activities).

The rate of CO_2 consumption increases during evasion towards the shallow reservoir as calcite and Mg-calcite precipitate partially, simultaneous with preferential leaching of Na^+ from Tr3–Cr2 formations, that takes up more aqueous SiO_2 from solution before inflow. Shallow recharges attain higher K/Na ratio by dissolution of dolomite impurities and hydrolysis of IWCP formations. The SRTW facies is then formed by mixing of both, destroying partial equilibration. The rate of inequilibration is somewhat lower towards the Sliače discharge zone. The Na/K increases simultaneously due to preferential Na^+ leaching during transition, answering to drop in CO_2 by preferential calcite deposition. Still, the K^+ is higher compared to DRTE. Alkali source is then not only in rock dissolution, but mixing with SRTW facies. Increase in Mg^{2+} instead of its consumption by Mg-calcite deposition and talc activation is a sign of secondary enrichment by dilution with S-CGW.

Definitely, numerical application of Na-K-Ca geothermometer (Appendix D) disqualifies any equilibration with the Na-K-Ca thermodynamic subsystem. Let all the facies originate in carbonates and form a chemistry by leaching of carbonates in major. Any reactions towards equilibrium

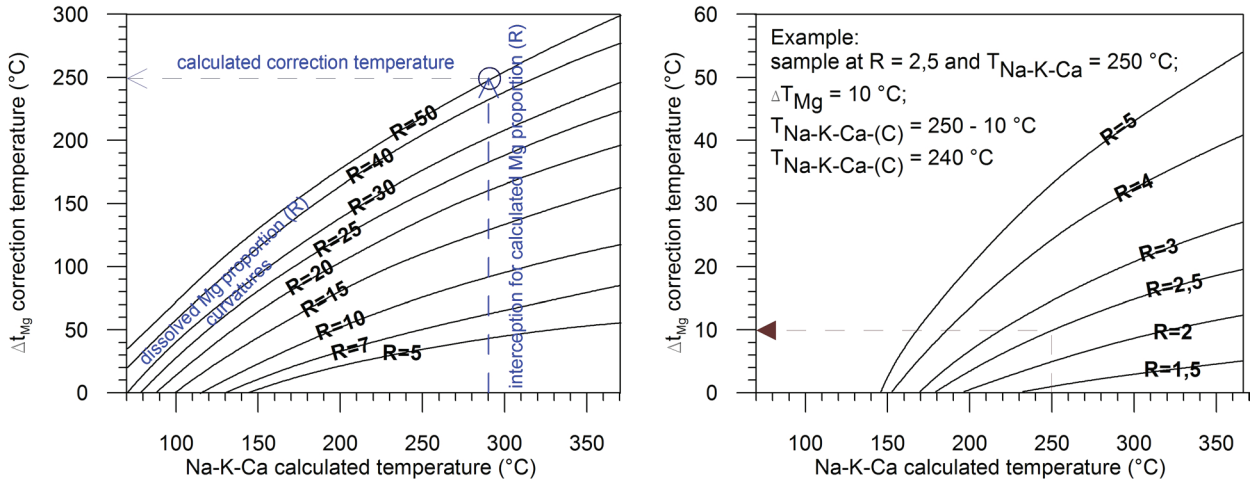

Fig. 14. Mg-correction derivation for $T_{Na\text{-}K\text{-}Ca}$ at 5 < R < 50 (left) and R < 5 (right).

with Ca-silicates are continuously destructed by excess CO_2.

Hydrochemical and thermodynamic maturity

In geochemistry of thermal waters, the maturity is understood as a quality referring to reservoir residency analysis and flow history (Giggenbach and Goguel, 1989); or equilibration to Na-K-Mg and Na-K-Ca subsystems (Giggenbach, 1981).

Equilibration to Na-K-Mg-Ca thermodynamic system and CO_2 is objective for cation geothermometry results reliability. This is because cation geothermometers are based on ionic ratios or stoichiometry derivation resultant to partitioning of alkalis (Fournier, 1989), with less focus on other (such as carbonate) systems. Inequilibration causes temperature estimation failure. In other words, immaturity prompts for precise interpretation of given results and allows detailed look on conceptual history and model of sampled waters.

Na-K-Mg subsystem

The Na-K-Mg subsystem composes of three thermodynamic pairs different in equilibration departure velocity and sensitivity to external dynamics (Fournier, 1982). The Na-K pair conserves primary equilibration well, whereas the K-Mg system re-equilibrates, for example by cooling, fast. The Na-Mg pair is of a robust response to any dynamics, pronounced in absence of Na-silicates to control the Na-Mg relation at LT conditions. Facies relation to all is usually inspected with the self-policing Na-K-Mg geoindicator (Giggenbach, 1988).

Use of tri-linear plots with absolute values upscaled and/or normalized to relative governs simultaneous correlation. To facilitate practical application, the concentration is scaled for $mg \cdot kg^{-1}$, whilst axes are normalized to accommodate geothermal waters of whatever geothermal system. Straight lines between Na/1000 proportion and $Mg^{0.5}$ apex represent equal ionic ratios of Na-K geothermometry (Giggenbach, 1988), either due to controlling assemblage or reservoir type and temperature (Giggenbach, 1986). Lines towards the Na/1000 apex at relative K/100 axis show constant $K\text{-}Mg^{0.5}$ ratios of K-Mg geothermometer (Giggenbach, 1988).

Intersection of isolines defines complex equilibration temperature to the Na-K-Mg system, termed the full-equilibrium line, above that thermal waters are classified "mature" or "equilibrated" and satisfactory for cation geothermometry application. Position of the curve depends on a choice of the Na-K geothermometer. The curve below represents arbitrary given line representing a dissolution line for "average crustal rock" at the Na-K-Mg system (Giggenbach, 1986). Samples positioned between are "partially equilibrated", due to mixing or water-rock reactions prior sampling, thus cation geothermometers must be

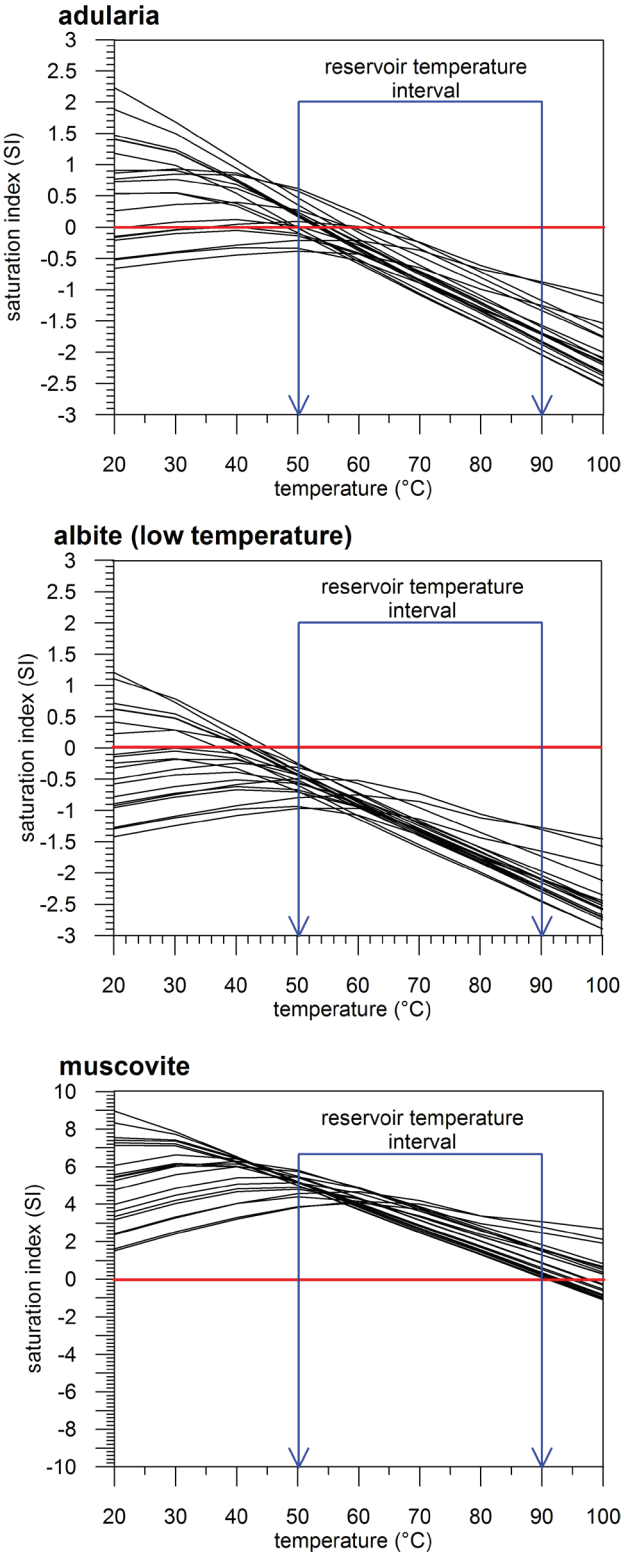

Fig. 15. Na-K-Mg-(SiO_2) alteration assemblage saturation.

used with a caution in order to assess formation temperatures. A cross-check using another Na-K geothermometer may prove or disapprove that partial equilibration (D'Amore and Arnórsson, 2000). Samples plotted below the average crustal rock dissolution line are "immature" and so "inequilibrated", and, in most cases, use of Na-K geothermometry for temperature estimation is ambiguous, whilst results of K-Mg geothermometry must be validated by more correlation (Fournier, 1989).

Derivation of the full-equilibrium line is the maturity index (Eq. 47) for geothermal waters regardless of origin, as being a linear combination of Na-K (Giggenbach, 1988) and K-Mg (Giggenbach, 1988) geothermometer:

$$MI = 0.315\, L_{km} - L_{kn} = 0.315 \left[\log\left(\frac{c^2K^+}{cMg^{2+}}\right)\right] \left[\log\left(\frac{cK^+}{cNa^+}\right)\right] \quad \text{(Eq. 47)}$$

where concentrations (c) are in mg·kg^{-1} and 0.315 is the van't Hoff's slope for linear combination of both geothermometers.

Mature waters yield the MI > 2, henceafter use of cation geothermometry is recommended for waters with a maturity index score of above 2 or close around. For mature, partially equilibrated, and rarely inequilibrated parental thermal waters, the corresponding springs plot departed towards the $Mg^{0.5}$ apex due to acquisition of Mg^{2+} by cooling, mixing or interaction with the wallrock (Marini, 2004). Parental fluids plotted closer to the $Mg^{0.5}$ corner than a spring or dilutant are signs of silicates or carbonates deposition prior sampling in the borehole, or incorrect steam separation at the wellhead. Meanwhile, the diagram is sensitive to reservoir environment, especially for carbonates, or admixture of low temperature waters (intense thermal – cold mixing) as both, carbonatogene reservoir waters or dilutants are routinely rich in Mg^{2+} and HCO_3^-. These tend to cluster solely in the $Mg^{0.5}$ corner.

The larger is the distance of the sample from the full equilibrium line, the less reliability gains application of cation geothermometry (Giggenbach, 1988), or, the more caution and cross-validation of partial geothermometry results must be accounted whether for temperature assessment or conceptual relations interpretation.

Application: maturity index analysis

Obviously, associated facies, regardless of position are definitely immature (Fig. 16). Thermal waters of DRTE score MI = –0.1 – 0.4 on maturity analysis, classifying them distinctly immature. Samples of SRTW, however, record increase to MI = 0.2–0.9. Previously identified subfacies (low-silica and high-silica) can not be distinguished according to MI. Samples of recharge zone yield MI = 0.49–0.56 for shallow and MI = 0.47–0.54 for deep approximated circulation regime. Highest score is obtained for VSH-1 samples, reaching up to MI = 0.8–0.99. Springs (S-CGW) of the Sliače area record MI = 0.51–0.57.

The maturity index increases with rNa^+ and cNa^+. This is most pronounced for VSH-1 samples, where maturity is inverse to Mg^{2+}. Enrichment in Na^+ realizes due to mixing of DRTE (Na^+ poor) with SRTW (Na^+ moderate), being followed by the second stage mixing (dilution) with S-CGW (Na^+ rich) prior sampling from the borehole.

Higher Na^+ level is not just because of its slower response to cooling. The S-CGW waters are expected to form and accumulate in siliciclastics. While the dilution balances Mg^{2+} lost in first stage, it adds Na^+. The relation of rNa^+ and cNa^+ or rMg^{2+} and cMg^{2+} to the MI vanishes within DRTE. The low score relates to Na^+ deficiency and to oversaturation with carbonates. Hence, the Na^+ level is controlled by aggressive CO_2 content in fluids.

Application: Na-K-Mg geoindicator analysis

The structure is immature to the Na-K-Mg subsystem (Fig. 16). To draw the Na-K-Mg diagram we used Na/K and K/Mg geothermometers by Giggenbach (1988). All samples plot as immature (Fig. 17), proving inequilibration to alkalis, thus ionic ratios overestimate temperatures. All populations score $T_{Na/K} > 350$ °C. While for K/Mg ratios the DRTE samples exceed a reservoir temperature by a factor of 1–2 ($T_{K\text{-}Mg} \approx 80$–$140$ °C), samples of VSH-1 cluster along a $T_{K\text{-}Mg} \approx 120$–$125$ °C, which does not correspond to the reservoir environment.

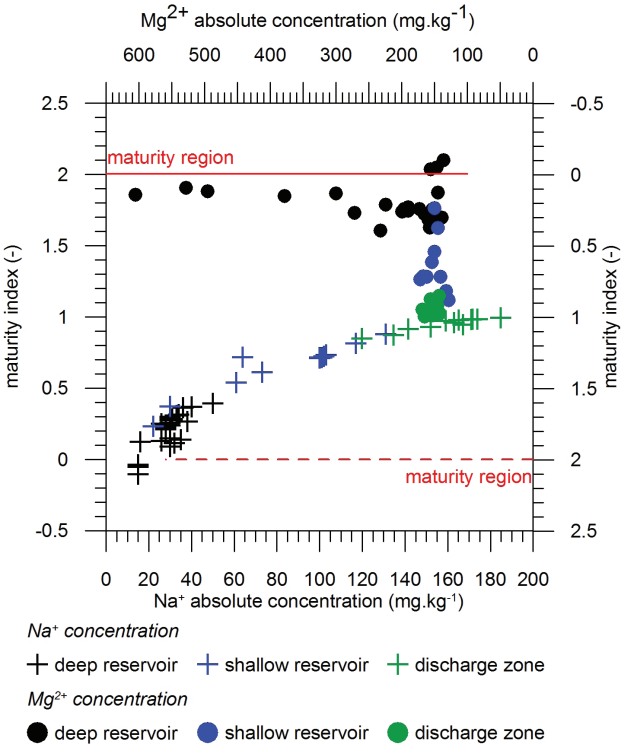

Fig. 16. Maturity index distribution versus sodium and magnesium concentrations.

Rock dissolution and mineral precipitation regime controls chemistry of all facies. This is, at the same time, controlled by rock dissolution or mineral precipitation. Compared to reservoir facies, samples of the Sliače springs depart towards cooling springs region, evidencig their S-CGW association. Samples of the VSH-1 organize off the cooling springs region from the DRTE facies. The position decreases a relative Mg^{2+} proportion compared to DRTE, combining losses of carbonates, dilution and alkali intake (Fig. 15). Increase in maturity of VSH-1 reflects Na^{+} enrichment over stable K^{+} level. Similar proportion in Mg^{2+} between SRTW and VSH-1 infers other magnesium source.

An idea of DRTE and SRTW mixing in the upflow zone (decrease in Mg^{2+}, increase in K^{+} and Na^{+}) recalled a first mixing stage preceding dilution of a mixture with S-CGW facies, assumed a second mixing stage (Na^{+} increase, Mg^{2+} decrease, K^{+} stability) may be satisfied, if the first realizes in Jurassic – Mid Cretaceous succession (Na^{+}/K^{+} source), while dilution takes part in the Mid Triassic dolomites or the Borové Fm. (K^{+} source).

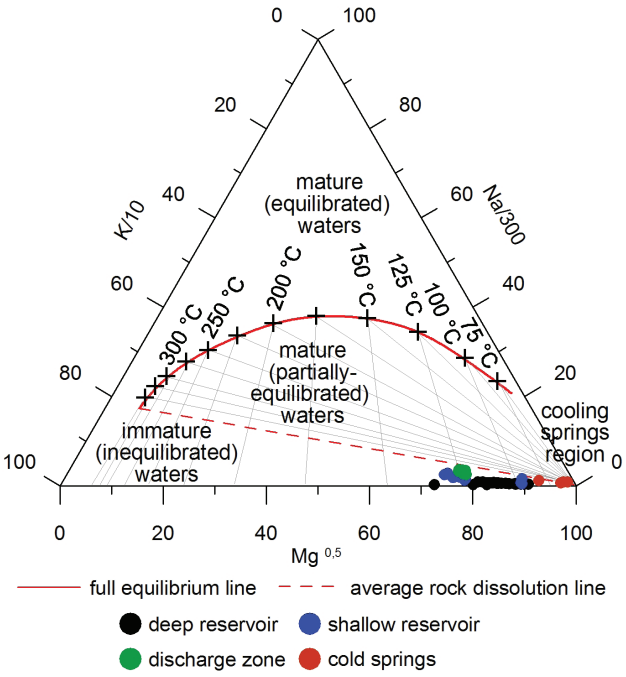

Fig. 17. Giggenbach maturity diagram (geothermometer). Modified after giggenbach (1986).

K-Mg-Ca subsystem

A limitation of Na-K-Ca geothermometer is its sensitivity to pCO_2 (Pačes, 1975) not too surprising in extensively magma-steam heated HT or carbonate reservoirs. In the HT equilibrated systems, the hydrolysis of calcium-alumno-silicates towards calcite production (Eq. 48) fixes the pCO_2 (Giggenbach, 1984) at given reservoir formation temperature (Eq. 49):

$$Ca-Al-silicate+K-feldspar+CO_2 \leftrightarrow CaCO_3+illite+SiO_2 \quad \text{(Eq. 48)}$$

where the Ca-Al-silicate is isochemically recrystallised stable Ca-mineral, and:

$$\log(fCO_2)=\log(PCO_2)=0.0168\cdot t-3.78 \quad \text{(Eq. 49)}$$

where t is temperature of formation in °C.

At initial conditions, the CO_2 fugacity is below that of (Eq. 49), so calcite can not precipitate. CO_2 equilibrium activity drops rapidly with drop in T, turning the fluid reactive with a CO_2 system (Ellis, 1970), recapturing equilibrium by calcite deposition (Eq. 50–51).

$$3K-feldspar+CO_2+Ca^{2+} \leftrightarrow muscovite+CaCO_3+6SiO_2+2K^{+} \quad \text{(Eq. 50)}$$

$$K_{eq}=\left[\frac{[K^{+}]^2}{[Ca^{2+}]+pCO_2}\right]\left[\frac{[mus\ \mathrm{cov}\ ite][CaCO_3][SiO_2]^6}{[microcline]^3}\right] \quad \text{(Eq. 51)}$$

In LT carbonate systems, the carbon dioxide originates by precipitation of calcite and generation of available CO_2 (Eq. 52), or by equilibration to carbonates and production of excess CO_2 by water-rock reaction at continuous contact with a source (Simmons and Christenson, 1993).

$$2HCO_3^{-}+Ca^{2+} \leftrightarrow CaCO_{3(solid)}+H_2O+CO_{2(g)} \quad \text{(Eq. 52)}$$

Under new equilibration (Eq. 48–50), involving the $CaCO_3$ deposition in a solid form, a correlation (Eq. 53) between concentration of major constituents for stated reactions (Ca^{2+} and K^{+}) and fugacity is given (Giggenbach, 1986):

$$\log\left[\frac{[c^2K^{+}]}{[cCa^{2+}]}\right]=\log(P_{CO_2})+3 \rightarrow \log(P_{CO_2})=L_{kc}-3 \quad \text{(Eq. 53)}$$

Presented L_{kc} system adapts to changes in CO_2 or concentrations of constituents fast. While concentrations for major components are a function of variations in temperature, especially cooling, the (Eq. 53) does not account for a CO_2 dependence neither on formation, nor on the equilibration temperature. Correlation of fugacity, geochemical composition and temperature is possible only if combining the L_{kc} system with a geothermometer likely adapting to reservoir dynamics, that is, the K-Mg (L_{km}) geothermometer (Giggenbach, 1988).

The K-Mg-Ca (K-Ca-p_{CO_2}) diagram plots samples with L_{kc} to the L_{km}. A solid black line represents a full equilibrium line for CO_2 partial pressures for a full equilibrium assemblage (Eq. 49). If water equilibrates with the K-Mg-Ca and Na-K-Mg system,

samples plot above the line and give a maturity index (Eq. 45) of MI > 2 considering them mature or equilibrated (Giggenbach, 1988). These waters are of CO_2 content too low to induce the rock alteration due to (Eq. 48). Low concentration may be a consequence of initial carbon dioxide attainment from the CO_2 deficient host-rocks prior sampling or dilution by magmatic waters with meteoric, or, either by a loss of CO_2 by boiling. A region between the full equilibrium curve and curve for calcite deposition fugacity (Eq. 53) involves samples able to deposit $CaCO_3$ during the upwell. Overall equilibrium to the K-Mg-Ca system is limited by the calcite deposition rate (Giggenbach, 1986). Samples below the dashed line are immature, with chemistry rather as a function of water-rock interaction then water-mineral equilibrium and alteration. Departure from the minimum calcite deposition line implies upflow velocity too fast for calcite alteration onset (Joseph et al., 2013).

Application: K-Mg-Ca geoindicator analysis

The theory expects immature samples to plot below the full equilibrium line. Actual records of all facies within a calcite formation and mature region (Fig. 18) may first be explained by extremely low K^+ concentrations, compared to Ca^{2+}, presumable for carbonate reservoirs.

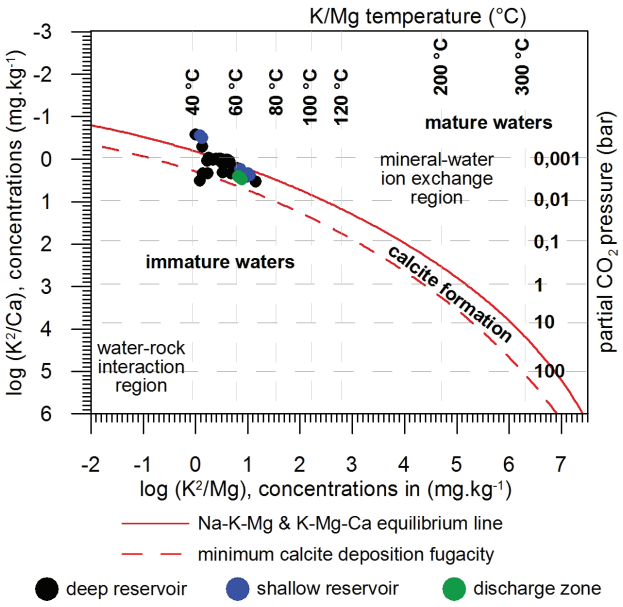

Fig. 18. K-Mg-Ca geoindicator analysis. Model modified after Giggenbach (1988).

DRTE samples plot along an equilibrium line due to low K^2/Mg and K^2/Ca ratios at TK-Mg ≈ 45–60 °C, which is somewhat below the reservoir interval, instantly due to inequilibration with the K-Mg-Ca subsystem. Assumed LT equilibration with calcite (Eq. 52) is not valid as $pCO_2 \approx 2.6 \cdot 10^{-4} - 3.2 \cdot 10^{-3}$ bar is too few to induce calcite precipitation. Calcite formation by hydrolysis of alumnosilicates (Eq. 46) yields better counts ($pCO_2 \approx 1.2 \cdot 10^{-3} - 2.3 \cdot 10^{-3}$ bar), allowing calcite deposition, which may be because of calcite saturation prior deep reservoir inlet. As there are no indices on boiling for calcite (Fig. 19), L_{kc} and L_{km} variation defining the fCO_2 results from vertical reservoir filtration at continuous contact with a wallrock.

In other words, the unit of calcite deposited hypothetically due to pressure change along a vertical upflow filtration is replaced by a unit of calcite dissolved during a vertical downflow in separate convection cells.

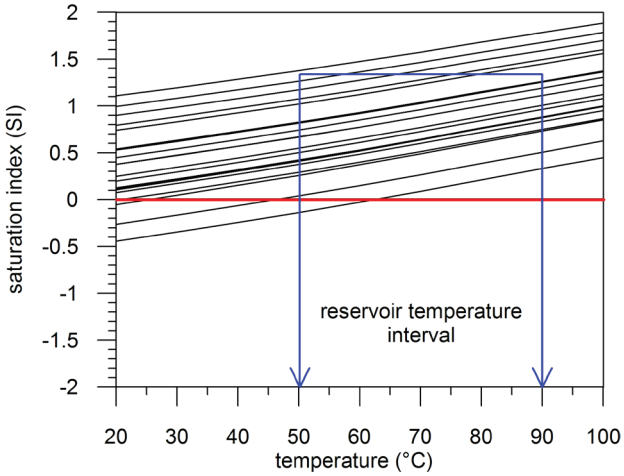

Fig. 19. Deep reservoir analysis: calcite saturation.

Temperature overestimate for the shallow reservoir, TK-Mg ≈ 45–65 °C, evidences unequilibration of SRTW facies to the K-Mg-Ca subsystem (Fig. 18), as the K^2/Mg ratio is too low. If we accept a genesis of the facies by mixing of recharges with thermal waters evaded from the deep reservoir, the excess Mg^{2+} reflects continuous dolomite dissolution within CHN dolomites and fresh intake, balancing the Mg^{2+} lost off the DRTE.

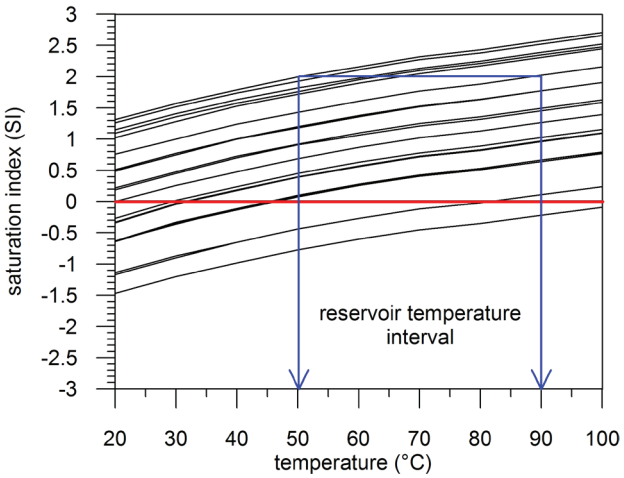

Fig. 20. Deep reservoir analysis: dolomite saturation.

Presumably, Mg-calcite precipitates (Fig. 20) after evasion from the deep reservoir. Calcite addition produces excess CO_2 and decreases an apparent pCO_2. Under low temperatures, the K^+ increases slower than Mg^{2+}, as K^+ leaching (simultaneous to alteration of Na-silicates to K-micas) is less intense with drop in CO_2.

In absolute concentrations, K^+ increases in VSH-1 samples, compared to DRTE, whilst keeping similarity to SRTW, either at lower Ca^{2+}. K^2/Ca and K^2/Mg ratios increase probably at a magnitude of calcite and dolomite deposition during DRTE and SRTW leaking towards discharge zone, conserving K^+ prior mixing and later enrichment of a mixture with K^+ and Mg^{2+} from dilution with S-CGW. After projection onto CO_2 fugacity line, the $T_{K\text{-}Mg} \approx 50$ °C, which evidences drop in aggressive CO_2 by some calcite and Mg-calcite deposition and ceasing of Na-silicates modification towards K-micas, calling the (Eq. 52) apparently valid.

Na-K-Mg-Ca geoindicator

The Na-K-Mg-Ca geoindicator (Giggenbach, 1988) combines Na-K-Mg and K-Mg-Ca thermodynamic subsystems, comparing relative proportions of Mg over Ca (carbonates) and Na to the K (alkali silicates). The solid line represents here a full equilibrium to both thermodynamic subsystems (Fig. 21). Samples plotted below the curve are already equilibrated without a tendency to dissolve host-rocks spontaneously (Wishart, 2015). Instead, the geochemistry of such samples is controlled by mineral-water equilibrium.

Average seawater (Na-Cl brine) region locates within high Mg^{2+}/low K^+ corner, whilst high Mg^{2+}/high K^+ corner represents a rock dissolution region. Here, samples plot outermost to the equilibrium, thus are immature and geochemical composition is controlled by a water-rock interaction (Giggenbach, 1995), i.e. dissolutio p well n, hydrometasomatism or hydrolysis. Affinity to subregions representing average crustal rock composition (Taylor, 1964) is controlled by relative ratios of the samples. Transition of samples towards equilibrium line in a direction of X axis indicates a possible seawater influence on their final geochemistry. A diagonal transition trend is an indice of mixing or dilution (Giggenbach, 1988).

Ionic ratios in a crustal rock region represent those needed to attain a full equilibrium to a specific rock. Drawing a vertical line onto X axis conserves Na/K ratio and can account on expected L_{kn} temperature. A horizontal line projected onto Y axis gives an estimation by L_{km} (Giggenbach, 1988). Interpretation must, however, take a caution onto both values as they can not gain same values in an essence. This plot is then, rather, used to outline reservoir or conceptual relations.

Application: Complex maturity analysis

Organization of all facies along and nearby the rock dissolution region is distinct evidence on immaturity and unequilibration to both subsystems as they plot outermost to the full equilibrium line (Fig. 21), recording three facies trends meanwhile.

Deep reservoir samples plot within or to the right of rock dissolution region. The equilibrium attainment realizes along an Y axis, evidencing the equilibration due to saturation of waters with carbonates. A drop in Mg/Ca ratio is observed along a DRTE/SRTW trend (1), implying Mg-calcite precipitation rate above that of "pure" calcite, or its acquire from Jr-Cr2 horizon. Apparent increase in Na/K towards the shallow reservoir gives some evidence on Na-silicates modification deceleration with drop in CO_2 and possible enrichment within.

Some equilibration to the wallrock is possible for residential SRTW subfacies, destructed by a mixing with DRTE originated subfacies instantly. At cooler downflow temperatures (2), limestone is leached easier than dolomite, which dissociation starts after the reservoir accommodation. Increase in alkalis in downflow is inverse to filtration velocity decline in the Borové Formation that is a source of Na^+. The K^+ originates by dissolution of silicates and impurities in dolomite, with questionable contribution of Na-silicates modification.

VSH-1 facies record somehow a most evident trend towards partial equilibration, off the rock dissolution region. In fact, only weak relation may be found between SRTW, DRTE and VSH-1 facies (3) as a sign of poly-

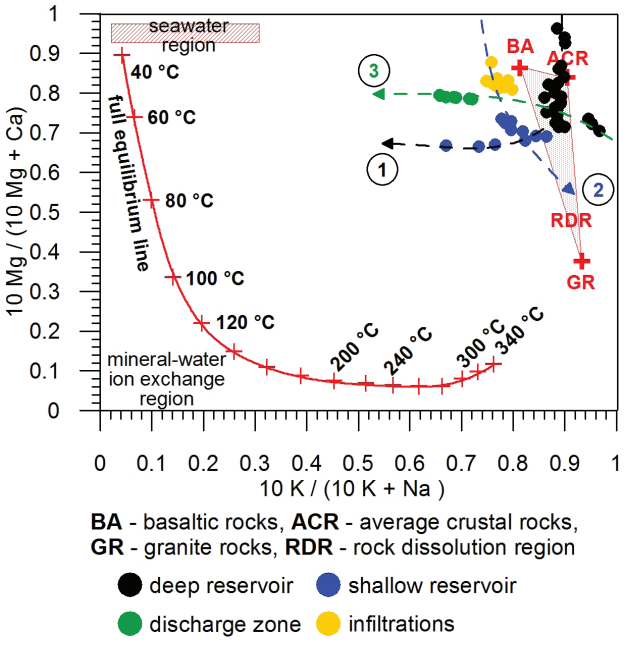

Fig. 21. Facial analysis: Na-K-Mg-Ca geoindicator. Modified after Giggenbach (1988).

stageous mixing. Some increase in Na^+, compared to parental conditions is either because of fair conservation of alkalis from SRTW and dilution with S-CGW hosted in IWCP (second mixing stage), however, effect of minor Na^+ preferential leaching in Jr-Cr2 horizon can not be excluded.

CO_2 induced modification of dissolved alkali silicates must be terminated already due to its consumption in deposited carbonates and activation of Mg-silicates, such as talc.

Quantitative cation geothermometry application

Na/K geothermometers (GN1–GN11) yield temperatures of over 100 °C for each zone, consequent to in-equilibration with Na/K system, excess CO_2 and deficient source. Variation by a magnitude of orders is also general for Na/Li geothermometers (GLN1–GLN5), resultant to combination of lack in either Na^+ and Li^{2+}. Temperature overestimates by a factor of 2–5 result from Na/Ca (GNC), K/Ca (GKC) and Na-K-Ca (GNKC) application, consequent to oversaturation of fluids with calcite and excess CO_2 in the system available, immediately restraining any equilibration to given thermodynamic pairs (Appendix D).

K-Mg geothermometry

Deep reservoir waters are oversaturated with dolomite under permanent contact producing excess Mg^{2+} and CO_2^-. The K^+ is consumed in activation of K-tectosilicates due to Na-silicates modification under aggressive CO_2 (cf. Giggenbach, 1986). Both factors cause high Mg/K ratio, underestimating DRTE temperatures by a factor of about 2 (Fig. 22). Apparent match of GKM3 (Giggenbach, 1988) at $T_{Mg/K} \approx 30–41$ °C is observed for the SRTW. Equilibration with Mg/K-silicates is not possible, rather the result is underestimated with respect to DRTE evaded subfacies by balancing Mg^{2+} lost during Mg-calcite deposition with its leaching from dolomites and enrichment from recharges, more intense than K^+ intake from the IWCP formations. Indeed, the K-Mg-SiO_2 relation aids assumption on fluent rewashing of the zone and residency too short for any equilibrium attainment. Depending on a depth of sampling, GKM3 scores reasonable estimates for the SRTW as long as $K/Mg^{0.5} = 0.5–14$. GKM3 yields $T_{Mg/K} \approx 31–33$ °C at VSH-1 (Fig. 22). Following qualitative applications, the temperature is definitely underestimated, as $T_{Mg/K} \approx T_{samp}$. Inflow temperature of waters from both reservoirs prior mixing must be, at least, of T = 45 °C or T = 40 °C respectively. We would not recommend K/Mg geothermometry quantitative application in local conditions.

Li-Mg geothermometry

A difference in lithium concentrations from early years (1987–1992) of deep reservoir production ($cLi^{2+} \approx$

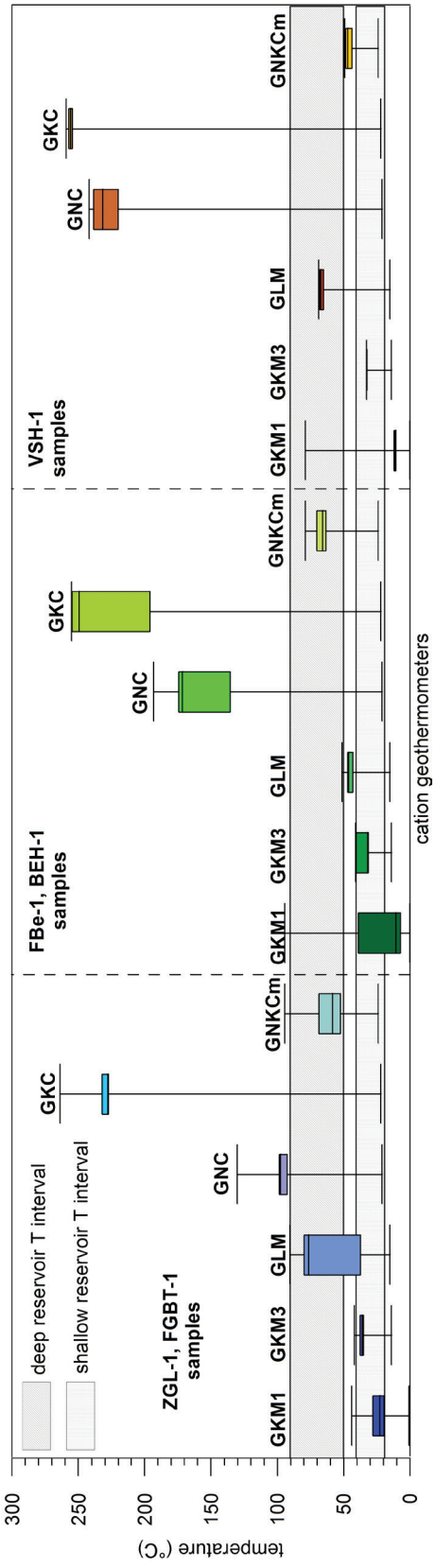

Fig. 22. Review on cation geothermometry quantitative application. See Appendix B for references and symbols.

1.4–2.5 mg·kg^{-1}), compared to steady lithium lowers that has been monitored at ZGL-1 or FGTB-1, henceforth (cLi^{2+} ≈ 0.2–0.3 mg·kg^{-1}) varies Li/Mg estimations from $T_{Li/MgO}$ ≈ 65–83 °C towards current $T_{Li/MgO}$ ≈ 27–37 °C. This is easily explained by the disproportion between low Li$^+$ and Mg^{2+}, even magnesium is upscaled by a root of square. There is just no sign on Li-clays equilibration (Eq. 45–46).

Such a drop may then be because of initial marinogene residuals removal or due to increasing an overall deep filtration velocity within the structure, as not only Li$^+$, but Cl$^-$ decreases in comparable scale (Fig. 23). Definitive rewashing of long-term and long-residential waters while building up the hydraulic gradient between recharge and accumulation zone towards pseudo-steady state would also drop the Li$^+$.

Stable Li$^+$ concentrations are recorded in the shallow reservoir (cLi$^+$ ≈ 0.3–0.6 mg·kg^{-1}) during its production (1979–2015) yielding $T_{Li/MgO}$ ≈ 39–52 °C, with no relation to sampling depth. The lithium content comes off its conservation during DRTE upwelling or leaching from IWCP and Jr-Cr2 positions in a downflow regime of recharges. Either the way, Li$^+$ appears conserved only, not entering any ion exchange reactions, questioning Li/Mg geothermometry application as no equilibrium is attained.

With given VSH-1 samples (see Appendix C) the score in temperature ($T_{Li/Mg}$ ≈ 62–69 °C) estimation at (cLi^{2+} ≈ 1.0–1.4 mg·kg^{-1}) is rather a hint on additional Li^{2+} addition from a host rock while waters of deep and shallow reservoir laterally leak towards discharge zone. For this interpretation, we would prefer the influence of transition at a contact with sufficient source, such as IWCP, or with Jurassic–Mid Cretaceous succession.

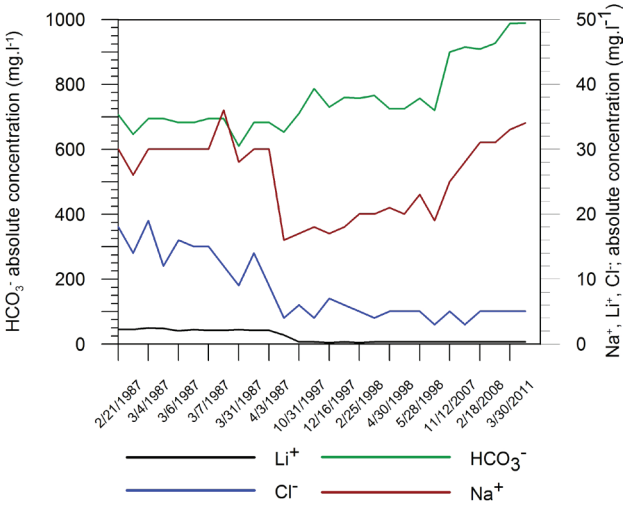

Fig. 23. Time-domain variability in selected ion constituents at ZGL-1.

Too few correlations for lithium geothermometry exist, available for detailed look on lithium origin. The deep reservoir waters are of higher temperature, thus may dissolve Li$^+$ intensively, thus do not need a long water-rock contact. Shallow reservoir waters are of half a lower temperature, but remain constantly in potential lithium source rock. If both facies mix together, the resultant lithium is then proportional to rate of mixing. A process to control the lithium level is, most probably, a simple enrichment, as association of lithium clays in ion-exchange reactions is unlikely. As far as uncertainty onto lithium origin exists up to a recent state, use of lithium geothermometry in local conditions is rather not recommended.

Na-K-Ca-Mg corrected geothermometry

Thermal waters of the Bešeňová elevation, regardless of facies affinity are acid, referring to volatile CO_2 content, thus with calcite and dolomite precipitation in control on aqueous pH, explaining why most of cation geothermometers fail in quantitative application (Appendix D). Besides saturation of calcite, aragonite or dolomite (Figs. 19–20), structures hosted in carbonates are usually rewashed, fast in filtration and diluted by recharges or during upwell in discharge zones, thus rich in excess Mg^{2+}.

For the deep reservoir, the excess Mg^{2+} is obviously controlled by magnesium (dolomite, calcareous dolomites, talc) saturation cycle. Using the Mg-correction, the initial T_{NKC} ≈ 211–325 °C decreases to T_{NKCm} ≈ 27–95 °C, out of that 24 % of samples (8/33) do not match the reservoir interval, with one overestimate only. There is no external Mg^{2+} source than dissolution of dolomites and LT alteration of impure dolomites. Correction estimation range implies rather variation in saturation of dolomite and talc thermodynamic activation.

Even after correction temperatures are overestimated, both in shallow reservoir (T_{NKCm} ≈ 61–79 °C) and VSH-1 samples (T_{NKCm} ≈ 42–49 °C). For both, the function can not be used in equilibrium conservation correlation to the origin of formation. The mismatch points to excess Mg^{2+} due to additional dolomite dissolution or mixing (dilution) with recharges, aiding previous balance of Mg-calcite deposited during lateral leaks or vertical evasion.

COMMENTS ON SOLUTE GEOTHERMOMETRY

Isotope and gaseous geothermometry

Use of solute geothermometry is grounded by conception of relative stable upflow during which a fluid does not undergo any mixing with cooler groundwater or is at sub-boiling conditions. Development of gas and isotope geothermometers responded to problem of inconsistency of many thermal springs with an obligatory conception in essence. As both are not a scope of our paper, we deal with either only in a brief review.

Thermal springs are not the only surface geothermal propagations. Many fields manifested by fumaroles do not involve springs, as the water table remains deep in grounds, thus aqueous geothermometers can not be applied (Giggenbach, 1991). The fact resulted in development of the gas geothermometers based on gas–gas equilibria, gas–mineral equilibria and mineral–residu-

al gas equilibria, related to CO_2, H_2S, H_2 or CH_4 (e.g. Arnórsson and Gunnlaugsson, 1985; Arnórsson et al., 1998). Steam geothermometry is more difficult to handle, because: (a) gas concentrations are affected by water–steam ratio; (b) in fumaroles, the gas content of a steam is affected by mechanism of boiling and condensation, and; (c) gaseous components fluxes from external reservoir or magmatic source may be of influence overprinting initial mineral–gas equilibria (D'Amore and Arnórsson, 2000). Application of these is ambiguous for low enthalpy systems with steam phase separated artificially.

In natural systems, equilibrium achievement for isotope exchange reactions is temperature dependent (Ellis and Mahon, 1977). Isotope geothermometers are less sensitive to thermal water flow dynamics, as achievement on chemical equilibrium is obligatory prior isotope redistribution into equilibration (Lyon, 1974). Out of many proposed, most frequently used geothermometers for high enthalpy fluids are those based on $CO_2 – CH_4$, $CH_3D – H_2$ and $HD – H_2O$, $CO_2 – H_2O$ and $SO_4 – H_2S$, whilst for low enthalpy systems, applicable isotope geothermometers refer to $SO_4 – H_2O$ and $CO_2 – H_2O$ (D'Amore and Arnórsson, 2000).

Critique on solute (cation) geothermometry

Criticism accents violating principal aspects of formal chemistry in setting assumptions for grounding and application of cation geothermometers. In balancing equilibrium reactions (e.g. Eq. 17), solids on both sides are not the same and there can not be a free ion in equilibrium reaction, thus the equation can not be in equilibrium, and mixed minerals are not pure phases, so their activity coefficients can not equal one. Another impossibility is in existence of a fraction of atom in formula (e.g. Eq. 39). In practical aspects of computational solute geothermometry, adds imbalance in physical units within solute geothermometers equations, as there are numbers on a one, and variable with a unit on the other side (Verma, 2012).

Silica geothermometry has also been subjected to criticism of its basics. Experimental solubilities of silica decrease along a water-vapor saturation curve at temperatures above 300 °C, neglecting a vapor formed fraction. It is mandatory to account on total silica discharge, thus to include a silica in the vapor fraction, in construction of silica solubility basics. To know that, correct knowledge on reservoir temperature is crucial. Then a role of silica geothermometers limits to reservoir water-rock interactions and equilibrium states (Verma, 2000). Nor SiO_2 geothermometry models are balanced in physical units (Verma, 2012).

Isotope geothermometry techniques and understanding on isotope cycles in thermal waters is in a constant development. There is, however, a rising accent on their relation not only to temperature, but onto influence of reservoir pressure and salinity addition as well, which is not included in conventional isotope geothermometry calculations (Horita, 2005). At the same time, variation in isotope thermodynamic history due to mixing is frequently missed out.

MULTICOMPONENT EQUILIBRIUM GEOTHERMOMETRY (MCG)

Instead of solubility of one or a few minerals and semi-empirical correlations, the multicomponent geothermometry uses complete fluid analysis and a solid thermodynamic background at given assemblage. The complexity provides the multicomponent geothermometry with the advantage of a great precision, if applied correctly. Exactly, minimum assumptions grounding the MCG turn this method most reliable, whether in temperature estimation, saturation states analysis, equilibrium correlations and CSM construction.

Mineral equilibria

Saturation state

Chemistry of thermal waters is not only a print of coexisting dissolved phases (Arnórsson et al., 1982; Reed, 1982), but a record of its conceptual history either. One of consequences of the conceptual history is an equilibrium state (Eq. 53), at which the activity quotient and equilibrium constant (Eq. 54) are equal, so the saturation index SI = 0 (Reed and Spycher, 1984).

$$SI = \log\left(\frac{Q_k}{K_{eq}}\right) \qquad \text{(Eq. 53)}$$

where Q_k is the activity quotient for aqueous species formed by the dissolution of a mineral "k" and K_{eq} is the equilibrium constant for the dissolution reaction of a mineral "k":

$$K_{eq} = \frac{\prod^{i} a_{i,k}^{vi,k}}{a_k}, \; and \; Q_k = \prod^{i} a_{i,k}^{vi,k} \qquad \text{(Eq. 54)}$$

where "$a_{i,k}$" – activity coefficient, "$v_{i,k}$" – stoichiometric coefficient for species "i" in equilibrium mass action expression for phase "k", "a_k" – activity coefficient of „k-th" phase.

If the phase is undersaturated (SI < 0), the thermal water tries to approach its equilibrium by dissolving/leaching activation from a wallrock or onset of equilibration ion-exchange reactions, or, in other words, the phase and its components remain in solution. At oversaturation (SI > 0), the water lets the phase to contribute on equilibration reactions or deposits, the phase after loosing a contact with a source rock or if p-T conditions change dramatically (e.g. onset of cooling, boiling).

A frequent technique in analysis of saturation states for one or more minerals is plotting the SI over an optional range of T, which implicitly displays thermodynamic state of mineral phases of various composition, instead of using activity diagrams where only two compositional variables are plotted at fixed temperature (Reed and Spycher, 1984).

Approach

The recalled complexity is, at early exploration stages, of greatest disadvantage for the MCG, requiring not only at least some knowledge on associated mineral suite, but a solid concept on reservoir dynamics, i.e. generation of adiabatic boiling and processes of heating and cooling during conceptual history. For the MCG, only deep reservoir is evaluated, as this is identified the only zone not affected by any mixing or dilution.

In a sake of review, geochemical models (Fig. 2) together with geothermometry (e.g. Figs. 6 and 7) give a solid supposition on conductive heating/cooling controlling reservoir intake or runoff temperature variations regardless of direction.

Computation module

The MCG targets saturation states of associated mineral phases. Several notes onto the problem have been listed e.g. in Remšík et al. (1998), as well as Vandrová et al. (2011), aimed at actual, sampling temperature saturation of the deep and shallow reservoir. The MCG, however, requires analysis over desired temperature interval, which usually means between reservoir base and reservoir outlet, or, rather, geothermal infrastructure intake temperature, with possible extension to reference temperature assuming constant p-T conditions.

Under local conditions, we set the temperature interval for T = 20–100 °C, referring to usual reference temperature and basal temperature extended by ~ 10 % for better precision at the base. Saturation calculations (Eq. 53–54) were carried using Phreeqc (USGS) and WATCH/WAIN (ÍSOR) scripta, applying cooling springs, no boiling ≈ conductive cooling/conductive heating modules off the sampling temperature. At this setup, both modules are able to vary thermodynamic properties and SI or desired solids, not changing macrochemistry of analysed solution.

Selection of fluid samples

Whether for simple saturation indexes (SI) or advanced multicomponent geothermometry (TSI, RMED) analysis, we limited calculations to deep reservoir waters only. The reservoir has been selected because it represents the only zone within the structure not affected by any mixing or dilution. Obviously, the reservoir intake from the deep infiltration channels is expected to be of quasi-isochemical regime. To narrow the population, the modelling procedure involves only samples of complete chemical analysis in referenced literature (see Appendix C). We itinered then the selection towards samples which yielded relevant temperature estimate at chalcedony geothermometer (Fournier, 1977) simulation in WATCH. To tighten homogeneity of samples, the last population reduction selected samples taken at wellhead only through a sampling campaigns since 1988.

Complex equilibrium temperature (T_{CEQ})

Type curve method

Interpretational procedures using SI vs. T diagrams are based on convergence and shape analysis. In T_{CEQ} evaluation, equilibrated assemblage intercepts the SI zero level at a definite temperature, or, at least, at a narrow temperature interval reservoir boundary conditions (Pang, 1988). In fact, no more than 10–12 phases coexist in equilibrium (Arnórsson et al., 1982). More interception clusters imply inequilibration or partial re-equilibration. Conceptual decision is rather a question of the interpreter. Equilibration to a relevant assemblage may be well seen by sharp maxima and irregular skewness of histograms (Reed and Spycher, 1984).

Boiling effects upon saturation states relate to an immediate change in pH and loss of CO_2 or H_2S respectively. For silicates, the SI = 0 intersection temperature increases as SiO_2 concentration in residual fluid is higher as of an initial (Tole, 1988). Mineral phases containing sulphide, aluminum and iron shift equilibration compared to the pre-boiling conditions as speciation of H_2S, Al^{3+} and $Fe^{2+,3+}$ changes with an increase of CO_2. However, the loss of CO_2 definitely causes supersaturation with respect to carbonates (Reed and Spycher, 1983). Boiling plots irregular dispersion and shifting of SI curves generally (Neupane et al., 2014).

By mixing with cooler thermal water or mineralized groundwater, the convergence temperature for particular phases shifts irregularly, and there is usually neither equilibrium attained, nor convergence clusters may be identified. A contact with dilutant (Fig. 11c), however, shifts apparent equilibrium to negative or causes "re-equilibration", or, simply, double interceptions for phases or complete assemblage (Tole, 1988).

Application: Selection of solids procedure

Numerous methods have been developed since the concept of equilibrium (saturation) analysis was introduced (e.g. Reed and Spycher, 1984). Besides computation and analysis principles, these methods vary in mineral assemblage selection/definition. Complex equilibrium analysis selects the assemblage by arbitrary.

Together 18 solids were selected to represent reservoir and conceptual model conditions, assigned into groups of master- primary (calcite, dolomite, chalcedony, gypsum, talc), alteration (albite, adularia, fluorite, kaolinite, illite, muscovite, chlorite) and hypothetical- minor phases (montmorillonites, gibbsite). Master and alteration phases control geochemistry of reservoir waters by their saturation states. Minor phases were introduced for additional control on stability for major components and pH. Neither

alteration, nor hypothetical phases must necessarily precipitate because of oversaturation. Their state of equilibrium is called to control ability of master components (OH^-, K^+, H^+, Na^+, F^-, Al^{3+}) to enter wallrock dissolution or ion exchange reactions, with respect to CO_2 reservoir cycle.

Application: Complex equilibrium temperature analysis

Derivation of complex equilibrium temperature requires calculation of temperature at which the saturation state (Eq. 53) equals SI = 0 for each of selected phases (Tab. 1) per every sample. With this procedure, the overall temperature varies T_{CEQ} = 56–79 °C, as median values of T_{SI} = 0. Because of skeweness of results, the representative temperature of complex equilibrium equals T_{CEQ} = 66 °C. Out of 20 samples, only two were disqualified, as number of equilibrated phases within T = 20–100 °C has not reached 50 % (9/18). The T_{CEQ} = 66 ° corresponds to upper half of the deep reservoir.

Quantitative equilibration analysis may be referred to reservoir temperature (T_{res} = 56–79 °C) or entire temperature (T = 20–100 °C) interval. The first approach inspects reservoir conditions only, whilst the latter allows evaluation of not only reservoir, but runoff conditions simultaneously, assuming no mixing and maintaining conductive heat loss as a controlling cooling process only.

Only 8 phases equilibrate at over 50 % frequency at T_{res}. Only chalcedony, Na- and K- montmorillonites equilibrate completely. Chalcedony saturation proves its control on silica solubility (Fig. 5). Equilibration of montmorillonites proves the adularia–albite system is not in control on Na/K stability (see Fig. 15). Adularia (mean T_{CEQ} = 55 °C) equilibrates in 16 samples at (T_{CEQ} = 40–65), however, in 8 samples within the reservoir. Albite (mean T_{CEQ} = 42 °C) intercepts SI = 0 in 9 samples only (T_{CEQ} = 30–46), not reaching equilibrium within reservoir. Anhydrite and fluorite never converge to SI = 0 at reservoir temperature as well. Inequilibration with anhydrite aids control of gypsum saturation on SO_4^{2-} content within deep reservoir. Gibbsite, kaolinite and chlorite (Tab. 2) equilibrate in over 15 samples. First two simulate available OH^- and Al^{3+} for alkali hydrolysis reactions. The Mg^{2+} available by chlorite saturation variation allows its re-attainment within LT metamorphosis of detritic dolomites, activating talc, leaching Mg-calcite and producing additional CO_2.

Tab. 1
Deep reservoir: review on CEQ of selected samples

Mineral phases	Wellhead samples codes																			
	z21/2/1987	z4/3/1987a	z4/3/1987b	z5/3/1987	z6/3/1987a	z6/3/1987b	z7/3/1987	z22/3/1987	z31/3/1987	z2/4/1987	z3/4/1987	z20/2/1992	z12/11/2007	z17/12/2008	z18/2/2008	z26/2/2009	z30/3/2011	z13/4/2011	f15/3/2011	f30/3/2011
	Equilibrium temperature (°C)																			
Adularia	50	49	61	U	51	59	U	55	U	40	U	58	48	55	53	53	56	54	65	63
Albite	37	U	U	U	U	U	U	43	U	U	U	43	U	31	42	42	46	43	U	U
Anhydrite	20	22	25	20	22	24	22	21	20	21	O	O	O	O	O	O	O	O	O	O
Calcite	O	O	20	45	O	O	62	O	25	O	O	O	O	O	O	O	O	O	O	O
Ca-mont.	71	78	O	O	88	91	O	80	86	84	84	74	76	80	71	73	74	74	85	86
Dolomite	O	31	82	82	46	45	U	O	45	32	29	O	O	O	O	O	O	O	O	20
Fluorite	O	O	O	O	O	O	O	O	O	O	O	O	O	O	O	O	O	O	O	O
Am. pyrite	56	45	O	U	U	U	U	22	U	57	U	55	U	60	46	55	55	62	79	80
Gibbsite	53	62	69	67	65	65	70	58	64	64	62	48	58	58	51	53	50	53	58	61
Chalcedony	56	64	94	81	72	81	94	67	67	67	67	72	58	67	60	62	66	62	77	79
Chlorite	61	85	97	99	94	91	O	73	88	87	83	44	77	74	53	60	52	60	74	80
Illite	49	U	64	U	55	61	U	55	U	52	52	51	51	54	50	52	52	52	59	60
Kaolinite	72	83	O	O	88	90	O	79	87	84	84	71	77	79	71	73	72	73	81	84
K-mont.	62	67	90	81	75	79	99	69	73	71	71	63	65	69	61	64	64	64	75	72
Mg-mont.	73	80	O	O	89	92	O	81	88	85	85	75	77	81	72	75	75	75	86	87
Na-mont.	62	68	92	84	76	80	O	70	74	73	73	63	66	70	62	64	64	65	74	75
Talc	38	63	74	81	71	66	83	49	66	64	60	O	54	44	27	35	25	35	45	52
Muscovite	91	95	O	O	O	O	O	98	O	O	O	92	95	98	91	93	93	93	O	O

Explanations: O – oversaturated; U – undersaturated

Tab. 2
Deep reservoir: review on CEQ of selected samples

Mineral phase	Reservoir equilibration frequency		Main SI = 0 interval
	x = n	%	(°C)
Adularia	8	40	50–55
Albite	0	0	35–40
Anhydrite	0	0	20–25
Calcite	1	5	25–30
Ca-mont.	17	86	70–75
Dolomite	2	10	80–85
Fluorite	0	0	–
Am. pyrite	9	45	55–60
Gibbsite	15	75	55–60
Chalcedony	20	100	65–70
Chlorite	17	85	70–75
Illite	2	10	45–50
Kaolinite	18	90	80–85
K-mont.	20	100	60–65
Mg-mont.	17	85	70–75
Na-mont.	20	100	70–75
Talc	9	45	65–70
Muscovite	9	45	90–95

Application: Type curve analysis

The type curve analysis applies to inspect reservoir dynamics. In previous, we already plotted chalcedony (Fig. 5), calcite (Fig. 19), dolomite (Fig. 20), and adularia–albite–muscovite suite (Fig. 15). Primary phases record uniform trend in SI-curves throughout the analysed interval. Alteration minerals, however, plot some minor variation (Figs. 15 and 24) at T < 65 °C. Because most of these are alkalis, we interpret the observed break as due to unstable contact with reservoir Na^+ and K^+ source (at T > 65 °C), and variable CO_2 saturation, which boosts or limits Na-silicates conversion into K-micas or phyllosilicates, with some secondary effect on aqueous Al^{3+} during the onset of conductive cooling as the sample is simulated to leave the reservoir.

A unifying feature of all phases plotted against temperature is variation in SI = 0 convergence, much above tolerated $\delta T_{SI} = 0$ difference of 10 % (± 9 °C). This is some sign of intraformation mixing, however, in pseudo-isochemical and pseudo-isothermal regime. The only possible scheme to fit this postulate is intraformation mixing of waters in vertical filtration due to formation of isolated, induced-convection cells, with steady, accommodated waters within upper parts of the reservoir.

Multicomponent equilibrium

Since the MEG was introduced (Reed and Spycher, 1984) and modified (Pang and Reed, 1998; Palandri and Reed, 2001), the application of some conceptual approaches aimed either at T_{res} derivation (e.g. Tole et al., 1993; Neupane et al., 2014), or initial reservoir fluids and formation brines reconstruction with onward temperature predictability improvements (e.g. Peiffer et al., 2013; Peiffer et al., 2014; Spycher et al., 2014). Hundreds of minerals can be easily plotted onto the SI vs. T diagram, making it all but useful. Moreover, dozens of assemblages may be misleadingly analysed, if these are selected inappropriately. Crucial for multicomponent equilibrium geothermometry is to know the assemblage and the procedure searches for, thus, the assemblage that is in control of chemistry of water samples.

Phase rule

The Gibb's phase rule identifies a number of minerals that may equilibrate with the geothermal fluid by defining degrees of freedom (Eq. 55), controlling a real number of components ready to equilibrate (Eq. 56), if temperature and pressure is fixed in the system, e.g. in the case of water saturated with steam (Cooper et al., 2013):

$$F = C - P + 2 \quad \text{(eq. 55)},$$

where F is a number of independent variables, C is a number of components and P is a number of phases in the system, so the number of equilibrium minerals (M) becomes:

$$M = C - F \quad \text{(Eq. 56)}$$

The phase rule gives an upper and theoretical limit for number of minerals that may coexist in equilibrium, even a real number of equilibrated minerals may be significantly less (Palmer et al., 2014), as this is due to combination of conceptual history of a fluid and p-T conditions.

In this paper, we have continuously accented multiple geothermometry application, however, temperature estimation resonates as the principal. Reservoir temperature may be derived by applying the TSI (Cooper et al., 2013) or CSI/RMED (Spycher et al., 2011; Spycher et al., 2014) methods.

Total saturation index (TSI)

Assemblage selection does not necessarily impede unreadability of SI vs. T plots if disarranged clustering or several re-equilibrations are displayed. The optimizing function for considered mineral assemblage is termed as

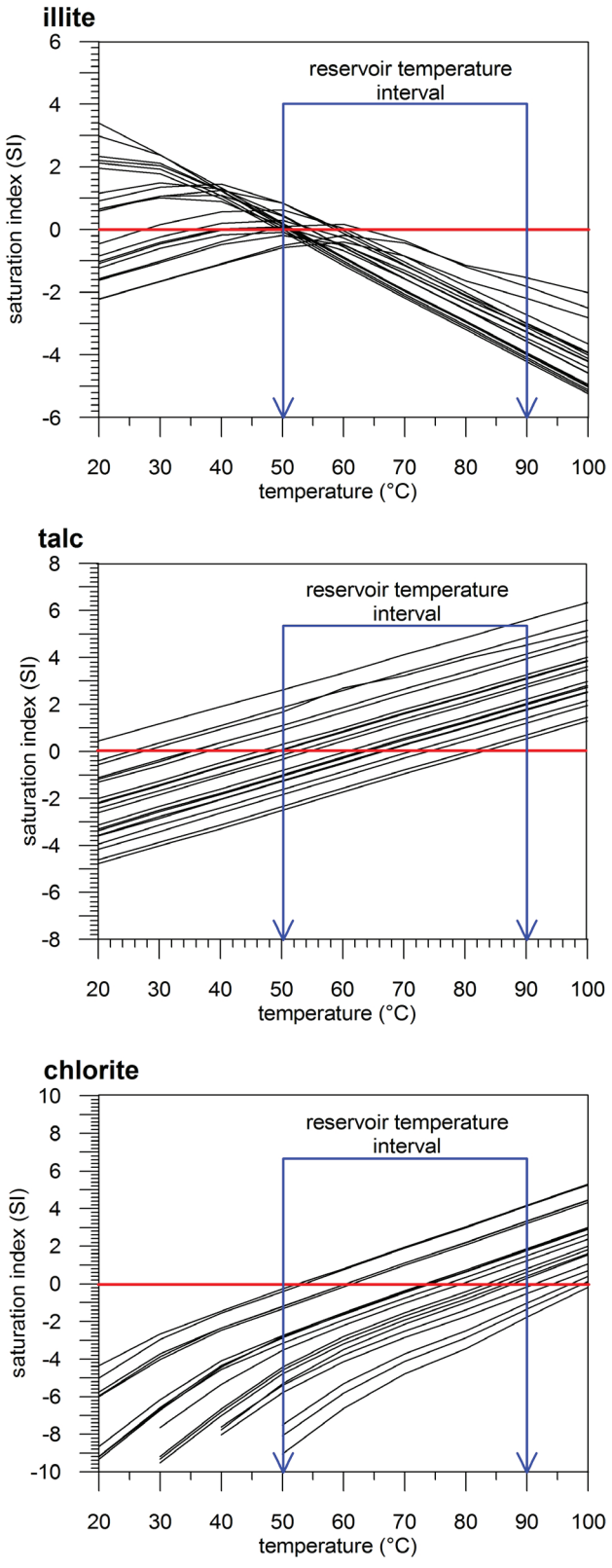

Fig. 24. K-Mg-(SiO_2) alteration assemblage saturation.

the Total Saturation Index – TSI (Cooper et al., 2013). In cited publication, the function is squared (Eq. 57) to search for loss in volatiles and reconstruction of amount of CO_2 degassed. However, if there is no boiling in the reservoir, alternative linear form (Eq. 58) can be used to search for absolute saturation states and yield hints on overall reservoir situation (Fričovský, 2014).

$$TSI = \sum_{i=1}^{n} (SI_i / wt_i)^2 = \sum_{i=1}^{n} \left[\left(\log \frac{Q_{k-i}}{K_{eq-i}} \right) / wt_i \right]^2 \qquad \text{(Eq. 57)}$$

$$TSI = \sum_{i=1}^{n} (SI / wt_i) = \sum_{i=1}^{n} \left[\left(\log \frac{Q_{k-i}}{K_{eq-i}} \right) / wt_i \right] \qquad \text{(Eq. 58)}$$

The (Eq. 57) is square-termed, thus always greater than zero. Temperature is estimated by plotting possible amounts of evaded CO_2 and searching for a function with one minima converging to zero TSI level. Then, the point at which the curve converges the TSI = 0 may be a solid hint on reservoir temperature (Palmer et al., 2014).

This allows to check for accuracy in degassing coefficient evaluation for SI calculations or, reversely, the optimized CO_2 loss may be revisioned by evaluation of degassing coefficient by trial-and-fail procedure while calculating SI of partial assemblage components. Initial CO_2 level estimation helps to reconstruct initial fluid composition prior sampling (if the fluid flashed before the action) or boiling respectively.

Use of linear function (Eq. 57) gives rough estimation of total equilibrium states in the reservoir, and, apparently, gains robust estimation of prevailing undersaturation or oversaturation. A hint on reservoir temperature may be read of the TSI = 0 line interception. Both functions equal for non-boiled, equilibrated waters.

TSI type curve analysis

Linear TSI functions (Eq. 58) are similar to those plotted as SI vs T, grouping number of phases together instead of plotting them individually. An assumption is the equilibration (no boiling, no mixing) of records TSI = 0 interception at narrow (δT_{TSI} < 10 % of T_{btm}-T_{top}) temperature interval and stable shape.

Fluids mixed prior sampling record unstable interception because of various cooling and changed saturation states of particular phase. Vertical reservoir flows cause the re-equilibration due to instable contact with sources of controlling assemblage components, which is of relative effect on thermodynamic activity stability of the phases. Irregularity in shape and wide δT_{TSI} dispersion is a sign of dilution, responding to destruction of initial fluid composition. Reservoir boiling or (uncontrolled) borehole flashing gives TSI curves shifting in total saturation, maintaining one of saturation extremes or distributed irregularly. Yet

vertical resolution in TSI is a function of SI extremes of selected assemblage (Fričovský, 2014).

Quadratic function (Eq. 57) respects possible analyti- cal and sampling errors disqualifying possibility of TSI = 0. The type curve analysis is used rather to evaluate a possible degassing effect as it should be a curve of closest approach to the TSI = 0 line and with one minima and more-or-less concave shape in a solid (e.g. Cooper et al., 2013). Because of squared term, the curve reflects SI by changing a shape or introducing several local extremes.

Upscaling and weighting factors

By definition, SI is a function of reaction stoichiometry (Smith et al., 2012). Both transcriptions defining the total saturation index (Eq. 57–58) are weighted by a factors (wt_i) ensuring all assemblage minerals are considered equally and a TSI (or TSI temperature) estimation is not skewed by stoichiometry (Neupane et al., 2014). Even numerous methods to upscale the total saturation index exist, such as thermodynamic activity, inverse of reservoir alteration frequency etc., the upscaling by thermodynamic components defined in (Cooper et al., 2013) entering reactions is the one used most frequently, still developing continuously (Cannon et al., 2014; Cooper et al., 2013; Neupane et al., 2014).

Application: Weighting factors and assemblage definition

We preferred the approach based on number of thermodynamic components. In that principle, the factor is derived from number of thermodynamic components for i-th mineral and a number of times each component enters dissolution or (equilibrium) ion exchange reaction (Tab. 3) of the i-th solid. This scales up the weighting factors as 1 mole of ion is added into solution (Cooper et al., 2013).

To ensure analysis coincidence, we kept the assemblage selected arbitrary and described in complex equilibrium analysis (Tab. 2). A reason for that is in a simple fact that the use of different assemblage would account different solids, skewing onward interpretations as referring to different equilibration or alteration conditions.

Application: TSI temperature calculation

Even there is no boiling, we used linear and quadratic total saturation index models for temperature estimation. TSI temperature is inferred by TSI = 0 interception for linear, and TSI = 0 convergence for quadratic approach.

Only two samples (Tab. 4) remained oversaturated through the entire interval (T = 20–100 °C), that disqualified them out of representative temperature assessment immediately. The rest has been determined to equilibrate

Tab. 3
Weighted factors calculation for normalized assemblage

Mineral	Thermodynamic components	wt_i
Albite	1* Al, 1* Na, 3* SiO_2	5
Adularia	1* Al, 1* K, 3* SiO_2	5
Anhydrite	1* Ca, 1* SO_4	2
Calcite	1* Ca, 1* CO_3	2
Ca-mont.	1* Ca, 2* Al, 2* Mg, 2* OH, 4* SiO_2	11
Dolomite	1* Ca, 1* Mg, 2* CO_3	4
Fluorite	1* Ca, 2* F	3
Gibbsite	1* Al, 3* OH	4
Chalcedony	1* SiO_2	1
Chlorite	2* Al, 3* SiO_2, 8* OH, 5* Mg, 5* Fe	23
Illite	1* K, 2* Al, 3* SiO_2, 2* OH	8
Kaolinite	2* Al, 4* OH, 4* SiO_2	8
K-mont.	1* K, 2* Al, 2* Mg, 2* OH, 4* SiO_2	11
Mg-mont.	1* Ca, 1* Na, 2* Al, 2* Mg, 4* SiO_2, 2* OH	12
Muscovite	1* K, 3* Al, 3* SiO_2	7
Na-mont.	1* Na, 2* Al, 2* Mg, 2* OH, 4* SiO_2	11
Am. Pyr.	1* Fe, 2* H_2S	2
Talc	1* Mg, 2* OH, 4* SiO_2	7

within T_{TSI} = 72–94 °C. Low coefficient of variation (c_v = 0.682) supports the median temperature T_{TSI} = 79 °C as representative, that corresponds to lower half of the reservoir (Fig. 25).

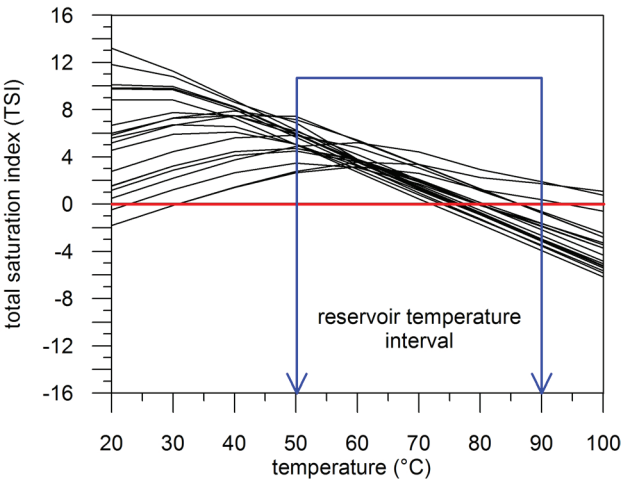

Fig. 25. TSI: linear approach.

Same two samples have been eliminated for squared T_{TSI} analysis (Fig. 26). The method is more sensitive to local SI minima and maxima extremes. In total, 18 samples converged closest to TSI = 0 at T_{TSI} = 69–89 °C (Tab. 4), with a median of T_{TSI} = 74 °C. The difference between both is δT_{TSI} = 5 °C, which is less than 10 % of reservoir temperature coverage interval, forth it is possible to refer the difference to extremes individual phases attain. Henceforth the temperature corresponds to middle/lower half part of the reservoir again.

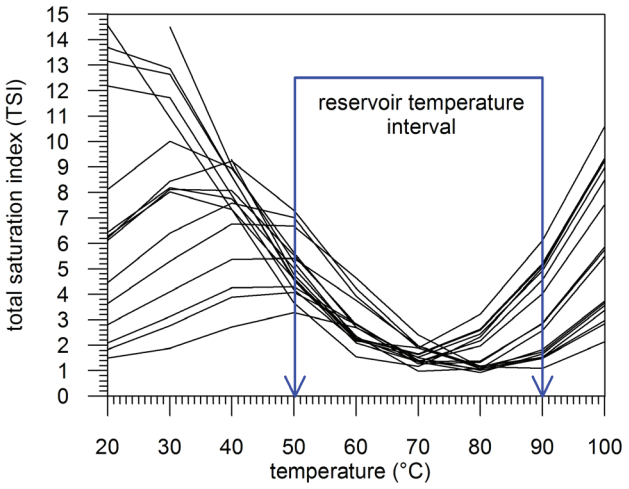

Fig. 26. TSI: quadratic approach.

Application: TSI type curve analysis

Two groups of linear TSI are identified (Fig. 25). Six samples record linear, or quasi linear shape, intercepting the TSI = 0 line with 5 °C dispersion (T_{TSI} = 72–77 °C). The rest equilibrates at T_{TSI} = 73–94 °C, however, records a break in TSI increase at T_{TSI} = 35–50 °C, out of reservoir conditions. Yet no break is observed within the reservoir temperature interval. Moreover, three samples plot some re-equilibration potential at T = 23, 30 and 31 °C.

The reservoir temperature difference between a top and a base equals δT_{res} = 40 °C. If we take the entire group, the δT_{TSI} = 22 °C (> 50 %), that is over tolerance. Uniform run of TSI functions contrast to high δT_{TSI} is indicative of reservoir immaturity. Either a minor change in concentration of major constituents disperses curves out of median TSI. This is proportional to instability in dissolution of macrocomponents, whether it may be due to quasi-isochemical mixing at reservoir intake (= reservoir is sensitive to recharge dynamics) or due to intraformation mixing between residential and vertically filtrating waters (= reservoir is sensitive to rate of convection). Stability is indicative of no boiling environment.

The use of squared function determined a convex (linear TSI) and sinusoidal (linear with break below 50 °C) lines. The number of samples per group equals to distribution of linear analysis (Tab. 4). The break, which gives the sinusoidal shape realizes at T_{TSI} < 50 °C, similar to linear

Tab. 4
Multicomponent equilibrium comparison

Approach	z21/2/1987	z4/3/1987a	z4/3/1987b	z5/3/1987	z6/3/1987a	z6/3/1987b	z7/3/1987	z22/3/1987	z31/3/1987	z2/4/1987	z3/4/1987	z20/2/1992	z12/11/2007	z17/12/2008	z18/2/2008	z26/2/2009	z30/3/2011	z13/4/2011	f15/3/2011	f30/3/2011
CEQ	56	65	74	–	72	79	–	67	70	65	71	63	65	68	56	61	60	62	75	75
TSI (L)	72	76	94	–	81	86	–	78	80	80	80	77	74	80	74	76	77	77	86	86
TSI (SQ)	70	71	89	–	81	89	–	73	79	80	80	70	70	75	69	70	69	70	80	80
RMED	80	50	30	–	60	80	70	80	–	80	–	30	50	80	50	60	60	–	80	80
n-RMED	2	7	7	–	4	6	1	6	–	2	–	2	8	7	6	10	10	–	13	9
L-TSI T	L	A	A	A	A	A	A	A	A	A	A	L	A	A	L	L	L	L	A	A
SQ-TSI T	V	S	S	S	S	S	S	S	S	S	S	V	S	S	V	V	V	V	S	S

Explanations: n-RMED – number of equilibrated phases; L-TSI T – linear type curve; SQ-TSI T – squared type curve; L – linear shape; A – concave (break) shape; S – sinusoidal shape; V – convex shape

analysis. The variation in convergence δT_{TSI} = 20 °C narrows compared to linear analysis, however, still equals 50 % of reservoir temperature interval. We add the difference is just as sensibility of the method increases towards saturation extremes, meanwhile supporting previous interpretations.

Clustered saturation indexes approach (RMED)

Optimization procedure

The MEG analysis and reservoir temperature estimation is clearly a function of selected mineral assemblage, either set arbitrary, or by numerical optimization (Spycher et al., 2014). Saturation indexes of a wide assemblage are normalized by a weighting factor (e.g. Cooper et al., 2013) and calculated against desired temperature interval. First itineration eliminates the phases which SI does not converge to 0.05 in absolute over the analysed range. Then, a median of SI (RMED) is calculated at each temperature step, normalized by a factor of 1.2. The suite to calculate temperature of overall equilibrium is narrowed by ignoring those solids violating SI ≤ /1.2RMED/. This eliminates skewing of TSI calculation, finally the reservoir temperature (T_{RMED}) is inferred from that of minimum median of absolute SI, yielded by residual phases – suite (Spycher et al., 2014).

Application: Assemblage upscaling

Similar to previous methods (CEQ, TSI), we decided to analyse the primary-alteration-hypothetical assemblage selected before to ensure conceptual homogeneity for onward correlation and analysis. Saturation indexes are, analogously, weighted as according to Tab. 3. The assemblage has been eliminated with calcite and muscovite, both not reaching $-0.05 < SI < 0.05$ throughout the reservoir temperature interval. Later upscaling itinerations have been conducted individually. The Ca- and Mg- montmorillonites were disqualified as most (Tab. 5), whilst chlorite, chalcedony and gibbsite were involved in each calculation.

Application: Upscaling implicatons

Elimination of calcite is more or less expected, as thermal waters simply must be oversaturated with calcite (Fig. 19) even before intake into the reservoir zone. The oversaturation to calcite, simultaneous to a permanent contact with a source rock is then one source of excess CO_2 in deep reservoir waters. As thermal waters are hosted in impure limestones and dolomites (and their transient forms) at low enthalpy conditions, the oversaturation with muscovite (Fig. 15), restraining its reaction activity, allows us to assume the LT alteration of siliceous (detritic) dolomites, which does not involve the metamorphic ion-exchange reactions, but activates talc, produces Mg-calcite and increases CO_2. Muscovite oversaturation consumes the SiO_2 and available Mg^{2+} into chlorite alteration. Yet chlorite and talc record confident equilibration. Their declining saturation tendency (Fig. 24) with decreasing temperature aids the process. With the use of this approach, the dolomite equilibrates well at T < 50 °C (80 % of equilibration records of $SI_w \leq RMED \cdot 1.2$), which corresponds to initial conception and assumption on some Mg-calcite precipitation while fluid experiences lateral leaking or vertical evasion, maintaining high CO_2 level at reservoir outlet, restraining balanced Na/K alteration (Fričovský and Tometz, 2014). Indeed, even with upscaled saturation, albite and dissociated Na-silicates are rather consumed to form illite or maintain muscovite uptorn, at least upon reservoir outlet.

Tab. 5
RMED summary table

Phase	Eliminations	Preferential RMEDx1.2 record	Preferential T_{RMED} contribution
Adularia	3	50	50
Albite	6	40	30
Anhydrite	18	20	20
Calcite	20	–	–
Ca-mont.	13	80	80
Dolomite	6	40	50
Fluorite	5	90	80
Am. pyrite	4	50	60
Gibbsite	0	60	60
Chalcedony	0	70	80
Chlorite	0	80	80
Illite	1	50	50
Kaolinite	1	80	80
K-mont.	3	70	80
Mg-mont.	11	80	80
Na-mont.	2	70	80
Talc	1	60	60
Muscovite	20	–	–

The other reason for inequilibration of albite–adularia system is relative good correlation of Na- and K- montmorillonites (or their activity coefficients), optionally controlling reservoir Na^+ and K^+ hydrolysis. Some loss in

CO_2, due to the precipitation of calcite and Mg-calcite, or because of consumption for talc activation, can not compensate its oversaturation referring to the Na/K system. Obviously, the rate of Na/K immaturity is a function of adularia-albite inequilibration, proportional to excess CO_2 level, supporting an idea of immaturity relation to dissociation of carbonates, but to low grade alteration of detritic (or impure) dolomites as well. Carbonates are deficient in alkalis, forth the metamorphis intensity depends on a water-rock contact with separate horizons containing siliciclastics. Instability of the water-source interaction relates then to variable vertical filtration. The deep reservoir is off any conditions for intrinsic convection. However, because of unconform base overheating, there are separate convection cells formed within, even not covering the entire effective profile. It is just obvious then that all reservoir reactions, whether do or do not producing CO_2 are a function of induced convection and so to the mass movement controlling final equilibration or re-equilibration. Further on, the rate of immaturity and inequilibration in Na/K relates explicitly to the rate of reservoir convection extension (vertical thickness, lateral impact), duration (vertical filtration velocity), and intensity (bulk mass movement).

Application: RMED temperature (T_{RMED}) calculation

Because of "hands on" elimination, we carried computations in 10 °C intervals, forth the real extension of inferred temperature is of $T_{RMED} \pm 5$ °C coverage. In total, 16 samples equilibrated according to RMED approach. The inferred temperature varies in $T_{RMED} \approx 30 \pm 5$ °C – 80 ± 5 °C interval, with medium (representative) temperature of reservoir equilibration at $T_{RMED} = 65$ °C (the average $T_{RMED} = 64$ °C). This is fairly similar to temperature of complex equilibration ($T_{CEQ} = 66$ °C), but is still less than that of total saturation index ($T_{TSI} = 79$ °C). The T_{RMED} versus T_{CEQ} similarity is fairly coincidental. With RMED, both most samples equilibrate and most equilibration records are observed for $T_{RMED} = 80 \pm 5$ °C (Tab. 6), which is, however, close to the temperature inferred by TSI. The consistency here is due to idem upscaling (weighting factors) application (Tab. 4).

Ternary chloride mixing model

Use of thermodynamic systems based on two or three components has been adopted within the Na-K-Mg (Giggenbach, 1988) and K-Mg-Ca (Giggenbach, 1986; Giggenbach, 1988) geoindicators. Both do, however, target the equilibrium temperature of initial spring and fail to provide relevant results while analysing mixed samples. Such samples are, however, rather scarce.

The ternary mixing model geoindicator expects the sampled water is a solution of parental and shallow thermal or cold groundwater, which is of some relation to aqueous chloride (Cioni et al., 1992). Then, constituents involved in particular geothermometers are regressed to the chloride. If their concentrations are fixed by primary

Tab. 6
T_{RMED} summary table

Temperature (°C)	Adularia	Albite	Anhydrite	Calcite	Ca-mont.	Dolomite	Fluorite	Am. pyrite	Gibbsite	Chalcedony	Chlorite	Illite	Kaolinite	K-mont.	Mg-mont.	Na-mont.	Talc	Muscovite	n-RMED	T_{RMED} contribution records
100	–	–	–	–	–	–	1	–	–	–	–	–	–	–	–	–	–	–	1	1
90	–	–	–	–	–	–	–	–	–	–	–	–	–	–	–	–	–	–	0	0
80	2	–	–	–	3	–	5	2	3	6	7	1	7	3	5	3	1	–	13	48
70	–	–	–	–	–	–	–	–	1	–	–	–	–	–	–	–	–	–	1	1
60	3	1	–	–	–	1	–	3	4	2	2	3	2	2	–	2	2	–	12	27
50	5	4	1	–	–	2	1	1	4	1	2	4	–	–	–	–	1	–	11	26
40	–	5	–	–	–	–	–	–	–	–	–	–	–	–	–	–	–	–	1	5
30	–	–	–	–	–	–	–	–	–	–	1	–	–	–	–	–	–	–	1	1
20	1	–	2	–	–	1	–	1	–	–	–	–	–	–	–	1	–	–	5	6

water–cold water mixing, their concentrations (cX) should fit a straight line and a simple linear regression should be obtained (Eq. 53).

$$cX = a \cdot cCl \pm b \quad \text{(Eq. 53)}$$

where "a" and "b" are coefficients of linear regression, while concentrations are in various units.

Still, if there is not any linearity between aqueous concentrations and mixed water with dilutant, other forms may occur. This is for example a case of irregular and unbalanced mixing. Linearity destruction may be of supplementary proof on no-mixing relations between selected geothermal–coldwater pairs.

Regressed concentrations are inserted into geothermometry functions (Antrodicchia et al., 1985; Marini, 2004). For these, at least necessary conditions of conceptual model, which is in control of particular geothermometer, must be met. Besides a silica geothermometer, various validated, and reasonable cation geothermometers may be included, such as that of Na/K (Eq. 55) and K-Mg (Eq. 56) as it is examined in (Chiodini et al., 1996; Marini, 2004):

$$T_{SiO_2}(^{\circ}\mathrm{C}) = \frac{X}{Y - \log(a.Cl \pm b)} - 273.15 \quad \text{(Eq. 54)}$$

$$T_{Na/K}(^{\circ}\mathrm{C}) = \frac{X}{Y \pm \log(a.Cl \pm b) - \log(a.Cl \pm b)} \quad \text{(Eq. 55)}$$

$$T_{K/Mg}(^{\circ}\mathrm{C}) = \frac{X}{Y - \mathrm{Z} \cdot \log(a.Cl \pm b) - \mathrm{W} \cdot \log(a.Cl \pm b)} \quad \text{(Eq. 56)}$$

where "X", "Y", and "Z" are generalized constants for SiO_2, Na/K and K-Mg geothermometers derived by different authors and Cl^- concentrations are in attributable units.

In next step, all temperatures are calculated for increasing chloride and plotted against it (Marini, 2004). If the fluid is in overall equilibrium, all functions converge some point, from that drawing a horizontal line onto Y axis gives an estimate of parental (primary) thermal water component, whilst a vertical line onto X axis gives an initial, reservoir chloride concentration at overall equilibrium (Chiodini et al., 1996). Admittedly, the given temperature must be validated due to a conceptual model of a system. If ternary function does not give any interception point, it is a sign on disequilibrium. However, geothermometry functions may intercept at a temperature that is far of reasonable, which must be interpreted immediately. Most probably, discrepancy in temperature to that expected in the reservoir is of error in magnitude of fluids disequilibration to one or more selected geothermometers.

A key advantage of a model is that functions of solute geothermometry may be, if validated, substituted by other geothermometers (Antrodicchia et al., 1985), such as isotopes or multicomponent equilibrium functions (Fričovský and Tometz, 2014), or involving a conservation enthalpy function (Cioni et al., 1992).

Application: Ternary combination approach

The selection of samples requires, at least, some record on affinity to parental reservoir fluid, besides the mandatory condition of mixing character. In local conditions, the parental endmember is considered the DRTE. Waters sampled at VSH-1 has been assigned as mixture according to geothermometry (this paper) and geochemical indicators (e.g. Fričovský and Tometz, 2013; Fričovský et al., 2015). Groundwaters, representing a dilutant, must be facially relative to the site. We used cold springs from southern margin of the Liptov Basin. The most important is, however, a controlling thermodynamic system selection, represented by most reliable geothermometers. To meet this condition, we used chalcedony geothermometer GSC3 (Fournier, 1991), in combination with GKM3 K^2/Mg model by (Giggenbach, 1988), and GLM $Li/Mg^{0.5}$ function (Kharaka and Mariner, 1989). Coupling of these refers to chalcedony control on dissolved SiO_2 in thermal waters, which try to equilibrate with K-Mg silicates by adapting the CO_2 cycle during lateral or vertical evasion from the reservoir, meanwhile conserving Li^+ concentration restraining its reaction with clay minerals.

Application: Deep reservoir analysis TCLM (with VSH-1 samples)

The TCLM plot of VSH-1 samples over increase in chloride shows no ternary convergence, either because of secondary dilution or involvement of more than one thermal water component in the mixture (Fig. 27). The SiO_2 – Li/Mg pair intercepts at $T_{TCLM} \approx 70$ °C. Low K^2/Mg ratio slips the GKM3 evolution with chloride down, converging with GSC3 at $T_{TCLM} \approx 30$ °C. The dispersion is rather due to high Mg^{2+} and some K^+ deficiency. Supposed magnesium consumption by activation of talc, chlorite alteration and Mg-calcite precipitation must be then compensated by additional Mg^{2+} from dilution. The GSC3/GLM interception is rather a sign of lithium concentration conservation, with minor enrichment only (if any). Definitely, the lithium is not added into solution by the ion exchange reactions.

Let that be the conservation of Li^+ from parental (DRTE) reservoir. The lithium clays are not able to form, as SiO_2 and Al^{3+} is consumed in Na-silicates transformation to K-micas (at least in terms of thermodynamic activities). Then, the Li^+ addition should be by dilution (S-CGW facies form in siliciclastics rich IWCP) or mixing with SRTW, at permanent contacts with IWCP or Jurassic/Mid Cretaceous succession. Either way, lithium clays may be conserved, dissolved, but do not enter the ion exchange reactions.

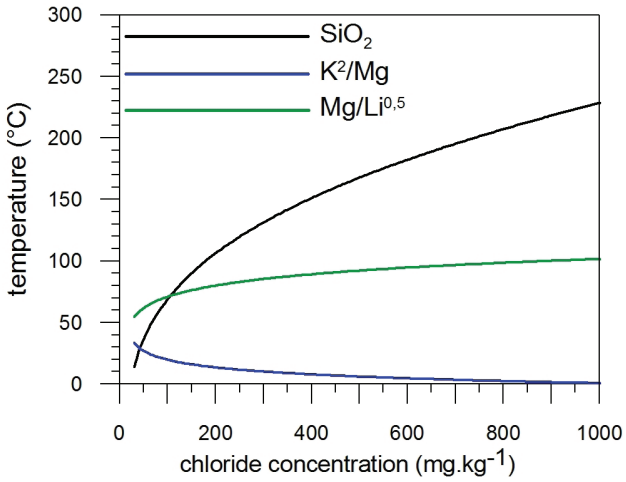

Fig. 27. TCLM analysis for DRTE/VSH-1 facies relation.

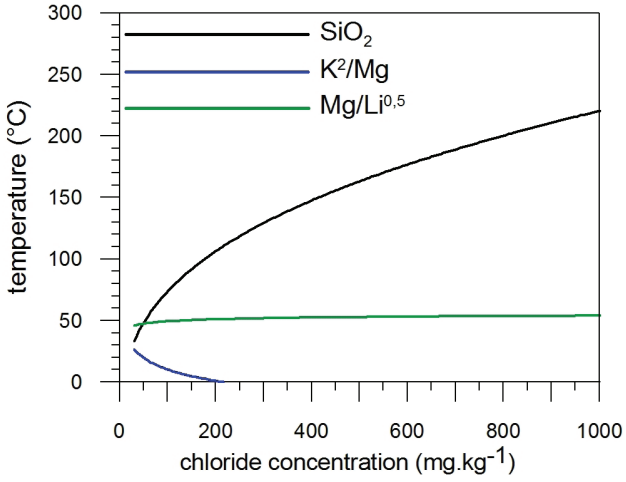

Fig. 28. TCLM analysis for DRTE/SRTW facies relation.

Application: Deep reservoir analysis (with BEH-1 and FBe-1 samples)

To verify secondary origin of the shallow reservoir, assuming mixing of parental DRTE waters with recharged (residential) waters, we let the BEH-1 and FBe-1 waters cool with springs from the Kľačianka valley. Excess SiO_2 in combination with low K/Mg ratio restrain the GSC3/GKM3 to intercept (Fig. 28). If we refuse some amorphous silica solubility activation at lower temperatures, the additional SiO_2 source must come from sufficient source, which is rather the IWCP (Borové Fm.), or Jurassic–Mid Cretaceous succession at a base.

As we have already discussed above, other SiO_2 source is fair to assume in the IWCP formations, that distinguished both subfacies in the SRTW (SiO_2 deficient BEH-1 and SiO_2 sufficient FBe-1). Neither Mg^{2+} deposition due to dolomite precipitation, nor its consumption in talc activation balances the Mg^{2+} enrichment by possible mixing (dilution) within shallow reservoir, or its simple increase by the local dissolution of dolomite from the host rock (expecting DRTE waters to get undersaturated to dolomite). All processes restrain equilibrium attainment to the K/Mg. The Li^+ concentration within shallow reservoir is more or less constant in time, compared to the deep reservoir. Convergence of GSC3/GLM gives a temperature estimate of $T_{TCLM} \approx 50$ °C, which corresponds to deep reservoir evasion temperature and may be a sign of conservation of lithium during vertical evasion, as with decreasing temperature, the activity to dissociate lithium clays decreases rapidly.

SUMMARY – CONCEPTUAL SITE MODEL UPDATE

First CSM models were developed in the late 1970s to conclude research of mineral in early (Zbořil et al., 1972; Franko et al., 1974) and shallow thermal waters of the Liptov Basin in a latter stage (Franko et al., 1979; Zembjak et al., 1982). A consensus on open hydrogeological character identified central discharge zone by travertine accumulations analysis in the Bešeňová vicinity (Franko et al., 1974), assigning the dome formations to thermal waters stored in deep reservoirs below. Drilling campaigns (Franko et al., 1979; Fendek et al., 1988) revealed stratified character of the accumulation zone. Numerical modelling (Fendek et al., 1988) and spatial piezometry analysis (Remšík et al., 1993) speculated the thermal waters to intake deep in permeable structures from the east (Liptovská Mara Depression), and leak laterally towards west after transition and some residency in central parts of the system. The open character of the structure has been proven continuously in time by total discharge analysis (Remšík et al., 1998), pumping tests (Vandrová et al., 2011), lumped parameter modelling (Fendek et al., 2013), or reservoir response analysis (Fričovský et al., 2014).

Geochemical methods paid favour onto geochemical origin and mineralization type (Franko et al., 1979; Fendek et al., 1988; Bodiš and Borosová, 1996), not much clearing up a contention on primary recharge zone position between the Lúčky area or the northern slopes of the Nízke Tatry Mts. The latter has been evidenced by isotope elevation analysis (Franko, 2002a, b). Application of boiling and mixing models (Fričovský and Tometz, 2013) provided more support to the assumption, emplacing the recharge zone to the Kľačianka valley area, that is in confidence with hydraulic (Fendek et al., 1988; Fendek et al., 2013), stationary temperature (Fričovský, 2014), dynamic hydrogeothermal (Fričovský et al., 2014) and reservoir response (Fričovský et al., 2015) models.

Application of several geothermometry techniques presented an ample scale of models and hypotheses, which is a must to interpret complexly for a CSM construction. In past, geothermometry has not gained a solid tribute, relieving importance of saturation (equilibrium) analysis methods by a few constraints on its inadequacy in local, low temperature, carbonate environment. An initial con-

ceptual model of simple infiltration, downflow transition and accumulation, with later westward expelling should then be, modified, as both, macrochemistry (boiling and mixing models) and geothermometry, aided with thermodynamic microanalysis, give some evidences on several mixing episodes, the primary model does not account.

Infiltration zone model

It is a must to pronounce the infiltration, based on spatial analogy and lithological homogeneity in seeping conditions, as there is no well available. Some indices on geochemistry of waters in early transition stages may be derived of springs and shallow wells in the valley, however, early infiltration stages taking part in prior must be assumed by lithology in a major.

We use the Rudolf well, LM springs (warm) and adjacent cold springs (e.g. Bočný prameň, pod Bielym etc.) to derive a model of the infiltration zone (Fig. 29). Previous studies (e.g. Franko, 1984; Fričovský and Tometz, 2013) localized the infiltration zone to the Kľačianka valley. The Rudolf and LM springs are analogized to represent early infiltration/transition facies, recording transient Ca-Mg-HCO_3-SO_4 type. By lithology, the only possible source of sulphate acquirement is the Late Triassic, found in the hydrogeological massif of the Nízke Tatry Mts. Application of Mg-correction (Fournier and Potter, 1979) to the T_{NKC} (Fournier and Truesdell, 1973) yields overrated temperatures, implying excess Mg^{2+}, that can not simply be adjusted to oversaturation with Mg-carbonates. This is, moreover, accented by positive T_{NKC} – pH correlation for springs pointing to various Mg^{2+} and Ca^{2+} source.

We prefer hypothesis based on two flow channels; a deeper one off the Nízke Tatry Mts. in deep and relatively slow circulation controlled by fissured and karst-fissured permeability, and the shallow one associated with fast downflows along a fissure swarms at the periphery of the basin. Both mix together at the periphery in TCM (thermal-cold-mixing) regime, satisfying excess Mg^{2+} objection and relatively stable Na/K ratio compared to cold springs by reciprocal leaching of Na/K silicates, not destructed by CO_2 saturation at this stage.

By the excess Mg^{2+}, the mixing rate is over 50 %, which is, in fact, a partial dilution. The TCM is then objected to realize prior differentiation for downflow (transition-accumulation donation) and upflow (springs upwelling) regime. Indeed, there is a difference between cold and warm springs in pH. Then, the mixing must realize in CHN Mid Triassic carbonates or KNA Jr-Cr2 succession (satisfying stable Na/K ratio).

Transition zone model

The entire structure of the Bešeňová elevation is considered open in hydrogeological regime referring to both reservoir zones. To satisfy this objection, recharge must be supplied in at least two effective profiles, separated spatially and horizontally. This calls the transition zone to split for a shallow and deep channels, obviously just after a short period of conjoint submersion off the infiltration zone.

Shallow transition/shallow recharge channel

Comparison of facies defined by wells and springs from the infiltration zone with the shallow reservoir (BEH-1, FBe-1): At an early stage, the transition realizes in weathered or fissured upper zone of the Jurassic–Mid Cretaceous KNA horizon, involving dissolution of limestones primary. Increase in Na/K reflects partial temperature build-up and decrease in filtration velocity prior effective inflow into shallow reservoir that allows preferential Na^+ leaching out of Jr–Cr2 bedrock. Releasing of K^+ from silicates in the IWCP is obviously less intense. A slow transition in silica metastability from the LT opal to chalcedony regime gives a supportive proof onto decrease in filtration velocity with depth and distance from the infiltration zone, maintaining a contact with silicates-dominated environment (Fig. 29). Still, there is no sign of equilibrium attainment with carbonates, which dissolution alternates spatially. While dissolution of limestones realizes in early shallow transition stage (increase in Ca/Mg ratio) within Jurassic–Mid Cretaceous succession, this is soon altered by dissolution of impure dolomites from the Borové Formation and the CHN Mid Triassic dolomites (decrease in Ca/Mg ratio).

Deep transition/deep recharge channel

A model of deep transition is interpreted by comparing infiltration zone and deep reservoir facies (FGTB-1, ZGL-1), analogously to previous. Obviously, Na-silicates are dissociated from the Jurassic–Mid Cretaceous horizon preferentially along with calcite. By decrease in absolute CO_2 content between infiltration and accumulation/reservoir production zone, along with a better fit of pCO_2 related to dissociation of Ca-silicates (hypothetical phase), derived of the K-Mg-Ca geoindicator (Fig. 18) saturation of submerging thermal waters with calcite must take part before effective inflow to the production zone (CO_2 is consumed in activity and saturation variation in the deep reservoir variation). Preferential (primary) saturation with respect to calcite during downflow projects into equilibration with an average crustal rock by acquiring Ca^{2+} on the Na-K-Mg-Ca plot (Fig. 21). Qualitative Na/K geothermometry analysis (Figs. 10 and 11) defines the Na^+ and K^+ addition of preferential rock leaching origin. Decrease in Na/K ratio with the depth and temperature reflects aggressive CO_2 accretion during submersion (or at least its conservation from the infiltration zone), supplied through a

contact with carbonates of variable impurity, progressively setting on a modification or restriction of easily leached albite into K-silicates.

An initial, transient type chemistry (Ca-Mg-HCO_3-SO_4) may be partially altered towards Ca-Mg-SO_4-HCO_3, acquiring some SO_4^{2-} at a contact with Late Triassic horizon and Carpathian Keuper shales and slates during downflow, modifying peripheral character of recharges towards immature. Attaining, or conserving the transient character supports then an assumption of quasi-isochemical mixing with residential thermal waters at an effective inflow towards production zone, implied e.g. by high $\delta T_{TSI} = 0$ dispersion (Figs. 25 and 26).

A presented model is based on geometry of the structure and interpolation of records between both production zones and infiltration area. Probability of identified processes is than a matter of uncertainties of the CSM.

Deep reservoir (accumulation/production zone) model

CSM for the deep reservoir (Fig. 30), referred as to Mid Triassic carbonates of the Krížna Nappe, is constructed as based on results of geothermometry and essential mixing models applied to samples of the ZGL-1 and FGTB-1 well, with simultaneous comparison with the infiltration zone to respect a conceptual histories of samples.

The deep reservoir is all but homogeneous referring to its vertical profile (already documented on both production wells), hydrogeochemistry and intraformational processes. The effective inflow realizes most probably towards base. Because of similarity in a macroscale (deep reservoir basal facies and recharges are of Ca-Mg-HCO_3-SO_4 to Ca-Mg-SO_4-HCO_3), the inflow is most probably of quasi iso-chemical TTM (thermal-thermal-mixing) regime. However, the velocity of submerging filtration controls initial intake geochemistry, that is definitely not constant. A sensitivity to recharges is then documented through a dispersion of $\delta T_{TSI} = 0 > 50$ % of the reservoir range (Figs. 25 and 26). Apparent similarity in TDS content and geochemistry type between reservoir zone recharges and residential waters plots as quasi-logarithmic distribution of samples on the silica – total carbonate model (Fig. 7), where the organization of the population follows the SiO_2 – CO_3 equilibrium function (by Arnórsson, 1985) trend, departed towards no-boiling region due to general silica lows.

Discussion on reservoir convection

In previous, the studies took the deep reservoir as a relatively homogeneous aquiferous body of "simple" tectonics bound vertical evasion towards surface, referring to the transition/accumulation zone. Yet already (Fričovský et al., 2014) presented an idea of minor convection as based on reservoir base overheating analysis, inferring formation of isolated convection cells of various spatial extension. Application of the reservoir geothermometry and thermodynamics (this paper) reveals, however, several more indices to combine with initial hypothesis.

A domestic convention on silica geothermometry inadequacy gainsays its principles in essence. Let the reservoir carbonates be impure (siliciclastics intercalations, beds, lenses, grains) and limited in spatial extension. A variation in absolute SiO_2 (Fig. 4) gives a fair evidence on instable contact of samples with its source (stable accommodation

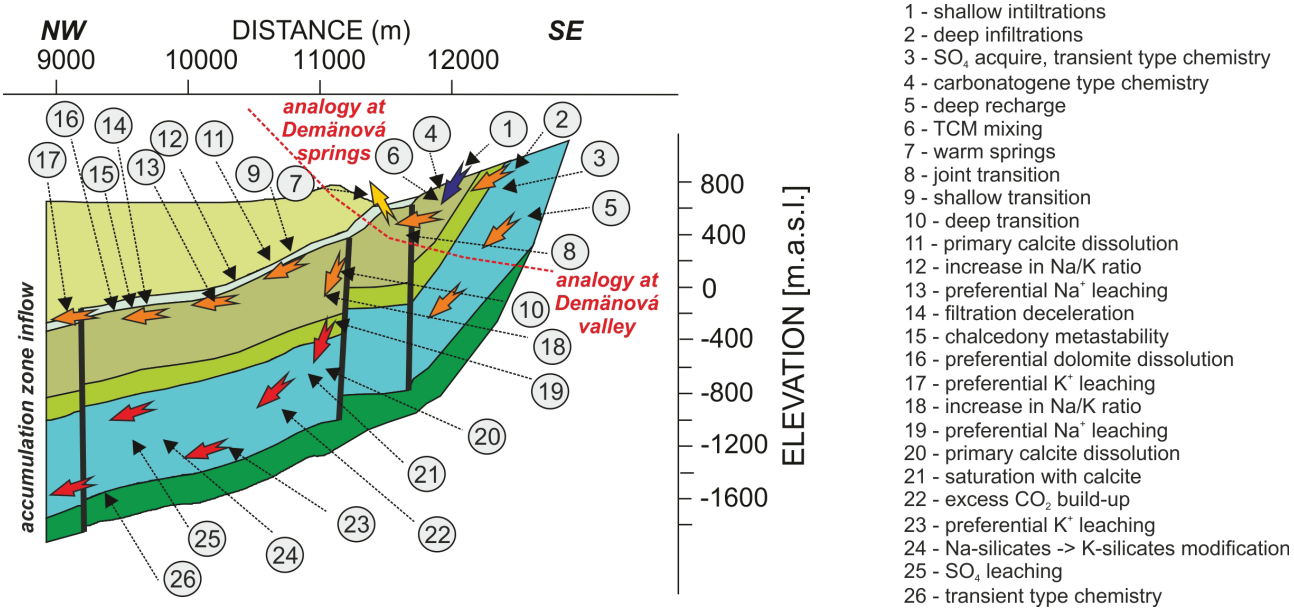

Fig. 29. Infiltration and transition zone CSM. For its localization see Fig. 1.

in reservoir positions would result just in SiO_2 lows), projected consequently onto quantitative temperature estimations (Appendix D).

A most vivid evidence on some vertical mass movement in the reservoir is provided by a use of K-Mg-Ca geoindicator (Fig. 18) or geobarometer (Giggenbach, 1988). The model reveals the reservoir partial CO_2 off a range to induce a calcite precipitation, thus its saturation realizes already in downflow to the production zone. In details, variations in pCO_2 are equal to differences in the L_{kc} and L_{km} functions (Eq. 47). This is because reservoir Mg^{2+} varies (e.g. according to Mg-SiO_2 alteration system analysis, Fig. 13) along with the Mg/Ca ratio, resultant to instable saturation of thermal waters with respect to carbonates during a consistent contact with a source rock. The variation must than be an effect of even minor changes in temperature and pressure, possible only through intraformation vertical movements.

In combination to base overheating implications, thermal waters partially enter separated and spatially limited, insulated convection cells, however, through the entire vertical profile of the body because of building up a density and p-T gradient between its top and a base, as the latter is heated unconformly.

Discussion on carbonates equilibria

The entire geothermal structure is predominantly hosted in carbonates. These are involved in the infiltration and transition zone, even variably impure, or as a compound of calcareous pelites and sandstones. In reservoir positions, dolomites prevail over limestones, along with the occurrence of transient and impure or intercalated forms.

Application of the K-Mg-Ca geoindicator (K-Ca-pCO_2 geobarometer) baffles expectations of CO_2 regime by assigning the CO_2 fugacity to Ca-alumosilicates hydrolysis. This is not possible in local conditions. In other words, the notice points to saturation of thermal waters with calcite (Fig. 19) prior effective intake into reservoir (production zone) position. Then, because thermal waters become saturated with calcite, samples organize towards an equilibrium with a wallrock (Na-K-Mg-Ca model, Fig. 21) by preferential dissolution of dolomite, increasing the Mg/Ca ratio continuously. However, thermal waters become oversaturated with dolomites soon, maintaining a contact with a source (Fig. 20). Onset of induced convection causes unit variation in saturation of carbonates. Because of a stable contact with a source rock, the unit of carbonate which has precipitated due to change in temperature and pressure in the vertical upflow is subsequently replaced by a unit dissolved in a downflow. This produces an excess CO_2 towards reservoir base, controlling immaturity of thermal waters by restraining a principal, Na-K, K-Mg and Na-Mg thermodynamic subsystems equilibrium attainment.

Discussion on silica regime

A silica regime has not been subjected to detailed analysis in previous. At deep reservoir conditions, use of saturation stability analysis (Fig. 4) records unbalanced distribution of records between conductive quartz solubility, chalcedony and LT opal polymorphs. At a given tem-

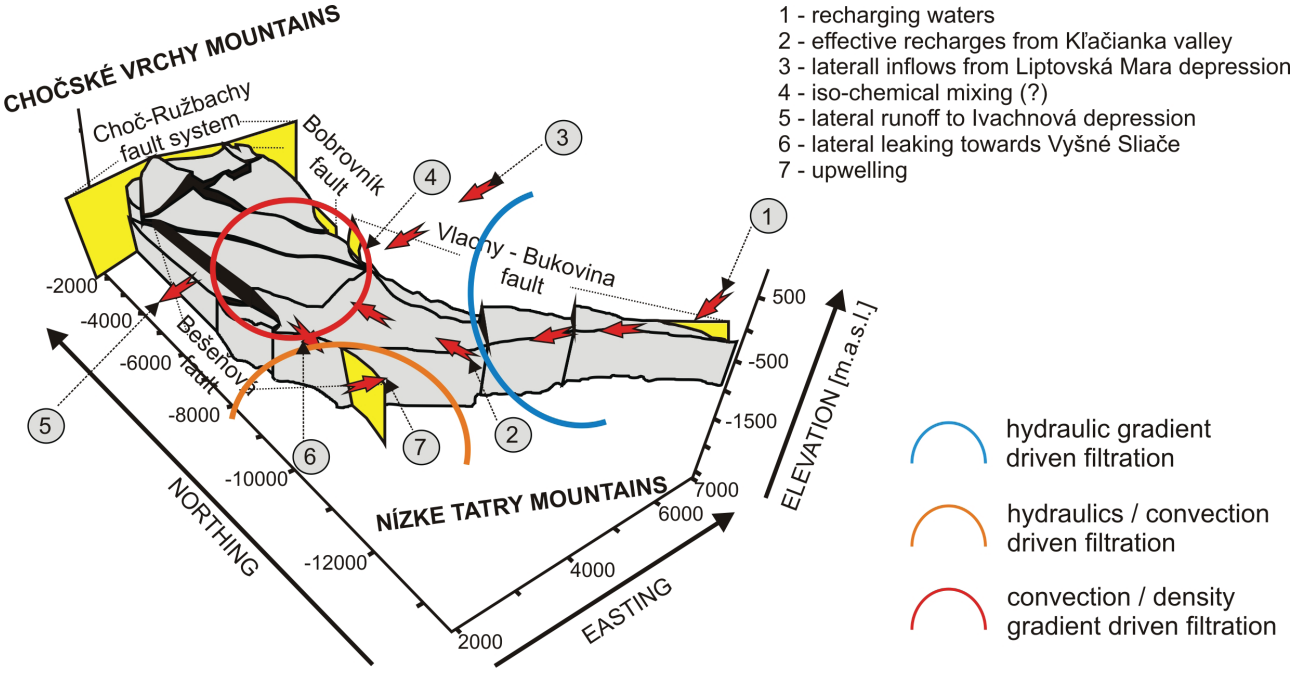

Fig. 30. Deep reservoir mass movements controls.

perature range, the variation is rather assigned to uneven silica content due to instable contact with its source. At deep reservoir conditions, chalcedony becomes metastable and in control on reservoir aqueous silica content (Fig. 5), attaining equilibration with a median of $T_{SI = 0} \approx 67$ °C. Application of silica geothermometers yielded reasonable results for chalcedony as well with median for conductive cooling models of T ≈ 75 °C. We assume the difference is not only a record of various sensitivity of functions to the dissolved silica content, but due to the instable contact of samples with a silica source and reaction time as well.

If the chalcedony becomes saturated, it is possible that some dissociated H_4SiO_4 becomes available for onward alteration of silicates. In vertical filtration regime, only a minor part of chalcedony can be deposited by a drop in p-T conditions, rather more is incorporated into Na/K silicates alteration and chlorite-talc activation.

Contribution to deep reservoir hydrochemical regime

Reservoir hydrochemical regime is controlled usually by primary lithology, temperature, pressure and residential period of thermal waters in the structure. In carbonates-hosted environment, a fluid saturation and available CO_2 plays a crucial role. Thermal waters of the deep reservoir are deficient in absolute Na^+ and K^+ content, expectable under insufficient source conditions. Compared to infiltration zone, the Na/K, K/Ca and K/Mg ratios decrease dramatically by conservation of absolute alkali concentrations and increase in Ca^{2+} and Mg^{2+}.

Application of Na/K qualitative geothermometry records samples organized in the rock dissolution region (Fig. 10) away of any alteration equilibration (Fig. 9), causing quantitative estimates (Appendix E) overrated. Under high CO_2 content, the inequilibration reflects modification of Na-silicates into K-silicates, restraining albite equilibration while increasing adularia, illite and muscovite activity. While complex equilibrium of albite (9/18 samples) is roughly of T_{CEQ} = 30–46 °C, adularia equilibrates at T_{CEQ} = 40–65 °C.

The immaturity of reservoir fluids (MI = –0.1–0.4; Fig. 16) is promoted by easier activation of Na- and K- montmorillonites (Tabs. 5 and 6), reaching equilibration (even in a magnitude of equilibration activity) with the reservoir fluid. Excess CO_2 and muscovite activity (Fig. 15) allows LT alteration of impure siliceous reservoir dolomites not involving metamorphic ion exchange reactions, but with LT talc activation, secondary Mg-calcite, calcite and CO_2 production. The incoming CO_2 is available to contribute further on a unit-scaled calcite – dolomite – Mg-calcite dissolution/precipitation cycle during reservoir convection.

These processes are controlled by equilibration temperature and depth. The talc equilibrates at T_{CEQ} = 65–70 °C and T_{RMED} = 60 °C preferentially (Tabs. 2 and 5). The chlorite records a balance in equilibration constant and thermodynamic activity at T_{CEQ} = 70–75 °C and T_{RMED} = 80 °C with some preference. Then, the excess Mg^{2+} in the reservoir is assumed to persist up to 50–60 °C, which corresponds to upper reservoir zones, maintaining low K/Mg and Na/Mg ratios (Fig. 31).

Both carbonates tend to precipitate in evasion regime, simultaneously allowing some equilibration of alkalis with consumed CO_2 as a rate of Na-silicates modification decreases proportionally. Under given trend between DRTE and SRTW (1) at Na-K-Mg-Ca geoindicator (Fig. 21), Mg-calcite is lost more intensively as the fluid breaks a contact with a source rock.

Discussion on deep reservoir adiabatic boiling

A boiling as one of crucial reservoir dynamics has been studied simultaneously with qualitative geothermometry analysis. A basis for this study was a discussion of boiling and mixing models (Fričovský and Tometz, 2013; Fričovský et al., 2015). After carried qualitative geothermometry analysis, we conclude that the boiling is definitely disqualified as:

• samples plot deep in the non-boiling region (Fig. 7) at the silica–total carbonate mixing model (missing any trend organization towards a boiling line)

• enthalpy and silica fraction functions intercept (Fig. 8) implying rather polystadial mixing instead of steam-loss induced silica deposition

• saturation curves (Figs. 5, 15, 19, 20 and 24) of particular solids are conserved in shape, not varying saturation states transitions

• total saturation index curves (Figs. 25 and 26) plot as continuous in shape, not varying complex saturation states transitions

Shallow reservoir (accumulation/production zone) model

With analogy to deep reservoir, a shallow aquifer hosted in CHN Mid Triassic carbonates and upper zone of KNA Jr-Cr2 succession is compared to infiltration zone in CSM construction procedure. Reservoir geochemistry is represented by the samples of BEH-1 and FBe-1 wells of different depths, thus screening different zones of an aquiferous body.

Thermal waters are of secondary origin that is well documented on:

- facies difference in silica content, inverse to depth and temperature distribution in the reservoir body (Fig. 4)
- temperature overestimates on the silica-enthalpy mixing model (Fig. 6)

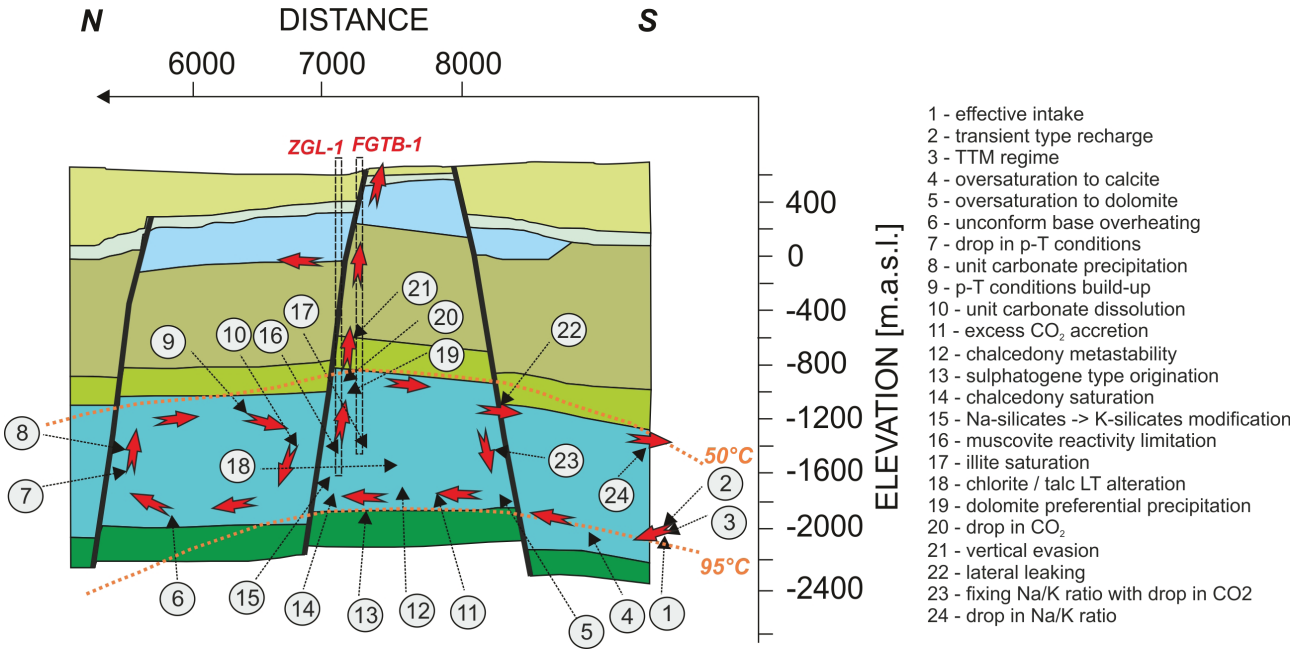

Fig. 31. Deep reservoir CSM. For its localization see Fig. 1.

- transition between rock dissolution and preferential alkali leaching observed at Na/K (Fig. 11) equilibrium plot (variable Na/K, K/Mg and Na/Mg ratio in a formation); and
- inconsistent plot of samples on Mg-SiO_2 alteration plot (Fig. 13) varying equilibrium temperatures between quartz and chalcedony stability at persistently low K/Mg ratio
- A reference is also given to use of mixing models in SRTW conditions (Fričovský and Tometz, 2013; Fričovský, 2014; Fričovský et al., 2015). Two reservoir facies are then recognized as:
- deep reservoir originated facies (vertically invading the shallow aquifer)
- shallow transition recharged facies (laterally recharging the shallow aquifer)

Deep reservoir originated facies

We expect the deep reservoir thermal waters to evade the bearing horizon at temperatures about 50–55 °C, initially saturated with chalcedony and oversaturated with carbonates. The vertical evasion realizes at open fault systems and quasi-vertical fissure swarms.

By the geochemical type, it is possible the evading waters preserve deep reservoir originated transient (Ca-Mg-HCO_3-SO_4 to Ca-Mg-SO_4-HCO_3) character.

Because of a loss of a contact with a source rock and change in p-T conditions, Mg-calcite is of higher tendency to precipitate spontaneously, consuming CO_2 and magnesium at various magnitude. Onset of calcite deposition is expected to realize at late evasion stages. A drop in aqueous aggressive CO_2 stabilizes modification of Na-alkalis, slowly increasing the Na/K ratio, progressively fixing a portion of dissolved SiO_2 in increasing thermodynamic activity of Na-silicates with its minor precipitation only. This is documented on an increase in albite saturation inverse to temperature (Fig. 15).

Some loss in silica in deeper reservoir parts or prior intake is also documented on silica-enthalpy mixing model by overestimating deep reservoir temperatures considered of end-member quality. An inverse overview, provides an option of post-mixing silica release from the IWCP Borové Formation.

Shallow transition originated facies

The separate recharge towards the shallow reservoir is expected due to an open hydrogeological character of a system, aided by facies analysis commented above. At shallow transition, the hydrochemical character of intakes into aquiferous zone may vary between transient and carbonatogene type, controlled by early dilution prior submersion. Thermal waters sampled at FBe-1 well are facially affine to infiltration zone facies at the Na/K, conserving the relative ratio (Fig. 11) with simultaneous increase in alkali concentrations. Because of their position within preferential Na^+ and K^+ leaching regime we expect the sodium intake realizing by minor hydrolysis of sodium-silicates in the KNA Jr-Cr2 profile, altered with the slow, but progressive K^+ dissociation from the CHN Mid Triassic dolomites and IWCP formations after the intake into production zone (Fig. 12).

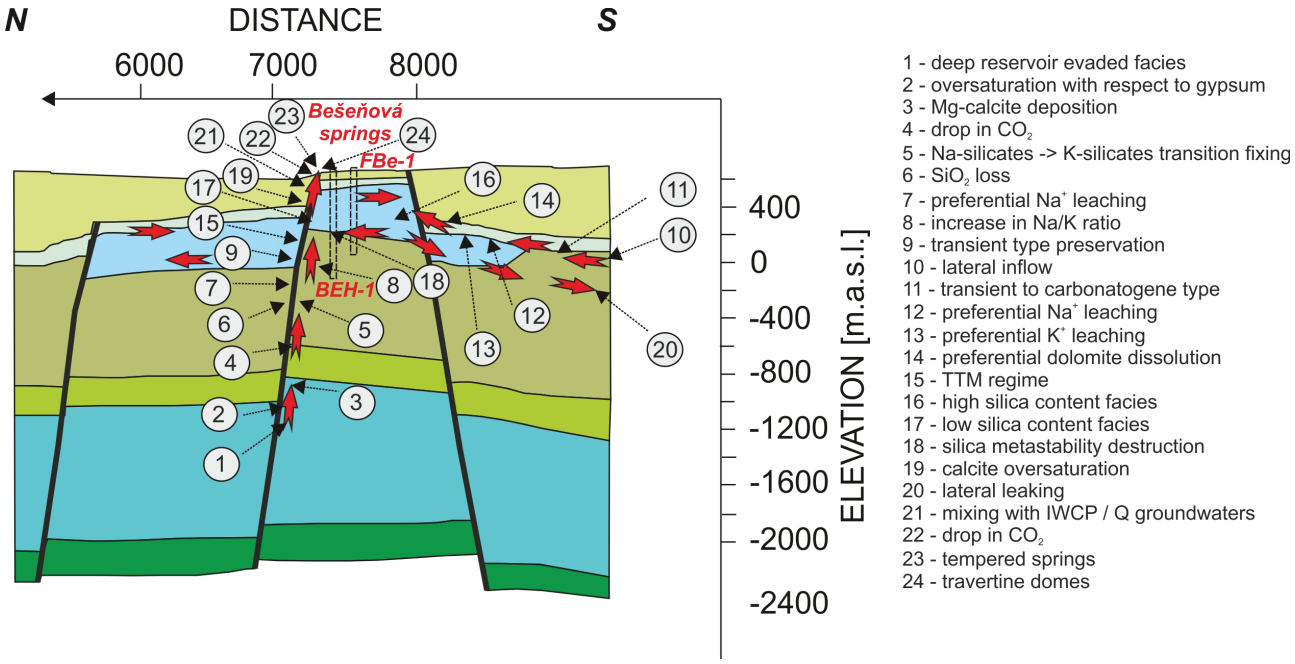

Fig. 32. Shallow reservoir CSM. For its localization see Fig. 1.

Discussion on shallow reservoir mixing

Both facies mix in the shallow reservoir, in the TCM (thermal-cold-mixing) regime. Even sampled waters are clearly of thermal character (T_{res} > 20 °C), only deep reservoir facies can be recognized as thermal end-member. A hydrochemical type of associated thermal waters may vary by a magnitude of modifications between transient and carbonatogene character, controlled by a mixing rate (Fig. 32).

A mixing event off any iso-chemical and iso-thermal parameters destructs any optional equilibration attained. By mixing of both facies, the Mg^{2+} increases as residential waters are enriched by magnesium from shallow transition.

The silica content also increases as shallow intake waters dissociate silicates from the IWCP and dolomite impurities, as well as a minor contribution from a contact with KNA Jr-Cr2 bedrock formations can not be excluded.

Vyšné Sliače (secondary) discharge zone model

There is no questioning of primary discharge zone location nearby the town of Bešeňová, associated with open faults-bound vertical upwelling of geothermal waters from the deep and shallow reservoir respectively. The mixed type of springs in Bešeňová is consequent to a definite dilution of reservoir thermal waters by the groundwater from the IWCP and Quaternary cover respectively, yet conserving oversaturation with respect to carbonates, equilibrated by deposition of travertines forming dome structures.

However, the existence of dry CO_2 fluxes and thermal springs in the Vyšné Sliače area provided some early note on possible thermal waters occurrence in its nearby deep territory. A first hint on some facies relations has been provided by application of mixing models (Fričovský and Tometz, 2013; Fričovský, 2014).

Silica-enthalpy-carbonate variation

There are distinguished facies of the Vyšné Sliače territory. We assigned the VSH-1 well to represent thermal waters prior upwelling, while thermal springs represent a surface propagation of waters, with primary end-member in the deep reservoir at a first assumption.

Facies relation of VSH-1 and springs yields overestimated temperatures of well facies, contravening expected SiO_2 deficiency of loosing-by-cooling (in precipitation or association of silicates), however, there is some silica lost between DRTE and VSH-1 facies, recorded by overestimate of deep reservoir temperatures (Fig. 6). The silica-enthalpy fraction model (Fig. 8) provides an amorphous silica check-test with excess resultant temperature and overestimate in the temperature by post-mixing silica dissolution. Two subfacies have been, however, identified on a silica – total carbonate model (Fig. 7) with deficient (D-LTC) and excess (D-HTC) total carbonate content, relative to DRTE and SRTW facies. Probably, the D-LTC records a "primary" subfacies evading deep reservoir with loosing silica fixed in activation of sodium-silicates due to loss of CO_2, mixing with shallow reservoir waters to give an origin of D-HTC, to form a resultant VSH-1 facies. Because of the

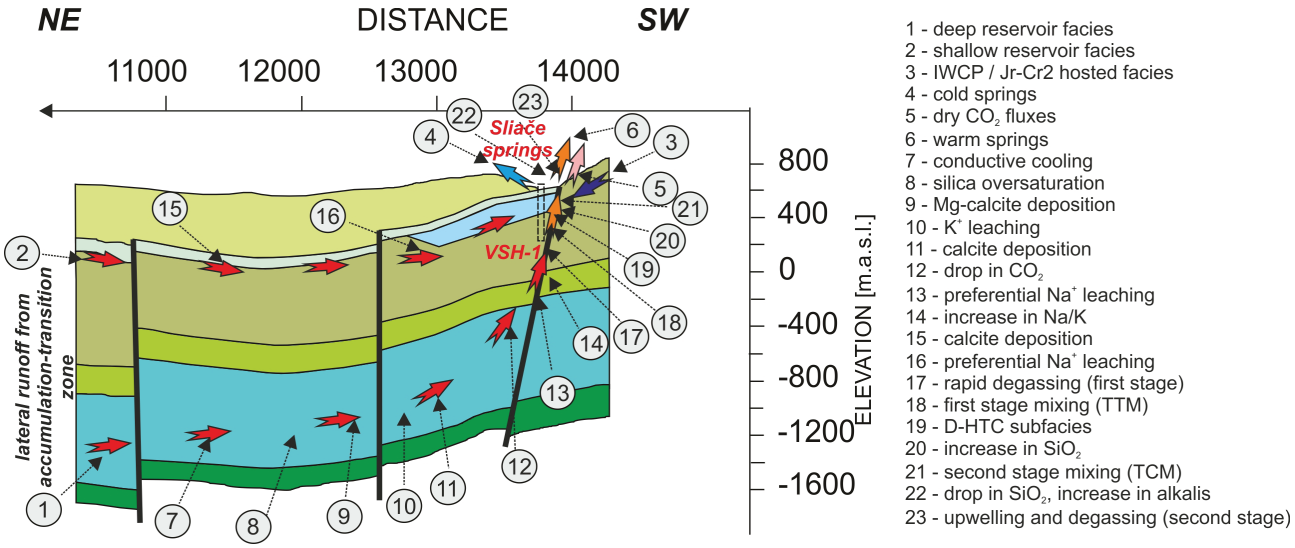

Fig. 33. Vyšné Sliače minor discharge zone CSM. For its localization see Fig. 1.

silica enthalpy results, the TTM regime must be realized in the Jurassic–Mid Cretaceous profile, to increase the SiO_2 content. Then, VSH-1 facies are most probably cooled and diluted rapidly by shallow groundwater (SCGW) to drop the silica and carbonate content prior upwelling as tempered springs. A dramatic cooling (by dilution and fast upflow at open faults and fissure swarms) along with rapid drop in pressure causes induced CO_2 separation of different preferential propagation towards the surface.

Discussion on equilibrium and alteration

A carbon dioxide saturation plays an essential role in evaluation of geochemical processes related to lateral runoff of deep and shallow reservoir thermal waters towards the Vyšné Sliače zone. An increase in Na/K ratio compared to DRTE is expected through the drop in available CO_2 by deposition of carbonates, mostly Mg-calcite (increase in MI inverse to Mg^{2+}; Fig. 16) combined with the preferential leaching of Na-silicates from KNA Jr-Cr2 profile (Fig. 11). Such an increase in absolute sodium concentration owes to mixing with the shallow groundwaters (second stage) and shallow reservoir evading thermal waters at a persistent contact with a source rock, and, probably, filtration deceleration, prolonging a water-rock contact sufficient for preferential leaching. Yet the maturity index is still low (MI = 0.8–0.9).

By comparing the SRTW and VSH-1 facies, an onset of calcite deposition realizes along a leaking due to runoff velocity low enough to enable its loss. The resultant increase in K/Ca ratio (Fig. 18) is rather to drop in Ca^{2+} as the absolute K^+ level is almost stable. Meanwhile, the K/Ca ratio increases between DRTE and VSH-1 facies, as a combination off loss in Ca^{2+} (calcite deposition) and some increase in K^+. Under relatively low K/Mg ratio, the GKM3 (Giggenbach, 1988) geothermometer yields temperatures conform to upper deep reservoir zones ($T_{K/Mg}$ = 59–63 °C at GKM3). Probably a leaching of potassium is fixed by adularia (Fig. 15) and illite (Fig. 24) oversaturation, controlled by CO_2 reduction of precipitation of Mg-calcite. An absolute concentration of alkalis in VSH-1 may then be a consequence of mixing between SRTW and DRTE facies in the KNA Jurassic–Mid Cretaceous horizon.

We also inspected facial and maturity relations on the Na-K-Mg geoindicator (Fig. 17). Thermal waters of VSH-1 are different in Mg^{2+} compared do DRTE, however, relatively conform to SRTW facies. On the Na-K-Mg-Ca geoindicator (Fig. 21), the VSH-1 shows, however, no relation to reservoir facies. In coincidence to silica – enthalpy conclusions, an expected loss in Mg^{2+} by deposition of carbonates at low temperatures is partially replaced by mixing of VSH-1 waters with S-CGW hosted in IWCP prior they upwell as thermal springs in the Vyšné Sliače area (Fig. 33). The polystageous mixing explains overrated dilution ratio at silica-enthalpy fraction model (Fig. 8).

A contribution to lateral leaking mechanisms

There has not been, however, any debate on probable driving mechanisms of lateral leakings towards the Sliače area. Hydraulic models presented in Fendek et al. (1988); Remšík et al. (1993); Remšík et al. (1998) provided some idea on preferential piezometry gradients from the central elevated parts towards SW. This may then be an option for general runoff, not providing conditions for some residency of thermal waters in the structure (within the accumulation/transition zone).

In fact, the mechanism has not been subjected to study neither in this paper. However, there are two more options

to be added into a complex CSM. The lateral leaking of thermal waters may then be induced by combination of:

- piezometric gradient
- build-up of density gradient (deep reservoir)
- difference in reservoir pressure

CONCLUSIONS

Tens of decades have passed since the geothermometers were successfully applied in the reservoir temperature estimation (e.g. Fournier, 1979; Arnórsson et al., 1983; Giggenbach, 1988) or the conceptual site models construction and analysis of geochemical regime and origination of thermal waters (e.g. Truesdell et al., 1977; Kharaka et al., 1982; Antrodischia et al., 1985). Only a few notes on isotope (Remšík et al., 1998) and sulphate (Bodiš and Borosová, 1996) geothermometry application were discussed with reference to the Bešeňová elevation geothermal structure. In fact, many techniques failed in temperature estimation (quantitative application) in local conditions (e.g. Fendek et al., 1988; Remšík et al., 1993; Remšík et al., 1998), because of the immaturity, low temperature conditions or predominat carbonate-hosted reservoirs. Being based on thermodynamics and hypothetical fluid-mineral equilibrium, geothermometers, however, represent a powerful tool for conceptual site models construction once correlated with the water chemistry (boiling and mixing) models, geology, alteration mineralogy, hydrogeology, and geothermics.

The Bešeňová elevation may be concluded as a complex hydrogeothermal structure of open hydrogeological character. Besides expected lateral inflow from the Liptovská Mara depression (e.g. Fig. 30), realized in the quasi-isochemical and isothermal regime, the correlation of ionic ratios with mixing models (presented e.g. in Fričovský and Tometz, 2013) has identified a minor recharge zone towards the Kľačianka valley that correlates with the local hydraulics and piezometry. Infiltration originates by at least one mixing episode between shallow and deep filtration channels (Fig. 29) prior separation from upwelling as tempered (warm) springs or descent into transition–accumulation zone. Deep reservoir waters are recharged in quasi-isochemical regime. Thermal waters are saturated with the calcite prior intake (Fig. 18), whilst attaining saturation with dolomite just after an inlet. Increase in CO_2 content under oversaturation with carbonates (Figs. 19 and 20) modifies Na-silicates towards K-silicates, simultaneous to preferential K^+ leaching from reservoir impurities (Fig. 31). Meanwhile, it is possible the LT alteration of impure dolomites realizes on a thermodynamic activity scale, altering a talc-chlorite-muscovite (illite) subsystem. Immaturity of thermal waters because of low Na/K ratio and possible modification of preferential thermodynamic activities of alkali silicates is driven and proportional by vertical separate filtration in convection cells due to unconform base overheating. Possibility of silicates alteration is documented by saturation of waters with chalcedony (Figs. 4 and 5). In vertical evasion regime, thermal waters rise up along open faults towards the shallow reservoir, where they mix with recharges from a shallow filtration, prior upwelling as springs, depositing travertine according to secondary saturation with calcite or travertine (Fig. 32). In the Sliače springs area (Fig. 33), it is possible that shallow and deep reservoir leakages mix in a first stage under TTM regime, prior dilution by shallow groundwaters (TCM regime). Rapid ascent along faults from the deep reservoir causes drop in pCO_2 driving formation of dry carbon dioxide fluxes on a surface, supported by second degassing stage after dilution. The mixture propagates as warm springs. Besides, a part of thermal waters leaks laterally towards the Ivachnová depression, due to regional piezometry (Fig. 30). Yet available geothermometers have been applied quantitatively as well. A silica–chalcedony conductive models appear of a best match referring to reservoir temperature conditions instead of comparing results to the wellhead measurements (Fig. 9, Appendix A). More precise results have been, however, derived of saturation index temperature (T_{CEQ} for chalcedony; Tabs. 1 and 2). For the deep reservoir environment, cation geothermometers are definitely skewed by immaturity (Figs. 16 and 17), with an exception of Mg-corrected Na-K-Ca geothermometer (Fig. 22). Multicomponent equilibrium geothermometry pointed on some complex equilibrium attainment in deeper (descending) parts of the deep reservoir (Figs. 25 and 26). Other zones were analysed in details in the main text.

Because of complexity and immaturity of a deep reservoir (assumed as a most potential of the entire basin), we rather recommend continuing studies focused at definition of local geoindicators (such as chalcedony, gypsum) for onward exploitation monitoring and relation analysis of thermal waters to other structures associated with the basin.

If not for quantitative temperature estimation and correlation, geothermometry techniques are distinctively valid for qualitative analysis either in low enthalpy or carbonates-hosted systems, if correlated together and applied with caution and reference to their essential principles.

Acknowledgement. Authors would sincerely like to thank the Andrea Vranovská, PhD. (Water Research Institute, Slovakia), prof. Peter Szucs (University of Miskolc, Hungary) and Peter Bajtoš, PhD. (State geological institute of Dionýz Štúr, Slovakia) for their contribution to this paper.

References

Antrodicchia, E., Cioni, R., Chhiodini, G., Gagliardi, R. & Marini, L., 1985: Geochemical temperatures of the thermal waters of Phlegraean Fields (Naples, Italy). *Geothermal Resources Council Transactions, 9, 287–292.*

Arnórsson, S., 1985: The use of mixing models and chemical geothermometers for estimating underground temperatures in geothermal systems. *J. Volcanol. Geotherm. Res., 23, 299–335.*

Arnórsson, S., 2000a: Mineral saturation. *In: Arnórsson, S. (ed.): Isotopic and chemical techniques in geothermal exploration, development and use, IAEA, Vienna, 152–200.*

Arnórsson, S., 2000b: Assessment of reservoir fluid composition from wet steam well data. *In: Arnórsson, S. (ed.): Isotopic and chemical techniques in geothermal exploration, development and use, IAEA, Vienna, 212–228.*

Arnórsson, S. & Gunnlaugsson, E., 1985: New gas geothermometers for geothermal exploration – calibration and application. *Geochim. Cosmochim. Acta, 49, 1 307–1 325.*

Arnórsson, S., Sigurdsson, S. & Svavarsson, H., 1982: The chemistry of geothermal waters in Iceland I. Calculation of aqueous speciation from 0° to 370 °C. *Geochim. Cosmochim. Acta, 46, 1 513–1 532.*

Arnórsson, S., Gunnlaugsson, E. & Svavarsson, H., 1983: The chemistry of geothermal waters in Iceland III. Chemical geothermometry in geothermal investigations. *Geochim. Cosmochim. Acta, 47, 567–577.*

Arnórsson, S., Andrésdóttir, A., Gunnarsson, I. & Stéfansson, A., 1988: New calibration for the quartz and Na/K geothermometers – valid in the range 0–350 °C. *In: Proceedings Geoscience Society of Iceland Annual Meeting, Reykjavik, Iceland, 42–43.*

Arnórsson, S., Fridriksson, Th. & Gunnarsson, I., 1998: Gas chemistry of the Krafla geothermal field, Iceland. *In: Proceedings International Symposium on Water-Rock Interaction, Auckland, New Zeeland, 613–66.*

Axelsson, G., 2009: Conceptual models of geothermal systems – introduction. *In: Proceedings Short Course V on Conceptual Modelling of Geothermal Systems, Santa Tecla, El Salvador, 1–12.*

Bodiš, D. & Borosová, S., 1996: Hydrogeochemical evaluation of the mineral and thermal waters of the Liptovská kotlina Basin: Application of the factor analysis. *Geol. Práce, Spr., 102, 65–70. (In Slovak with English summary.)*

Browne, 1978: Hydrothermal alteration in active geothermal fields. *Ann. Rev. Earth Planet. Sci., 6, 229–250.*

Cannon, C., Wood, T., Neupane, G., McLing, T., Mattson, E., Dobson, P. & Conrad, M., 2014: Geochemistry sampling for traditional and multicomponent equilibrium geothermometry in Southeast Idaho. *Geothermal Resources Council Transactions, 38, 425–431.*

Chiodini, G., Cioni, R., Frullani, A., Guidi, M., Marini, L., Prati, F. & Raco, B., 1996: Fluid geochemistry of Montserrat Island, West Indies. *Bull. Volcanology, 58, 380–392.*

Cioni, R., Fanelli, G., Guidi, M., Kinyariro, J. K. & Marini, L., 1992: Lake Bogoria hot springs (Kenya): geochemical features and geothermal implications. *J. Volcanol. Geotherm. Res., 50, 231–246.*

Cooper, D. C., Palmer, C. D., Smith, R. W. & McLing, T. L., 2013: Multicomponent equilibrium models for testing geothermometry approaches. *In: Proceedings 38th Workshop On Geothermal Reservoir Engineering, Stanford University, California, paper No. SGP-TR-198, 1–10.*

Cumming, W., 2009: Geothermal resource conceptual models using surface exploration data. *In: Proceedings the 34th Workshop on Geothermal Reservoir Engineering, Stanford University, CA, USA, 6 pp.*

Činčura, J., & Köhler, E., 1995: Paleoalpine karstification: the longest paleokarst period in the Western Carpathians (Slovakia). *Geol. Carpath., 46, 5, 343–347.*

Davraz, A., 2014: Application of hydrogeochemical techniques in geothermal systems; examples from eastern Mediterranean region. *In: Baba, A., Bundschuh, J. & Chandrasekharam, D. (eds.): Geothermal systems and energy resources: Turkey and Greece. CRC press, London, UK, 336 p.*

D'Amore, F. & Arnórsson, S., 2000: Geothermometry. *In: Arnórsson, S. (ed.): Isotopic and chemical techniques in geothermal exploration, development and use, IAEA, Vienna, 152–200.*

Ellis, A. J., 1970: Quantitative interpretation of chemical characteristics of hydrothermal systems. *Geothermics, 2, 516–528.*

Ellis, A. J. & Mahon, W. A. J., 1977: Chemistry and geothermal systems. *Academic Press, New York, 392 pp.*

Fendek, M., Bodiš, D., Biely, A., Kullmanová, A., Gašparíková, V., Snopková, P., Král, M. & Janči, J., 1988: The report on the investigation geothermal borehole ZGL-1 in the Bešeňová locality – the verification of the prognostic sources of geothermal energy in the Liptovská kotlina Basin – West. *Manuscript – Final report, State geological institute of Dionýz Štúr, Bratislava, 85 pp. (In Slovak.)*

Fendek, M., Fendeková, M., Daniel, S. & Kultan, V., 2013: Bešeňová – usable quantity of geothermal energy, supplementary hydrogeological survey. HYDROFEN Bratislava, 91 pp. *(In Slovak.)*

Fouillac, R. & Michard, S., 1981: Sodium/lithium ratio in water applied to geothermometry of geothermal reservoirs. *Geothermics, 10, 55–70.*

Fournier, R. O., 1973: Silica in thermal waters: laboratory and field investigations. *Proceedings International Symposium on Hydrogeochemistry and Biogeochemistry, Tokyo, 1970, vol. 1, Hydrochemistry, Washington, DC, 1973, 122–139.*

Fournier, R. O., 1977: Chemical geothermometers and mixing models for geothermal systems. *Geothermics, 5, 41–50.*

Fournier, R. O., 1979: A revised equation for the Na-K geothermometer. *Geothermal Resource Council Transactions, 3, 221–224.*

Fournier, R. O., 1980a: Application of water geochemistry to geothermal and reservoir engineering. *Spanish Institute of Geology and Mineralogy, 5–56.*

Fournier, R. O., 1980b: The interpretation of Na-K-Mg relations in geothermal waters. *Geothermal Resources Council Transactions, 14, 2, 1 421–1 425.*

Fournier, R. O., 1981: Applications of water chemistry for geothermal exploration and geothermal engineering. *In: Rybach, L. & Muffler, L. P. J. (eds.): Geothermal Systems – Principles and Case Histories, Willey PH, New York, USA, 109–143.*

Fournier, R. O., 1982: Geochemistry in geothermal exploration and production. *In: Proceedings 5th New Zeeland Geothermal Workshop, Auckland, New Zeeland, 209–215.*

Fournier, R. O., 1989: Lectures on geochemical interpretation of hydrothermal waters. United Nations Geothermal Training Programme, Reykjavik, Iceland, 77 pp.

Fournier, R. O., 1991: Water geothermometers applied to geothermal energy. *In: D'Amore, R. (ed.): Application of geochemistry in Geothermal Reservoir Development, UNITAR, Rome, 37–69.*

Fournier, R. O. & Rowe, J. J., 1966: Estimation of underground temperatures from the silica content of water from hot springs and wet-steam wells. *Amer. J. Sci., 264, 685–697.*

Fournier, R. O. & Truesdell, A. H., 1971: An empirical geothermometer based on Na, K and Ca dissolved in natural waters (abstract). *Geol. Soc. Amer. Abstr., 3, 570.*

Fournier, R. O. & Truesdell, A. H., 1973: An empirical Na-K-Ca geothermometer for natural waters. *Geochim. Cosmochim. Acta, 37, 1 255–1 275.*

Fournier, R. O., White, D. E. & Trusdell, A. H., 1974: Geochemical indicators of subsurface temperature – Part 1, basic assumptions. *J. Res. U. S. Geol. Survey, 2, 259–261.*

Fournier, R. O. & Potter, R. W. II., 1978: A magnesium correction for the Na-K-Ca chemical geothermometer. *U.S. Geological Survey Open-File Report, 78–986, 24.*

Fournier, R. O. & Potter, R. W. II., 1979: Magnesium correction to the Na-K-Ca chemical geothermometer. *Geochim. Cosmochim. Acta, 43, 1 543–1 550.*

Fournier, R. O. & Potter, R. W. II., 1982: A revised and expanded silica (quartz) geothermometer. *Geothermal Resources Council Bulletin, 11, 3–12.*

Franko, O., 1984: Bešeňová – carbonated thermal waters. In: Hydrogeologický sprievodca VIII celoštátnej hydrogeologickej konferencie. *GÚDŠ, Bratislava. (In Slovak.)*

Franko, O., 2002a: Recent views on hydrogeological structure of mineral waters in Lúčky locality. *Podzemná voda, VIII, 2, 123–132. (In Slovak.)*

Franko, O., 2002b: New data for suggestion of protection zones of natural healing resources in Lúčky locality. *Manuscript – Final report, Kúpele Lúčky, 39 pp. (In Slovak.)*

Franko, O., Biely, A., Hricko, J., Szalaiová, V. & Mateovič, L., 1974: Evaluation of the Demänová area in the Liptovská kotlina Basin for searching for the thermal waters. *Manuscript – Final report, State geological institute of Dionýz Štúr, Bratislava, 50 pp. (In Slovak.)*

Franko, O., Bodiš, D., Gazda, S. & Michalíček, M., 1979: Hydrogeological evaluation of the Liptovská kotlina Basin from the view of the mineral waters occurrence. *Manuscript – Final report, State geological institute of Dionýz Štúr, Bratislava, 79 pp. (In Slovak.)*

Fričovský, B., 2014: Composite conceptual model and hydrogeothermal evaluation of the Bešeňová elevation hydrogeothermal structure, Liptov Basin, Slovakia. *Manuscript – Doctoral (Ph.D.) Thesis, Institute of Geosciences, Technical University of Košice, 301 pp.*

Fričovský, B. & Tometz, L., 2013: Reservoir boiling and mixing models overview and application: case study on the Bešeňová elevation hydrogeothermal structure (northern Slovakia). *In: Proceedings on Hydrogeochemistry 2013 International Conference, XIV, Sosnowiec, Poland, 1–12.*

Fričovský, B. & Tometz, L., 2014: Use of the multicomponent geothermometry at formation of the conceptual model of hydrogeothermal structures, Bešeňová Elevation, Slovakia. *In: Geochémia 2014 – zborník vedeckých príspevkov z konferencie. Št. Geol. Úst. D. Štúra, Bratislava, 42–46.(In Slovak.)*

Fričovský, B., Tometz, L., Vizi, L. & Štiaková, J., 2014: Update on stationary temperature model on carbonates dominated, stratified, low enthalpy hydrogeothermal system of the Bešeňová Elevation, Slovakia. *In: Proceedings 14th SGEM Conference, Vol. II – Hydrogeology, engineering geology and geotechnics, Albena, Bulgaria, 1 003–1 011.*

Fričovský, B., Tometz, L., Fendek, M. & Gumáňová, J., 2015: Update on composite geochemical conceptual model for the Bešeňová elevation hydrogeothermal structure, Liptov Basin, northern Slovakia. *In: Proceedings World Geothermal Congress 2015, Melbourne, Australia, paper No. 14 092, 1–11.*

Gibbs, R. J., 1970: Mechanisms controlling world water chemistry. *Science, 170, 1 088–1 090.*

Giggenbach, W. F., 1981: Geothermal mineral equilibria. *Geochim. Cosmochim. Acta, 45, 393–410.*

Giggenbach, W. F., 1984: Mass transfer in hydrothermal alteration systems. *Geochim. Cosmochim. Acta, 48, 2 963–2 711.*

Giggenbach, W. F., 1986: Graphical techniques for the evaluation of water/rock equilibration conditions by use of Na, K, Mg and Ca contents of discharge waters. *In: Proceedings 8th New Zeeland Geothermal Workshop, 37–43.*

Giggenbach, W. F., 1988: Geothermal solute equilibria. Derivation of Na-K-Mg-Ca geoindicators. *Geochim. Cosmochim. Acta, 52, 2 749–2 756.*

Giggenbach, W. F., 1991: Chemical Techniques in Geothermal Exploration. *In: D'Amore, F. (ed.): Application of geochemistry in geothermal reservoir development. UNITAR/UNDP publication, Rome, 119–142.*

Giggenbach, W. F., 1995: Geochemical exploration of a difficult geothermal system, Paraso, Vella Lavella, Solomon Islands. *In: Proceedings World Geothermal Congress 1995, Firenze, Italy, 995–1 000.*

Giggenbach, W. F. & Goguel, R. L., 1989: Collection and analysis of geothermal and volcanic water and gas discharges. DSIR report CD 2401, 4th ed., Pentone, New Zeeland.

Giggenbach, W. F., Gonfiantini, R., Jangi, B. L. & Truesdell, A. H., 1983: Isotopic and chemical composition of Parbati Valley geothermal discharges, NW Himalaya, India. *Geothermics, 12, 199–222.*

Giggenbach, W. F., Sheppard, D. S., Robinson, B. W., Stewart, M. K. & Lyon, G. L., 1994: Geochemical structure and position of the Waiotapu geothermal field, New Zeeland. *Geothermics, 23, 599–644.*

Giordano, T. H. & Swanberg, C. A., 1978: Influence of reservoir rock-type on the Na-K-Ca geothermometer. *Geological Society of America Abstracts with Programs, 2, 7, 433.*

Gíslason, S. R., Heaney, P. J., Oelkers, E. H. & Schott, J., 1997: Kinetic and thermodynamic properties of moganite, a novel silica polymorph. *Geochim. Cosmochim. Acta, 61, 1 193–1 204.*

Gross, P., Biely, A., Köhler, E. & Papšová, J., 1979: Geology of the Inner Carpathian Paleogene in the western part of the Liptovská kotlina Basin. *Manuscript – Technical report Sta-*

te geological institute of Dionýz Štúr, Bratislava, 32 pp. (In Slovak.)

Gross, P., Köhler, E., Biely, A., Franko, O., Hanzel, V., Hricko, J., Kupčo, G., Papšová, J., Priechodská, Z., Szalaiová, V., Snopková, P., Stránská, M., Vaškovský, I. & Zbořil, Ľ., 1980: Geology of the Liptovská kotlina Basin. *Št. Geol. Úst. D. Štúra, Bratislava, 236 pp. (In Slovak with English summary.)*

Gunnarsson, I. & Arnórsson, S., 2000: Amorphous silica solubility and thermodynamic properties of H_4SiO_4 in the range 0–350 °C at Psat. *Geochim. Cosmochim. Acta, 64, 2 295–2 307.*

Hanzel, V., Kullman, E. & Vrana, K., 2008: Lúčky – computation of quantities of mineral waters. Final report. *Manuscript. Archives of the State Geological Institute of Dionýz Štúr, Bratislava, 220 pp. (In Slovak.)*

Horita, J., 2005: Stable isotope thermometry: There is more to it than temperature. *Geochem. J., 39, 481–496.*

Johnson, J. W., Oelkers, E. H. & Helgeson, H. C., 1992: SUPCTR92: A software package for calculating the standard modal thermodynamic properties of minerals, gases, aqueous species and reactions from 1 to 5 000 bar and 0 to 1 000 °C. *Computers & Geosciences, 7, 899–947.*

Joseph, E. P., Fournier, N., Lindsay, J. M., Robertson, R., Denise, M. & Beckles, D. M., 2013: Chemical and isotopic characteristics of geothermal fluids from Sulphur Springs, Saint Lucia. *J. Volcanol. Geotherm.Res., 254, 23–36.*

Jurewycz, E., 2005: Geodynamic evolution of the Tatra Mts. and the Pieniny Klippen Belt (Western Carpathians): problems and comments. *Acta geol. pol., 55, 3, 295–338.*

Karingithi, C. W., 2009: Chemical geothermometers for geothermal exploration. *In: Proceedings Short Course on Exploration of Geothermal Resources, Lake Naivasha, Kenya, paper No. 22.*

Kharaka, Y. K. & Mariner, R. H., 1989: Chemical geothermometers and their application to formation waters from sedimentary basins. *In: Naeser, N. D. & McCulloh, T. H. (eds.): Thermal History of Sedimentary Basins. Springer, New York, 99–11.*

Kharaka, Y. K., Lico, M. S. & Lax, L. M., 1982: Chemical geothermometers applied to formation waters, Gulf of Mexico and California basins. *Amer. Assoc. Petrol. Geol. Bull., 66, 588.*

Klago, M. & Stuchliková, B., 1990: Liptovský Ján, Pod Bielym, hydrogeologický prieskum. Final report. *Št. Geol. Úst. D. Štúra, Bratislava, 40 pp.*

Lyon, G. L., 1974: Geothermal gasses. *In: Kaplan, I. R. (ed.): Natural Gases in Marine Sediments, Plenum Press, New York.*

Maďar, D., 1997: Liptovská kotlina Basin – regional hydrogeothermal evaluation, geophysical survey. *Manuscript – Final report, ESPRIT, s. r. o., Banská Štiavnica, 27 pp. (In Slovak.)*

Marini, L., 2004: Geochemical techniques for the exploration and exploitation of geothermal energy. *Viareggio, Italy, 106 p.*

Morey, G. W., Fournier, R. O. & Rowe, J. J., 1962: The solubility of quartz in water in temperature interval from 25 to 300 °C. *Geochim. Cosmochim. Acta, 26, 1 029–1 043.*

Němec, F. & Bartková, J., 1987: Paleogene of the Liptovská kotlina Basin and its underlier. *Manuscript – Final report, Naftoprojekt Bratislava, š. p., 181 pp.*

Neupane, G., Mattson, E., McLing, T., Palmer, D., Smith, R. W. & Wood, T. R., 2014: Deep geothermal reservoir temperatures in the Eastern Snake River Plain, Idaho, using multicomponent geothermometry. *In: Proceedings 39th Workshop on Geothermal Reservoir Engineering, Stanford University, California, SGP-TR-202, 1–12.*

Nicholson, K., 2012: Geothermal fluids: chemistry and exploration techniques. *Springer Science & Business Media, 263 pp.*

Nieva, D. & Nieva, R., 1987: Developments in geothermal energy in Mexico, part 12: A cationic composition geothermometer for prospection of geothermal resources. Heat Recovery Systems and CHP, 7, 243–258.

Pačes, T., 1975: A systematic deviation from Na-K-Ca geothermometer below 75 °C and above 10^{-4} atm P_{CO_2}. *Geochim. Cosmochim. Acta, 39, 541–544.*

Palmer, C. D., Ohly, S. R., Smith, R. W., Neupane, G., McLing, T. & Mattson, E., 2014: Mineral selection for multicomponent equilibrium geothermometry. *Geothermal Resources Council Transactions, 38, 453–459.*

Pang, Z. H., 1988: Multiple fluid-mineral equilibrium calculations and their applications to geothermometry and hydrochemical processes in geothermal systems. *Manuscript – United Nations University Geothermal Training Programme, Reykjavik, Iceland, report No. 5, 82 pp.*

Pang, Z. H., 2001: Isotope and chemical geothermometry and its application. *Sciences in China – series E, Technological Sciences, 44, 1, 16–20.*

Pang, Z. H. & Reed, M. H., 1998: Theoretical chemical thermometry on geothermal waters: problems and methods. *Geochim. Cosmochim. Acta, 62, 1 083–1 091.*

Palandri, J. & Reed, M. H., 2001: Reconstruction of in-situ composition of sedimentary waters. *Geochim. Cosmochim. Acta, 65, 1 741–1 767.*

Peiffer, L., Wanner, C., Spycher, N., Sonnenthal, E. L. & Kennedy, B. M., 2013: Multicomponent vs. classical geothermometry: An evaluation using reactive transport modeling. *Proc. Earth Planet. Sci., 7, 665–668.*

Peiffer, L., Wanner, C., Spycher, N., Sonnenthal, E. L., Kennedy, B. M. & Iovenitti, J., 2014: Optimized multicomponent vs. classical geothermometry: Insights from modeling studies at the Dixie Valley geothermal area. *Geothermics, 15, 154–169.*

Reed, M. H., 1982: Calculation of multicomponent chemical equilibria and reaction processes in systems involving minerals, gases and aqueous phase. *Geochim. Cosmochim. Acta, 46, 513–528.*

Reed, M. H. & Spycher, N., 1983: Calculated effects of boiling, cooling and oxidation on precipitation of ore and gangue minerals from hydrothermal solution. *In: Proceedings 4th International Symposium on Water Rock Interaction – Extended Abstracts, Misasa, Japan, 405–408.*

Reed, M. H. & Spycher, N., 1984: Calculation of pH and mineral equilibria in hydrothermal waters with application to geothermometry and studies of boiling and dilution. *Geochim. Cosmochim. Acta, 48, 1 479–1 492.*

Remšík, A., Fendek, M., Král, M., Bodiš, D. & Michalko, J., 1993: Geothermal energy of the Liptovská kotlina Basin. *Manuscript – Technical report, State geological institute of Dionýz Štúr, Bratislava, 97 pp. (In Slovak.)*

Remšík, A., Fendek, M., Mello, J., Král, M., Bodiš, D., Michalko, J., Maďar, D. & Vika, K., 1998: Liptovská kotlina Basin – regional hydrogeothermal evaluation. *Manuscript – Final report, Ministry of the Environment of the Slovak Republic, Bratislava, 94 pp. (In Slovak.)*

Remšík, A., Fendek, M. & Maďar, D., 2005: The occurrence and distribution of the geothermal waters in the Liptovská kotlina Basin. *Miner. Slov., 37, 123–130.*

Sanjuan, B., 2010: Use of a new Sodium/Lithium (Na/Li) geothermometric relationship for High-Temperature (HT) geothermal fluids derived from seawater/basalt interaction processes: Application to the Djibouti case. *In: Proceedings 3rd Third East African Rift Geothermal Conference ARGEO-C3-DJIBOUTI, Djibouti, 231–248.*

Sanjuan, B., Girard, J. P., Lanini, S., Bourguignon, A. & Brosse, E., 2003: Geochemical modelling of diagenetic illite and quartz cement formation in Brent sandstone reservoirs: example of the Hild Field, Norwegian North Sea. *In: Worden, R. H. & Morad, S. (eds.): Clay mineral cements in Sandstones. Intern. Assoc. Sedimentol. Spec. Publ., Blackwell Publishing, Oxford, 34, 425–452.*

Santoyo, E. & Díaz-González, L., 2010: A new improved proposal of the Na/K geothermometer to estimate deep equilibrium temperatures and their uncertainties in geothermal systems. *In: Proceedings World Geothermal Congress 2010, Bali, Indonesia, 1–9.*

Sheridan, M. F., Satkin, R. L. & Wohletz, K. W., 1980: Geothermal resource evaluation at Castle Hot Spring. *Manuscript – Final report, Arizona Geological Survey, Tuscon, AZ, 57 pp.*

Shikanozo, N., 1976: Thermodynamic interpretation of Na-K-Ca geothermometer in the natural water system. *Geochem. J., 10, 47–50.*

Simmons, S. F. & Christenson, B. W., 1993: Towards a unified theory on calcite formation in boiling geothermal systems. *In: Proceedings 15th New Zeeland Geothermal Workshop, Auckland, New Zeeland, 145–148.*

Simmons, S. F., 2013: Fluid-mineral equilibria in great basin geothermal systems: implications for chemical geothermometry. *In: Proceedings, 38th Workshop on Geothermal Reservoir Engineering, Stanford University, Stanford, California, 1–8.*

Smith, R. W., Palmer, C. D. & Cooper, D. C., 2012: Approaches for Multicomponent Equilibrium Geothermometry as a Tool for Geothermal Resource Exploration. *In: Proceedings American Geophysical Union Fall Meeting 2012, 12, abstract No. V23F-08, 1 p.*

Sonney, R. & Vuataz, F., 2010: Validation of chemical and isotopic geothermometers from low temperature deep fluids of Northern Switzerland. *In: Proceedings World Geothermal Congress 2010, Bali, Indonesia, paper No. 1 426.*

Spycher, N., Sonnenthal, E. L. & Kennedy, B. M., 2011: Integrating multicomponent chemical geothermometry with parameter estimation computations for geothermal explorarion. *Geothermal Resource Council Transactions, 35, 663–666.*

Spycher, N., Peiffer, L., Sonnenthal, E. L., Saldi, G., Reed, M. H. & Kennedy, B. M., 2014: Integrated multicomponent solute geothermometry. *Geothermics, 51, 113–123.*

Taylor, S. R., 1964: Abundance of chemical elements in the continental crust, a new table. *Geochim. Cosmochim. Acta, 28, 1 273–1 285.*

Tole, M. P., 1988: Geochemical sampling, laboratory analysis, and mineral equilibria calculations for fluids from selected areas in Iceland. United Nations University Geothermal Training Programme, Reykjavik, Iceland, report No. 7, 55.

Tole, M. P., Ármansson, H., Pang, Z. H. & Arnórsson, S., 1993: Fluid/mineral equilibrium calculations for geothermal fluids and chemical geothermometry. *Geothermics, 22, 17–37.*

Tonani, F., 1980: Some remarks on the application of geochemical techniques in geothermal exploration. *In: Proceedings Advances in European Geothermal Research, 2nd Symposium, Strassbourgh, France, 428–443.*

Truesdell, A. H., 1975: Geochemical techniques in exploration. *In: Proceedings 2nd UN Symposium on Development and Use of Geothermal Resources 1, 53–86.*

Truesdell, A. H., 1976: Summary of section III: geochemical techniques in exploration. *In: Proceedings 2nd UN Symposium on Development and Use of Geothermal Resources, San Francisco, USA, 1, 53–89.*

Truesdell, A. H. & Fournier, R. O., 1975: Calculation of deep temperatures in geothermal systems from the chemistry of boiling spring waters of mixed origin. *In: Proceedings 2nd U.N. Symposium on Geothermal Resources, San Francisco, CA, 837–844.*

Truesdell, A. H. & Fournier, R. O., 1977: Procedure for estimating the temperature of a hot water component in a mixded water using a plot of dissolved silica versus enthalpy. *J. Res. U.S. Geological Survey, 5, 1, 49–52.*

Truesdell, A. H., Nathenson, M. & Tye, R. O., 1977: The effects of sub-surface boiling and dilution on the isotopic compositions of Yellowstone thermal waters. *J. Geophys. Res., 82, 3 694–3 703.*

Vandrová, G. & Matejčeková, E., 1991: Liptovský Ján, Jánska dolina valley – thermal well "Rudolf", hydrodynamic tests. *Manuscript – Final report, State geological institute of Dionýz Štúr, Bratislava. (In Slovak.)*

Vandrová, G., Štefanka, P. & Červeňan, M., 2009: Bešeňová – revision of exploatation conditions of the sources ZGL-1 and FBe-1. *Manuscript – Final report, State geological institute of Dionýz Štúr, Bratislava, 101 pp. (In Slovak.)*

Vandrová, G., Štefanka, P., Hók, J. & Sýkora, M., 2011: Bešeňová – hydrogeothermal borehole FGTB-1, 1st and 2nd phase. *Manuscript – Technical report, State geological institute of Dionýz Štúr, Bratislava, 140 pp.(In Slovak.)*

Verma, S. P., 2000: Limitations in applying silica geothermometers for geothermal reservoir evaluation. *In: Proceedings 25th Workshop on Geothermal Reservoir Engineering, Stanford University, CA, 1–6.*

Verma, S. P., 2012: Cation exchange geothermometry: A critique. *Geotermia, 25, 1, 53–56.*

Verma, S. P. & Santoyo, E., 1997: New improved equations for Na/K, Na/Li and SiO_2 geothermometers by outlier detection and rejection. *J. Volcanol. Geotherm. Res., 79, 1–2, 9–24.*

Walther, J. V. & Helgeson, H. C., 1977: Calculation of thermodynamic properties of aqueous silica and the solubility of quartz and its polymorphs at high pressures and temperatures. *Amer. J. Sci., 277, 1 315–1 351.*

Wishart, DeBonne, N., 2015: Comparison of silica and cation geothermometers of Bath Hot Springs, Jamaica WI. *In: Proceedings World Geothermal Congress 2015, Melbourne, Australia, Paper No. 14 130.*

Zbořil, Ľ., Májovský, J., Takáčová, H. & Husák, Ľ., 1972: The Liptovská kotlina Basin – geoelectric, gas flux and thermometric measurements within the period 1971–1972. *Manuscript – Technical report, State geological institute of Dionýz Štúr, Bratislava, 40 pp. (In Slovak.)*

Zembjak, O., Biely, A., Bodiš, D., Fendek, M., Franko, O., Gabauer, G. & Bálint, T., 1986: Geothermal energy – investigation of the re-injection possibilities and evaluation of the SSR potential – investigation of the geothermal sources of the Liptovská kotlina Basin. *Manuscript – Final report, State geological institute of Dionýz Štúr, Bratislava, 51 pp. (In Slovak.)*

Využitie geotermometrie pri odhade rezervoárovej teploty a konštrukcii koncepčných modelov: Princípy, metódy a aplikácie v podmienkach hlbokého rezervoáru hydrogeotermálnej štruktúry bešeňovskej elevácie, Slovensko.

Aplikácia geotermometrov pre odhad teploty (napr. Fournier, 1979; Arnórsson et al., 1983; Giggenbach, 1988), objasnenie geochemického pôvodu, podmienok formovania termálnych vôd a tvorbu koncepčných modelov (hydro)geotermálnych štruktúr a polí (napr. Truesdell et al., 1977; Kharaka et al., 1982; Antrodischia et al., 1985) je celosvetovo uznávanou metódou na podporu realizovaných geologických, hydrogeologických a geofyzikálnych štúdií.

Využívanie metód geotermometrického výskumu a prieskumu bolo v podmienkach Západných Karpát dlhodobo zaznávané a obmedzené na niekoľko zmienok v lokálnych podmienkach štruktúry Bešeňovskej elevácie (Bodiš a Borosová, 1996; Remšík et al., 1998). Je pravdou, že mnohé z nich pravidelne zlyhávali pri odhade rezervoárovej teploty (napr. Fendek et al., 1988; Remšík et al., 1993; Remšík et al., 1998) termálnych vôd v dôsledku ich termodynamickej nevyzrelosti, nízkych teplôt a prevažne karbonátového prostredia. Avšak, nakoľko sú tieto metódy založené na striktných termodynamických zákonitostiach a predpoklade zachovania rovnovážneho stavu na rozhraní, napríklad, termálna voda – minerálna fáza, geotermometre predstavujú v skutočnosti dôležitý prostriedok pri konštrukcii koncepčných modelov hydrogeotermálnych a geotermálnych štruktúr, ak sú korelované s modelmi zmien makrochemického zloženia vody a súvisiacej alterácie hornín a alteračných asociácií, vyhodnotením geotermických parametrov, poznaním geologickej stavby a hydrogeologických pomerov.

Cieľom prezentovanej štúdie je poukázať na základné geotermometrické techniky celosvetovo využívané pri odhade rezervoárovej teploty a konštrukcii koncepčných modelov (hydro)geotermálnych štruktúr s ich následnou aplikáciou v lokálnych podmienkach bešeňovskej elevácie.

Hydrogeotermálna štruktúra elevácie Bešeňovej môže byť celkovo charakterizovaná ako zložitý, hydrogeologicky otvorený systém. Koreláciou iónových pomerov s makrochemickými modelmi zmiešavania (prezentované v práci Fričovský a Tometz, 2013) bola identifikovaná infiltračná zóna v okolí Kľačianskej doliny, čo je v súlade s lokálnymi hydraulickými podmienkami a distribúciou piezometrických napätí. Zároveň je stále opodstatnený predpoklad kvázi izochemického prítoku termálnych vôd od štruktúry depresie Liptovskej Mary na východe. V okolí Kľačianskej doliny dochádza minimálne k jednej epizóde zmiešavania medzi hlbokým a plytkým infiltračným kanálom, ktorá prebieha pred separáciou zostupných, dotačných od výstupných a výverových smerov (obr. 29). Termálne vody v hlbokom obehu dosahujú saturáciu voči kalcitu ešte pred vstupom do produkčnej časti rezervoáru (obr. 18) v centrálnej tranzitno-akumulačnej zóne. Zvyšovanie obsahu CO_2 podmieňuje modifikáciu Na-silikátov na K-silikáty, preferenčne disociovaných zo siliciklastických prímesí rezervoárových karbonátov (obr. 31). Výsledky multikomponentovej geotermometrie (tab. 5 – 6; obr. 27 – 28), analýzy saturačných stavov (obr. 20

a 24) a alteračných systémov (obr. 10 – 13) poukazuje na možnú aktiváciu nízkoteplotnej alterácie rezervoárových dolomitov so siliciklastickými prímesami a polohami, zvyšovaním reaktivity talku pri rozpúšťaní Mg-kalcitu, presýtení termálnych vôd voči dolomitu a produkcii CO_2.

Celková minimálna vyzrelosť hlbokých termálnych vôd je následne indikovaná nízkym iónovým pomerom Na/K a modifikáciou termodynamických reaktivít alkalických silikátov v súvislosti s vertikálnou filtráciou v izolovaných konvekčných bunkách pod vplyvom nerovnomerného prehrievania bázy (obr. 30). Alterácia na úrovni termodynamickej aktivity, respektíve čiastočnej ionovýmeny je podporovaná celkovou saturáciou termálnych vôd voči chalcedónu. Termálne vody vystupujú zároveň po otvorených zlomových systémoch v smere k plytkému rezervoáru, kde dochádza k ich zmiešavaniu s termálnymi vodami plytšieho obehu. Časť zmiešaných vôd následne pokračuje po tektonickom výstupe k povrchu, kde vyvierajú v podobe termálnych prameňov a podieľajú sa na tvorbe travertínových štruktúr (obr. 32). V prostredí sekundárnej výverovej zóny Vyšných Sliačov predpokladáme, že k prvej etape zmiešavania dochádza medzi termálnymi vodami z obidvoch rezervoárov pred ich následným zmiešavaním a nariedením plytkými podzemnými vodami (obr. 33). Rýchly výstup predovšetkým z hlbokého rezervoáru po otvorených zlomových systémoch spôsobuje prudký pokles parciálneho tlaku CO_2, čo podmieňuje vznik suchých výronov plynov dokumentovaných v minulosti, k čomu prispieva aj sekundárne odplyňovanie po prudkom ochladení nariedením. Kým časť termálnych vôd z hlbokého rezervoáru vyviera v podobe termálnych prameňov v okolí Vyšných Sliačov, časť termálnych vôd pokračuje v hlbokom prúdení v smere k depresii Ivachnovej (obr. 30).

Aplikácia geotermometrov pri odhade rezervoárovej teploty, eventuálne teploty posledného vyváženia termálnym vodám voči jednotlivým termodynamickým systémom, bola ovplyvnená termodynamickou nevyzrelosťou termálnych vôd (obr. 2, 16 – 17). Presvedčivé výsledky (obr. 9) boli dosiahnuté pri geochemickom modelovaní nasýtenia termálnych vôd štruktúry voči chalcedónu (obr. 4 – 5).

V podmienkach hlbokého rezervoáru sa ako perspektívny geotermometer ukázala Mg-korekcia Na-K-Ca geotermometra (obr. 22). Multikomponentová geotermometria poukázala na možnosť krátkodobého, celkového vyváženia termálnych vôd alebo prítomnosť geochemicky vyzretých termálnych vôd v hlbších častiach rezervoáru.

Na základe zložitosti nového predkladaného modelu štruktúry termálnych vôd, zreteľne odlišnej od predchádzajúceho modelu jednoduchej infilrácie a výveru (napr. Fendek et al., 1988) odporúčame pozornosť zamerať na určenie lokálnych geochemických geoindikátorov vychádzajúcich z chalcedónu, alebo sadrovca.

Okrem kvantitatívneho využitia pri dlhodobom monitoringu termálnych vôd a rezervoárovej odozvy je zároveň možné tieto geoindikátory s určitosťou využiť pri upresňovaní koncepčného modelu, definovaní koncepčnej histórie termálnych vôd a interpretácii vzájomných, genetických vzťahov termálnych vôd s termálnymi vodami Liptovskej kotliny.

Využitie geotermometrov preukázalo svoje opodstatnenie aj v podmienkach nízkoentalpických a karbonátových štruktúr, predovšetkým pri tvorbe koncepčného modelu a ako podporná metóda geochemického modelovania.

APPENDIX A – SILICA GEOTHERMOMETERS

Phase	Geothermometer	Author	Model	Code
Amorphous silica	$[731/(4.52 - \log CS)] - 273.15$	Fournier, 1977	conductive	GSA1
	$121.6 + 0.2694CS - 1.8101 \cdot 10^{-4}CS^2 + 7.5521 \cdot 10^{-8}CS^3 + 55.184 \log CS$	Gunarsson and Arnórsson, 2000	conductive	GSA2
Moganite	$30.7 + 0.53113CS + 1.2578 \cdot 10^{-4}CS^2 - 5.9241 \cdot 10^{-7}CS^3 + 19.57 \log CS$	Gíslason et al., 1997	conductive	CGM
Chalcedony	$[1\,032/(4.69 - \log CS)] - 273.15$	Fournier, 1977	conductive	GSC1
	$[1\,021/(4.69 - \log CS)] - 273.15$	Arnórsson et al., 1983	conductive	GSC2
	$[1\,112/(4.91 - \log CS)] - 273.15$	Fournier, 1991	conductive	GSC3
	$[1\,264/(5.31 - \log CS)] - 273.15$	Arnórsson et al., 1983	adiabatic	GSC4A
Quartz	$[1\,309/(5.198 - \log CS)] - 273.15$	Fournier, 1977	conductive	GSQ1
	$[1\,315/(5.205 - \log CS)] - 273.15$	Truesdell, 1975	conductive	GSQ2
	$[1\,157.7/(4.88 - \log CS)] - 273.15$	Verma, 2011	conductive	GSQ3
	$42.2 + 0.28831CS - 3.6686 \cdot 10^{-4}CS^2 + 3.1665 \cdot 10^{-7}CS^3 + 88.390 \log CS$	Fournier and Potter, 1982	conductive	GSQ4
	$55.3 + 0.3659CS - 5.3954 \cdot 10^{-4}CS^2 + 5.5132 \cdot 10^{-7}CS^3 + 74.360 \cdot \log CS$	Arnórsson et al., 1988	conductive	GSQ5
	$44.119 + 0.24469mS - 1.7414 \cdot 10^{4}mS^2 + 79.305 \log mS$	Verma and Santoyo, 1997	conductive	GSQ6
	$66.9 + 0.1378CS - 4.9727 \cdot 10^{-5}CS^2 + 1.0468 \cdot 10^{-8}CS^3 + 87.841 \log CS$	Arnórsson et al., 1988	adiabatic	GSQ7A
	$[1\,522/(5.75 - \log CS)] - 273.15$	Fournier, 1973	adiabatic	GSQ8A
	$[1\,164/(4.9 - \log CS)] - 273.15$	Arnórsson et al., 1983	adiabatic	GSQ9A
	$[1\,264/(5.81 - \log CS)] - 273.15$	Arnórsson et al., 1983	adiabatic	GSQ10A
	$[1\,498/(5.7 - \log CS)] - 273.15$	Arnórsson et al., 1983	adiabatic	GSQ11A
Opal	$[1\,000/(4.84 - \log CS)] - 273.15$	Fournier, 1977	conductive	GSOL
	$[781/(4.51 - \log CS)] - 273.15$	Fournier, 1977	conductive	GSOH

Explanations: CS – concentration of SiO_2 in $mg \cdot kg^{-1}$; mS – concentration of SiO_2 in $mol \cdot l^{-1}$

APPENDIX B – CATION GEOTHERMOMETERS

Phase	Geothermometer	Author	Code
Na/K	[777/(0.7 + log NK)] – 273.15	Fournier and Truesdell, 1973	GNK1
	[856/(0.857 + log NK)] – 273.15	Truesdell, 1976	GNK2
	[1 217/(1.483 + log NK)] – 273.15	Fournier, 1979	GNK3
	[883/(0.78 + log NK)] – 273.15	Tonani, 1980	GNK4
	[933/(0.993 + log NK)] – 273.15	Arnórsson et al., 1983	GNK5
	[1 319/(1.699 + log NK)] – 273.15	Arnórsson et al., 1983	GNK6
	[1 178/(1.47 + log NK)] – 273.15	Nieva and Nieva, 1987	GNK7
	[1 390/(1.75 + log NK)] – 273.15	Giggenbach, 1988	GNK8
	[1 289/(1.615 + log NK)] – 273.15	Verma and Santoyo, 1997	GNK9
	$733.6 – 770.55\log Y + 378.189\log Y^2 – 95.753\log Y^3 + 9.544\log Y^4$	Arnórsson et al., 1988	GNK10
	[876/(0.877 + log NK)] – 273.15	Santoyo and Díaz-González, 2010	GNK11
K^2/Mg	[2 330/(7.35 + log KM)] – 273.15	Fournier, 1991*	GKM1
	[1 077/(4.03 + log KM)] – 273.15	Fournier, 1991**	GKM2
	[4 410/(14 + log KM)] – 273.15	Giggenbach, 1988	GKM3
Na/Li	[1 590/(0.770 + log NL)] – 273.15	Kharaka et al., 1982	GNL1
	[1 000/(0.389 + log NL)] – 273.15	Fouillac and Michard, 1981***	GNL2
	[1 195/(0.13 + log NL)] – 273.15	Fouillac and Michard, 1981****	GNL3
	[1 049/(0.44 + log NL)] – 273.15	Verma and Santoyo, 1997***	GNL4
	[1 276/(0.07 + log NL)] – 273.15	Verma and Santoyo, 1997****	GNL5
	[2 002/(1.322 + log NL)] – 273.15	Sanjuan, 2010	GNL6
$Li/Mg^{0.5}$	[2 200/(5.47 – log LM)] – 273.15	Kharaka and Mariner, 1989	GLM
$Na/Ca^{0.5}$	[1 096.7/(3.08 – log NC)] – 273.15	Tonani, 1980	GNC
$K/Ca^{0.5}$	[1 930/(3.861 – log KC)] – 273.15	Tonani, 1980	GKC
Na-K-Ca	[1 647/(log NK + βlog CN + 2.24)] – 273.15 β = 1/3 for $T_{samp} < 100$ °C β = 4/3 for $T_{samp} > 100$ °C/log $Ca^{0.5}/Na < 0$	Fournier and Truesdell, 1973	GNKC

Explanations: NK – Na/K in mg·kg^{-1}; KM – K^2/Mg in mg·kg^{-1}, Y – Na/K in mol·l^{-1}; NL – Na/Li in mg·kg^{-1}; LM – $Li/Mg^{0.5}$ in mg·kg^{-1}; NC – $Na/Ca^{0.5}$ in mg·kg^{-1}; KC – $K/Ca^{0.5}$ in mg·kg^{-1}; CN – $Ca^{0.5}$/Na in mg·kg^{-1}; * – for log (K^2/Mg) > 1.25 in mg·kg^{-1}; ** – for log (K^2/Mg) < 1.25 in mg·kg^{-1}; *** – for mCl < 0.3 mol·kg^{-1} in mol·kg^{-1}; **** – for mCl > 0.3 mol·kg^{-1} in mol·kg^{-1}

APPENDIX C – DESCRIPTION OF SAMPLES (part 1)

Well, spring	Sample code	T_{samp}	pH	Ca	Mg	Na	K	HCO_3	Cl	SO_4	Li	SiO_2	fCO_2	TDS	REF
		°C	–	all concentrations in $mg \cdot l^{-1}$											
ZGL-1	z/21/2/87	61	6.8	510	159	30	23	707	18	1 384	2.2	35	400	2840	1
ZGL-1	z/4/3/87a	62	6.6	510	190	26	16	647	14	1 558	2.2	42	410	2978	1
ZGL-1	z/4/3/87b	61	6.1	510	159	30	23	695	19	1 397	2.5	80	1 307	2 844	1
ZGL-1	z/5/3/87	62	6.1	510	159	30	23	695	12	1 401	2.4	60	690	2 840	1
ZGL-1	z/6/3/87a	61	6.3	510	139	30	23	683	16	1 342	2	50	870	2 753	1
ZGL-1	z/6/3/87b	62	6.3	500	145	30	23	683	15	1 327	2.2	60	786	2 731	1
ZGL-1	z7/3/87	62	6	500	148	30	23	695	15	1 324	2.1	80	650	2 743	1
ZGL-1	z/22/3/87	62	6.6	506	153	36	23	695	12	1 377	2.1	45	452	2 820	1
ZGL-1	z/31/3/87	53	6.3	473	224	28	22	610	9	1 641	2.2	45	660	2 033	1
ZGL-1	z/2/4/87	61	6.4	495	160	30	22	683	14	1 408	2.1	45	645	2 838	1
ZGL-1	z/3/4/87	62	6.4	495	199	30	22	683	9	1 558	2.1	45	647	3 021	1
ZGL-1	z/20/2/92	51	7	548	145	16	12	653	4	1 433	1.4	50	484	2 878	2
ZGL-1	z/31/10/97	61	6.4	553	138	17	24	711	6	1 376	0.3	20	230	2 867	2
ZGL-1	z/27/11/97	61	6.4	546	150	18	25	787	4	1 370	0.3	34	420	2 959	2
ZGL-1	z/16/12/97	61	6.3	534	156	17	23	730	7	1 369	0.2	27	290	2 897	2
ZGL-1	z/21/8/91	61	6.3	597	130	18	23	760	6	1 371	0.3	24	400	2 920	2
ZGL-1	z/25/2/98	61	6.4	550	130	20	23	757	5	1 432	0.2	27	350	2 897	2
ZGL-1	z/27/3/98	61	6.3	567	141	20	27	766	4	1 360	0.3	27	320	2 905	2
ZGL-1	z/30/4/98	61	6.4	594	124	21	27	725	5	1 374	0.3	28	660	2 865	2
ZGL-1	z/17/5/98	61	6.4	594	142	20	28	725	5	1 374	0.3	23	660	2 860	2
ZGL-1	z/28/5/98	61	6.4	582	128	23	28	757	5	1 375	0.3	23	367	2 917	2
ZGL-1	z/11/6/98	61	6.3	547	134	19	27	720	3	1 355	0.3	29	558	2 823	2
ZGL-1	z/12/11/07	60	6.6	612	144	25	20	900	5	1 380	0.3	37	757	3 101	3
ZGL-1	z/17/12/07	61	6.6	609	153	28	25	915	3	1 470	0.3	45	751	3 225	4
ZGL-1	z/18/2/08	61	6.9	609	158	31	25	909	5	1 400	0.3	39	1 300	3152	4
ZGL-1	z/26/2/09	61	6.8	611	155	31	25	927	5	1 380	0.3	40	1 300	2 662	4
ZGL-1	z/30/3/11	61	6.9	611	153	33	26	988	5	1 420	0.3	44	751	3 253	5
ZGL-1	z/13/4/11	61	6.8	609	159	34	26	990	5	1 440	0.3	40	684	3 278	5
ZGL-1	z/7/3/87/1390	63	5.6	500	165	30	23	61	15	1 418	2.5	60	700	2 830	1
ZGL-1	z/19/3/87/1390	63	5.7	517	157	40	29	708	10	1 377	3.3	70	750	2 810	1
ZGL-1	z/2/4/89/1390	62	6	506	232	50	33	707	18	1 653	2.6	65	770	3 164	1
ZGL-1	z/4/3/87/1510	64	5.8	540	190	28	23	1 000	26	1 342	2.5	60	800	3 162	1
ZGL-1	z/21/3/87/1510	64	6.4	506	173	28	23	700	10	142	2	70	750	2 858	1
ZGL-1	z/23/3/87/1510	63	6.6	517	196	30	25	1 061	15	1 255	2.1	70	800	3 088	1
ZGL-1	z/1/4/87/1510	64	6.4	440	272	38	30	988	17	1 436	2	60	750	3 202	1
ZGL-1	z/6/3/87/1730	60	5.9	570	300	26	23	2 123	38	991	2	50	760	4 110	1
ZGL-1	z/22/3/87/1730	68	6.9	341	528	30	27	2 647	12	914	3	55	720	4 493	1
ZGL-1	z/1/4/87/1730	69	6.6	396	495	32	29	2 501	24	1 006	2.5	57	590	4 468	1
ZGL-1	z/6/3/87/1880	69	5.6	510	159	30	23	683	18	1 416	2.5	54	630	2 853	1
ZGL-1	z/23/3/87/1880	69	6.8	572	378	30	25	2 623	14	868	2.9	56	650	4 496	1
ZGL-1	z/1/4/87/1880	69	6.7	231	605	35	27	2 647	24	932	2.3	53	612	4 488	1
FGTB-1	f/15/3/11	61	6.5	568	136	15	44	695	34	1 480	0.2	55	768	3 021	5
FGTB-1	f/30/3/11	61	6.5	566	147	15	30	720	13	1 500	0.2	58	770	3 017	5
FGTB-1	f/13/4/11	61	6.6	563	156	15	26	714	8	1 480	0.2	54	628	3 008	5

Explanations: REF (References): 1 – Fendek et al. (1988); 2 – Remšík et al. (1998); 3 – Hanzel et al. (2008); 4 – Vandrová et al. (2009); 5 – Vandrová et al. (2011)

APPENDIX C – DESCRIPTION OF SAMPLES (part 2)

Well, spring	Sample code	T_{samp}	pH	Ca	Mg	Na	K	HCO_3	Cl	SO_4	Li	SiO_2	fCO_2	TDS	REF
		°C	–	all concentrations in $mg \cdot l^{-1}$											
BEH-1	B/8/7/74	34	7.2	625	150	22	14	1 159	7	1 238	0.4	17	1 476	3 236	6
BEH-1	B/13/7/74	33	7.1	625	145	30	14	1 135	7	1 258	0.4	15	1 729	3 233	6
BEH-1	B/18/7/74	33	6.9	615	141	64	13	1 135	11	1 284	0.5	15	1 654	3 278	6
BEH-1	B/23/10/74	34	6.5	601	150	61	33	1 208	11	1 230	0.6	10	1 757	3 305	6
BEH-1	B/18/5/74	32	6.6	600	132	117	38	1 336	21	1 180	0.4	15	1 826	3 430	6
BEH-1	B/30/8/74	33	6.4	600	128	131	36	1 342	21	1 186	0.3	16	1 823	3 450	6
BEH-1	B/12/9/74	34	6.5	650	154	73	33	1 445	37	1 168	0.4	3	1 580	3 568	6
Fbe-1	F/12/9/09	26	6.6	585	172	103	36	1 740	47	833	0.5	27	1 812	3 536	4
Fbe-1	F/26/2/09	26	6.4	593	170	102	37	1 763	47	830	0.5	27	1 621	3 564	4
Fbe-1	F/11309	27	6.6	593	167	101	39	1 793	47	843	0.5	30	1 398	3 606	4
Fbe-1	F/30/3/11	26	6.7	585	162	100	39	1 769	45	863	0.5	27	1 186	3 580	4
Fbe-1	F/13/4/11	25	6.8	588	167	100	39	1 757	44	873	0.5	25	1265	3 584	4
LM-45	Lm/15/7/87	22	6.3	670	284	51	16	2 136	26	844	0.4	20	1 367	3 909	7
LM-45	Lm/241085	20	6.6	682	197	53	17	2 172	24	824	0.4	37	1 781	4 009	7
LM-45	Lm/30/10/90	20	6.5	703	192	54	17	2 178	24	825	0.4	38	1 586	4 034	7
LM-140	Lm/27/8/5	28	6.1	668	197	47	17	2 111	25	818	0.4	23	1 523	3 024	7
LM-140	lm/15/7/85	30	6.1	649	186	47	16	2 025	24	808	0.4	22	1 254	3 280	7
LM-140	lm/9/10/90	29	6.6	644	195	51	17	2 056	23	979	0.4	40	1 736	3 827	7
RUDOLF	r/15/9/87	27	6.3	648	168	43	17	1 971	24	751	0.4	21	745	3 660	8
RUDOLF	r/28/10/87	28	6.3	621	181	37	11	1 990	23	851	0.2	15	350	3 783	8
RUDOLF	r/24/10/87	29	6.8	643	197	48	16	2 062	22	790	0.3	36	1 192	3 819	8
RUDOLF	r/30/10/90a	29	6.7	643	192	49	16	2 044	23	781	0.4	37	1 225	3 770	7
RUDOLF	r/30/10/90b	29	6.4	672	194	45	17	2 062	24	836	0.5	17	1 250	3 856	7
RUDOLF	r/30/10/90c	28	6.3	622	181	51	17	1 970	23	851	0.4	15	632	3 720	7
VSH-1	Vsh/1	31	7	397	153	171	33	1 756	70	485	1.3	30	479	3 066	4
VSH-1	Vsh/2	33	6	408	153	163	33	1 770	67	487	1.2	30	693	3 080	4
VSH-1	Vsh/3	30	7	407	153	152	33	1 745	63	484	1.2	30	782	3 042	4
VSH-1	Vsh/4	31	7	448	168	167	36	1 920	69	532	1.3	33	860.2	3 384	4
VSH-1	Vsh/5	33	6	429	165	185	36	1 896	76	524	1.4	32	517.3	3 356	4
VSH-1	Vsh/6	30	7	380	147	165	32	1 684	68	465	1.3	29	434.2	2 981	4
VSH-1	Vsh/7	31	7	395	153	172	33	1 751	70	484	1.3	30	451.5	3 100	4
VSH-1	Vsh/8	33	6	369	142	159	31	1 633	65	451	1.2	28	445.5	2 890	4
VSH-1	Vsh/9	30	7	403	156	174	34	1 785	71	493	1.3	30	484.5	3 158	4
Sliač	s/spring/3	31	7	426	156	135	34	1 768	57	493	1.1	31	1 125	3 105	9
Sliač	s/spring/4	33	6	392	143	120	31	1 616	51	451	1	28	1 086	2 837	9
Sliač	s/spring/5	30	7	388	145	142	31	1 656	59	460	1.1	29	788.4	2 918	9
Štiavnička	s/spring/6	9	7.1	133	31	22	4	391	50	133	0.1	0.2	22	766	9
Sliač	s/spring/7	12	7.1	77	23	13	1	317	10	42	0.1	0.5	11	484	9
Sliač	s/spring8	11	7	74	20	9	1.2	287	7	45	0.1	0.5	26	443	9
Sliač	s/spring9	16	7	75	11	9	0.4	269	6	11	0.1	0.1	14	410	9
Sliač	s/spring/1	20	7.1	475	142	97	35	1 770	56	470	0.7	5	1 580	3 052	9
Sliač	s/spring/2	16	7	603	180	53	19	1 598	27	1 040	0.8	7	1 360	3 530	9

Explanations: REF (References): 4 – Vandrová et al. (2009); 6 – Franko et al. (1979); 7 – Klago and Stuchlíková (1990); 8 – Vandrová and Matejčeková (1991); 9 – Zbořil et al. (1992)

APPENDIX D – SILICA GEOTHERMOMETRY RESULTS (part 1)

Well, spring	Sample code	Silica geothermometer temperature estimate (°C)																			
	GSA1	GSA2	GSM	GSOL	GSOH	GSC1	GSC2	GSC3	GSC4A	GSQ1	GSQ2	GSQ3	GSQ4	GSQ5	GSQ6	GSQ7A	GSQ8A	GSQ9A	GSQ10A	GSQ11A	
ZGL-1	z/21/2/87	–	–	18	28	–	55	51	57	62	85	86	108	104	72	11	73	89	74	62	87
ZGL-1	z/4/3/87a	–	–	24	35	–	63	60	65	70	93	94	118	113	80	0	81	96	82	70	94
ZGL-1	z/4/3/87b	6	4	50	64	26	97	93	97	98	124	125	159	147	112	–	111	122	115	98	121
ZGL-1	z/5/3/87	–	–	36	50	13	81	77	82	85	110	111	140	131	97	–	97	110	100	85	109
ZGL-1	z/6/3/87a	–	–	29	42	5	72	68	73	77	101	102	129	122	88	–	89	103	90	77	101
ZGL-1	z/6/3/87b	–	–	36	50	13	81	77	82	85	110	111	140	131	97	–	97	110	100	85	109
ZGL-1	z7/3/87	6	4	50	64	26	97	93	97	98	124	125	159	147	112	–	111	122	115	98	121
ZGL-1	z/22/3/87	–	–	26	38	0	67	63	68	73	96	97	122	116	83	–	84	98	85	73	97
ZGL-1	z/31/3/87	–	–	26	38	0	67	63	68	73	96	97	122	116	83	–	84	98	85	73	97
ZGL-1	z/2/4/87	–	–	26	38	0	67	63	68	73	96	97	122	116	83	–	84	98	85	73	97
ZGL-1	z/3/4/87	–	–	26	38	0	67	63	68	73	96	97	122	116	83	–	84	98	85	73	97
ZGL-1	z/20/2/92	–	–	29	42	5	72	68	73	77	101	102	129	122	88	–	89	103	90	77	101
ZGL-1	z/12/11/07	–	–	26	38	0	67	63	68	73	96	97	122	116	83	–	84	98	85	73	97
ZGL-1	z/17/12/07	–	–	21	32	–	60	56	62	67	90	91	114	109	76	5	78	93	79	67	91
ZGL-1	z/18/2/08	–	–	22	33	–	61	57	63	68	91	92	116	110	78	3	79	94	80	68	92
ZGL-1	z/26/2/09	–	–	25	37	–	66	62	67	72	95	96	121	115	82	–	83	97	84	72	96
ZGL-1	z/30/3/11	–	–	22	33	–	61	57	63	68	91	92	116	110	78	3	79	94	80	68	92
FGTB-1	f/15/3/11	–	–	33	46	9	77	73	78	81	105	106	135	126	93	–	93	106	95	81	105
FGTB-1	f/30/3/11	–	–	35	49	11	79	76	80	83	108	109	138	129	95	–	96	109	98	83	107
FGTB-1	f/13/4/11	–	–	32	46	8	76	72	77	80	105	106	133	125	92	–	93	106	94	80	104
ZGL-1	z/7/3/87/1390	–	–	36	50	13	81	77	82	85	110	111	140	131	97	–	97	110	100	85	109
ZGL-1	z/19/3/87/1390	0	–	43	57	20	90	86	90	92	117	118	150	139	105	–	105	117	108	92	115
ZGL-1	z/2/4/89/1390	–	–	40	54	16	86	82	86	88	114	115	145	135	101	–	101	113	104	88	112
ZGL-1	z/4/3/87/1510	–	–	36	50	13	81	77	82	85	110	111	140	131	97	–	97	110	100	85	109
ZGL-1	z/21/3/87/1510	0	–	43	57	20	90	86	90	92	117	118	150	139	105	–	105	117	108	92	115
ZGL-1	z/23/3/87/1510	0	–	43	57	20	90	86	90	92	117	118	150	139	105	–	105	117	108	92	115
ZGL-1	z/1/4/87/1510	–	–	36	50	13	81	77	82	85	110	111	140	131	97	–	97	110	100	85	109
ZGL-1	z/6/3/87/1730	–	–	29	42	5	72	68	73	77	101	102	129	122	88	–	89	103	90	77	101
ZGL-1	z/22/3/87/1730	–	–	33	46	9	77	73	78	81	105	106	135	126	93	–	93	106	95	81	105
ZGL-1	z/1/4/87/1730	–	–	34	48	10	79	75	79	82	107	108	137	128	94	–	95	108	97	82	107
ZGL-1	z/6/3/87/1880	–	–	32	46	8	76	72	77	80	105	106	133	125	92	–	93	106	94	80	104
ZGL-1	z/23/3/87/1880	–	–	34	47	10	78	74	79	82	106	107	136	127	94	–	94	107	96	82	106
ZGL-1	z/1/4/87/1880	–	–	31	45	7	75	71	76	79	104	105	132	125	91	–	92	105	93	79	104

APPENDIX D – SILICA GEOTHERMOMETRY RESULTS (part 2)

Well, spring	Sample code	Silica geothermometer temperature estimate (°C)																			
	GSA1	GSA2	GSM	GSOL	GSOH	GSC1	GSC2	GSC3	GSC4A	GSQ1	GSQ2	GSQ3	GSQ4	GSQ5	GSQ6	GSQ7A	GSQ8A	GSQ9A	GSQ10A	GSQ11A	
BEH-1	B/8/7/74	–	–	2	2	–	25	22	29	37	57	58	72	71	42	29	44	64	44	37	62
BEH-1	B/13/7/74	–	–	–	–	–	21	17	25	33	52	53	67	66	38	29	38	60	39	33	58
BEH-1	B/18/7/74	–	–	–	–	–	21	17	25	33	52	53	67	66	38	29	38	60	39	33	58
BEH-1	B/23/10/74	–	–	–	–	–	7	4	11	20	39	40	50	49	23	27	22	47	25	20	46
BEH-1	B/18/5/74	–	–	–	–	–	21	17	25	33	52	53	67	66	38	29	38	60	39	33	58
BEH-1	B/30/8/74	–	–	1	–	–	23	20	27	35	55	56	70	69	40	29	41	62	42	35	60
BEH-1	B/12/9/74	–	–	–	–	–	15	12	20	28	47	48	61	60	32	29	33	55	34	28	53
Fbe-1	F/12/9/09	–	–	12	18	–	44	40	47	53	74	75	95	92	61	21	63	79	62	53	78
Fbe-1	F/26/2/09	–	–	12	18	–	44	40	47	53	74	75	95	92	61	21	63	79	62	53	78
Fbe-1	F/11309	–	–	14	22	–	48	45	51	57	79	80	100	97	65	17	67	83	67	57	82
Fbe-1	F/30/3/11	–	–	12	18	–	44	40	47	53	74	75	95	92	61	21	63	79	62	53	78
Fbe-1	F/13/4/11	–	–	10	15	–	40	37	43	50	71	72	91	88	57	23	59	77	59	50	75
LM-45	Lm/15/7/87	–	–	5	7	–	31	28	35	42	63	64	80	78	49	27	50	69	50	42	67
LM-45	Lm/241085	–	–	20	30	–	57	54	60	65	87	88	111	107	74	8	76	91	76	65	89
LM-45	Lm/30/10/90	–	–	21	31	–	59	55	61	66	89	90	113	108	75	6	77	92	77	66	90
LM-140	Lm/27/8/5	–	–	8	12	–	37	34	40	47	68	69	87	85	54	25	56	74	56	47	72
LM-140	lm/15/7/85	–	–	7	10	–	35	32	39	45	66	67	84	83	52	26	54	72	54	45	71
LM-140	lm/9/10/90	–	–	22	33	–	61	57	63	68	91	92	116	110	78	3	79	94	80	68	92
RUDOLF	r/15/9/87	–	–	6	9	–	33	30	37	44	65	66	82	81	50	27	52	71	52	44	69
RUDOLF	r/28/10/87	–	–	–	–	–	21	17	25	33	52	53	67	66	38	29	38	60	39	33	58
RUDOLF	r/24/10/87	–	–	19	29	–	56	53	58	64	86	87	110	105	73	9	75	90	75	64	88
RUDOLF	r/30/10/90a	–	–	20	30	–	57	54	60	65	87	88	111	107	74	8	76	91	76	65	89
RUDOLF	r/30/10/90b	–	–	2	2	–	25	22	29	37	57	58	72	71	42	29	44	64	44	37	62
RUDOLF	r/30/10/90c	–	–	–	–	–	21	17	25	33	52	53	67	66	38	29	38	60	39	33	58
VSH-1	Vsh/1	–	–	14	22	–	48	45	51	57	79	80	100	97	65	17	67	83	67	57	82
VSH-1	Vsh/2	–	–	14	22	–	48	45	51	57	79	80	100	97	65	17	67	83	67	57	82
VSH-1	Vsh/3	–	–	14	22	–	48	45	51	57	79	80	100	97	65	17	67	83	67	57	82
VSH-1	Vsh/4	–	–	17	25	–	52	49	55	60	83	84	105	101	69	13	71	87	71	60	85
VSH-1	Vsh/5	–	–	16	25	–	51	48	54	60	82	83	104	100	68	14	70	86	70	60	84
VSH-1	Vsh/6	–	–	13	20	–	46	43	49	55	77	78	98	95	63	19	65	82	65	55	80
VSH-1	Vsh/7	–	–	14	22	–	48	45	51	57	79	80	100	97	65	17	67	83	67	57	82
VSH-1	Vsh/8	–	–	12	19	–	45	42	48	54	76	77	96	93	62	20	64	80	64	54	79
VSH-1	Vsh/9	–	–	15	22	–	49	45	51	57	79	80	101	97	66	17	68	84	68	57	82
VSH-1	Vsh/10	–	–	15	22	–	49	45	52	57	79	80	101	98	66	17	68	84	68	57	82
VSH-1	Vsh/11	–	–	13	19	–	45	42	48	54	76	77	96	94	62	20	64	81	64	54	79
VSH-1	Vsh/12	–	–	13	20	–	46	42	49	55	77	78	97	94	63	19	65	81	65	55	80

APPENDIX E – CATION GEOTHERMOMETRY RESULTS (part 1)

Well, spring	Sample code	Cation geothermometry temperature estimate (°C)																							
	GN1	GN2	GN3	GN4	GN5	GN6	GN7	GN8	GN9	GN10	GN11	GKM1	GKM2	GKM3	GLM	GLN1	GLN2	GLN3	GLN4	GLN5	GNC	GKC	GNKC	GNKCm	
ZGL-1	z/21/2/87	>	>	>	>	>	>	>	>	>	>	>	24	–	36	80	>	–	–	–	–	98	>	>	55
ZGL-1	z/4/3/87a	>	>	>	>	>	>	>	>	>	>	>	38	–	40	78	>	–	–	–	–	90	>	>	39
ZGL-1	z/4/3/87b	>	>	>	>	>	>	>	>	>	>	>	23	–	36	83	>	–	–	–	–	98	>	>	57
ZGL-1	z/5/3/87	>	>	>	>	>	>	>	>	>	>	>	23	–	36	82	>	–	–	–	–	98	>	>	57
ZGL-1	z/6/3/87a	>	>	>	>	>	>	>	>	>	>	>	21	–	35	79	>	–	–	–	–	98	>	>	57
ZGL-1	z/6/3/87b	>	>	>	>	>	>	>	>	>	>	>	21	–	36	81	>	–	–	–	–	98	>	>	57
ZGL-1	z7/3/87	>	>	>	>	>	>	>	>	>	>	>	22	–	36	80	>	–	–	–	–	98	>	>	57
ZGL-1	z/22/3/87	>	>	>	>	>	>	>	>	>	>	>	22	–	36	79	>	–	–	–	–	>	>	>	59
ZGL-1	z/31/3/87	>	>	>	>	>	>	>	>	>	>	>	30	–	38	76	>	–	–	–	–	96	>	>	38
ZGL-1	z/2/4/87	>	>	>	>	>	>	>	>	>	>	>	24	–	37	79	>	–	–	–	–	99	>	>	61
ZGL-1	z/3/4/87	>	>	>	>	>	>	>	>	>	>	>	28	–	38	76	>	–	–	–	–	99	>	>	54
ZGL-1	z/20/2/92	>	>	>	>	>	>	>	>	>	>	>	44	–	42	70	>	–	–	–	–	65	>	>	60
ZGL-1	z/12/11/07	>	>	>	>	>	>	>	>	>	>	>	20	–	35	37	>	–	–	–	–	89	>	>	69
ZGL-1	z/17/12/07	>	>	>	>	>	>	>	>	>	>	>	20	–	35	37	>	–	–	–	–	95	>	>	73
ZGL-1	z/18/2/08	>	>	>	>	>	>	>	>	>	>	>	20	–	35	37	>	–	–	–	–	95	>	>	69
ZGL-1	z/26/2/09	>	>	>	>	>	>	>	>	>	>	>	18	–	35	37	>	–	–	–	–	98	>	>	72
ZGL-1	z/30/3/11	>	>	>	>	>	>	>	>	>	>	>	19	–	35	37	>	–	–	–	–	>	>	>	69
FGTB-1	f/15/3/11	>	>	>	>	>	>	>	>	>	>	>	1	–	29	31	>	–	–	–	–	61	>	>	65
FGTB-1	f/30/3/11	>	>	>	>	>	>	>	>	>	>	>	13	–	33	30	>	–	–	–	–	61	>	>	94
FGTB-1	f/13/4/11	>	>	>	>	>	>	>	>	>	>	>	19	–	35	30	>	–	–	–	–	61	>	>	82
ZGL-1a	z/7/3/87/1390	>	>	>	>	>	>	>	>	>	>	>	23	–	36	83	>	–	–	–	–	98	>	>	52
ZGL-1a	z/19/3/87/1390	>	>	>	>	>	>	>	>	>	>	>	15	–	34	91	>	–	–	–	–	>	>	>	69
ZGL-1a	z/2/4/89/1390	>	>	>	>	>	>	>	>	>	>	>	17	–	34	80	>	–	–	–	–	>	>	>	35
ZGL-1a	z/4/3/87/1510	>	>	>	>	>	>	>	>	>	>	>	26	–	37	81	>	–	–	–	–	93	>	>	47
ZGL-1	z/21/3/87/1510	>	>	>	>	>	>	>	>	>	>	>	24	–	36	77	>	–	–	–	–	94	>	>	58
ZGL-1	z/23/3/87/1510	>	>	>	>	>	>	>	>	>	>	>	24	–	36	76	>	–	–	–	–	97	>	>	69
ZGL-1	z/1/4/87/1510	>	>	>	>	>	>	>	>	>	>	>	23	–	36	71	>	–	–	–	–	>	>	>	28
ZGL-1	z/6/3/87/1730	>	>	>	>	>	>	>	>	>	>	>	34	–	39	70	>	–	–	–	–	87	>	>	31
ZGL-1	z/22/3/87/1730	>	>	>	>	>	>	>	>	>	>	>	38	–	40	73	>	–	–	–	–	>	>	>	77
ZGL-1	z/1/4/87/1730	>	>	>	>	>	>	>	>	>	>	>	34	–	39	70	>	–	–	–	–	>	>	>	48
ZGL-1	z/6/3/87/1880	>	>	>	>	>	>	>	>	>	>	>	23	–	36	83	>	–	–	–	–	98	>	>	61
ZGL-1	z/23/3/87/1880	>	>	>	>	>	>	>	>	>	>	>	35	–	39	76	>	–	–	–	–	95	>	>	68
ZGL-1	z/1/4/87/1880	>	>	>	>	>	>	>	>	>	>	>	40	–	41	65	>	–	–	–	–	>	>	>	63

APPENDIX E – CATION GEOTHERMOMETRY RESULTS (part 2)

Well, spring	Sample code	Cation geothermometry temperature estimate (°C)																						
	GN1	GN2	GN3	GN4	GN5	GN6	GN7	GN8	GN9	GN10	GN11	GKM1	GKM2	GKM3	GLM	GLN1	GLN2	GLN3	GLN4	GLN5	GNC	GKC	GNKC	GNKCm	
BEH-1	B/8/7/74	>	>	>	>	>	>	>	>	>	>	>	39	–	41	43	>	–	–	–	–	77	>	>	63
BEH-1	B/13/7/74	>	>	>	>	>	>	>	>	>	>	>	38	–	40	43	>	–	–	–	–	92	>	>	63
BEH-1	B/18/7/74	>	>	>	>	>	>	>	>	>	>	>	40	–	41	48	>	–	–	–	–	>	>	>	65
BEH-1	B/23/10/74	>	>	>	>	>	>	>	>	>	>	>	11	–	32	51	>	–	–	–	–	>	>	>	70
BEH-1	B/18/5/74	>	>	>	>	>	>	>	>	>	>	>	5	–	31	44	>	–	–	–	–	>	>	>	79
BEH-1	B/30/8/74	>	>	>	>	>	>	>	>	>	>	>	6	–	31	39	>	–	–	–	–	>	>	>	79
BEH-1	B/12/9/74	>	>	>	>	>	>	>	>	>	>	>	11	–	33	43	>	–	–	–	–	>	>	>	66
Fbe-1	F/12/9/09	>	>	>	>	>	>	>	>	>	>	>	10	–	32	46	>	–	–	–	–	>	>	>	66
Fbe-1	F/26/2/09	>	>	>	>	>	>	>	>	>	>	>	9	–	32	46	>	–	–	–	–	>	>	>	62
Fbe-1	F/11/3/09	>	>	>	>	>	>	>	>	>	>	>	7	–	31	47	>	–	–	–	–	>	>	>	67
Fbe-1	F/30/3/11	>	>	>	>	>	>	>	>	>	>	>	7	–	31	47	>	–	–	–	–	>	>	>	66
Fbe-1	F/13/4/11	>	>	>	>	>	>	>	>	>	>	>	7	–	31	47	>	–	–	–	–	>	>	>	66
LM-45	Lm/15/7/87	>	>	>	>	>	>	>	>	>	>	>	46	–	42	37	>	–	–	–	–	>	>	>	33
LM-45	Lm/241085	>	>	>	>	>	>	>	>	>	>	>	37	–	40	40	>	–	–	–	–	>	>	>	51
LM-45	Lm/30/10/90	>	>	>	>	>	>	>	>	>	>	>	36	–	40	41	>	–	–	–	–	>	>	>	62
LM-140	Lm/27/8/5	>	>	>	>	>	>	>	>	>	>	>	37	–	40	40	>	–	–	–	–	>	>	>	51
LM-140	lm/15/7/85	>	>	>	>	>	>	>	>	>	>	>	38	–	40	41	>	–	–	–	–	>	>	>	49
LM-140	lm/9/10/90	>	>	>	>	>	>	>	>	>	>	>	37	–	40	41	>	–	–	–	–	>	>	>	46
RUDOLF	r/15/9/87	>	>	>	>	>	>	>	>	>	>	>	34	–	39	42	>	–	–	–	–	>	>	>	48
RUDOLF	r/28/10/87	>	>	>	>	>	>	>	>	>	>	>	52	–	44	28	>	–	–	–	–	>	>	>	46
RUDOLF	r/24/10/87	>	>	>	>	>	>	>	>	>	>	>	39	–	41	35	>	–	–	–	–	>	>	>	47
RUDOLF	r/30/10/90a	>	>	>	>	>	>	>	>	>	>	>	39	–	40	41	>	–	–	–	–	>	>	>	51
RUDOLF	r/30/10/90b	>	>	>	>	>	>	>	>	>	>	>	37	–	40	45	>	–	–	–	–	>	>	>	48
RUDOLF	r/30/10/90c	>	>	>	>	>	>	>	>	>	>	>	35	–	40	41	>	–	–	–	–	>	>	>	41
VSH-1	Vsh/1	>	>	>	>	>	>	>	>	>	>	>	11	–	33	68	>	–	–	–	–	>	>	>	49
VSH-1	Vsh/2	>	>	>	>	>	>	>	>	>	>	>	11	–	33	66	>	–	–	–	–	>	>	>	47
VSH-1	Vsh/3	>	>	>	>	>	>	>	>	>	>	>	11	–	33	66	>	–	–	–	–	>	>	>	44
VSH-1	Vsh/4	>	>	>	>	>	>	>	>	>	>	>	9	–	32	67	>	–	–	–	–	>	>	>	44
VSH-1	Vsh/5	>	>	>	>	>	>	>	>	>	>	>	10	–	32	69	>	–	–	–	–	>	>	>	49
VSH-1	Vsh/6	>	>	>	>	>	>	>	>	>	>	>	12	–	33	68	>	–	–	–	–	>	>	>	47
VSH-1	Vsh/7	>	>	>	>	>	>	>	>	>	>	>	11	–	33	68	>	–	–	–	–	>	>	>	48
VSH-1	Vsh/8	>	>	>	>	>	>	>	>	>	>	>	12	–	33	67	>	–	–	–	–	>	>	>	49
VSH-1	Vsh/9	>	>	>	>	>	>	>	>	>	>	>	11	–	32	68	>	–	–	–	–	>	>	>	43
VSH-1	Vsh/10	>	>	>	>	>	>	>	>	>	>	>	11	–	32	64	>	–	–	–	–	>	>	>	48
VSH-1	Vsh/11	>	>	>	>	>	>	>	>	>	>	>	12	–	33	63	>	–	–	–	–	>	>	>	46
VSH-1	Vsh/12	>	>	>	>	>	>	>	>	>	>	>	12	–	33	65	>	–	–	–	–	>	>	>	42

APPENDIX F – LIST OF ACRONYMS AND SYMBOLS IN TEXT

Symbol	Description	Unit (if any)
β	reaction stoichiometry coefficient	–
Δt_{Mg}	Mg-correction temperature	°C
a_k	activity coefficient of phase k	–
$a_{i,k}$	activity coefficient of species i in phase k	–
C	number of components in reaction	–
CSM	conceptual site model	–
CHN	Choč Nappe (system, succession, horizon)	–
cX	concentration of i-th component in water	ppm, $mg \cdot l^{-1}$, $mg \cdot kg^{-1}$
D-HTC	discharge zone, high total carbon subfacies	–
D-LTC	discharge zone, low total carbon subfacies	–
DRTE	deep reservoir thermal endmember	–
F	number of independent variables in reactions	–
H	enthalpy (in general)	$kJ \cdot kg^{-1}$
HL	enthalpy of liquid	$kJ \cdot kg^{-1}$
H_{res}	reservoir enthalpy	$kJ \cdot kg^{-1}$
HT	high temperature (conditions)	–
IWCP	Inner Western Carpathian Paleogene (Sub-Tatric Group) succession	–
Jr/Cr-2	(Krížna Nappe) Jurassic – Mid Cretaceous succession (duplexes)	–
K_{eq}	equilibrium constant	–
KNA	Krížna Nappe (system, succession, horizon)	–
L_x	Logarithm of ionic concentration ratios	–
LT	low temperature (conditions)	–
M	number of equilibrated minerals in solution	–
MCG	multicomponent geothermometers	–
MEG	multicomponent equilibrium geothermometry	–
MI	maturity index	–
P	number of phases in reactions	–
pCO_2	partial CO_2 pressure	bar, MPa
Pg	Paleogene	–
p-T	(thermodynamic) pressure – temperature conditions	–
Q_k	activity coefficient for aqueous species of phase k	–
r_x	relative concentrations	–, %
RMED	clustered median (multicomponent geothermometry) approach	–
S-CGW	Sliače springs – cold groundwater facies	–
SI	saturation index	–
SRTW	shallow reservoir thermal waters facies	–
T	temperature (general)	°C
T_{btm}	bottomhole temperature	°C
TCR	Tatricum Crystalline (bedrock)	–
TEU	Tatricum Envelope Unit (horizon)	–
Tr2	Mid Triassic (carbonates)	–
T_{est}	estimated temperature	°C
T_{res}	reservoir temperature	°C
T_{samp}	sampling temperature	°C
T_{wh}	wellhead temperature	°C
T_x	Geothermometer temperature	°C
TCM	thermal-cold mixing (regime)	–
TCLM	ternary chloride mixing model	–
TTM	thermal-thermal mixing (regime)	–
TSI	total saturation index	–
Tr3-Cr2	(Krížna Nappe) Late Triassic – Mid Cretaceous profile	–
$v_{i,k}$	stoichiometric coefficient for species i in phase k	–
X_{CS}	silica fraction correction	–
X_H	enthalpy fraction correction	–